Green Chemistry

TUTORIAL REVIEW

View Article Online
View Journal | View Issue

Cite this: *Green Chem.*, 2025, **27**, 2846

Recent advances in ex ante techno-environmental-economic assessment of thermochemical waste or biomass to energy technologies based on process simulation†

Jiehong Tang,[a,b] Yuting Tang, *[a,b] Hongyu Liu,[a,b] Xinfei Chen,[c] Xikui Zhang,[a,b] Yin Chen,[a,b] Shuang Liang,[a,b] Junxuan Huang,[a,b] Wen Teng,[a,b] Ziwei Sun[a,b] and Xiaoqian Ma[a,b]

Received 26th November 2024,
Accepted 27th January 2025

DOI: 10.1039/d4gc06016d

rsc.li/greenchem

Thermochemical waste or biomass to energy (W/BtE) technology is known for its high conversion efficiency, rapid reaction rate, and foreseeable scale-up potential. To elucidate the coexisting risks and opportunities of newly proposed or ready-to-be-retrofitted W/BtE systems, ex ante techno-environmental-economic (TEE) assessment can provide multidimensional quantified guidance, while process simulation is an effective tool to predict their performance based on the existing laboratory- or pilot-scale experiment results. This review aims to provide a comprehensive understanding of process simulation-based TEE assessment of W/BtE systems. It summarizes the establishment of applicable conditions for reactor-level modelling approaches. Next, the calculation methods and principles for TEE assessment are introduced. Furthermore, based on the review of studies published from 2020 to 2024, it fully investigates the advances in the optimization of thermochemical processes through process simulation and the performance improvement of W/BtE systems, including waste or biomass to power (W/BtP) and to fuel (W/BtF) systems. Eventually, it highlights that the enhancement of data source quality and in-depth consideration of realistic conditions are the key aspects to be improved in the future.

Green foundation

1. We discussed the basic structures, calculation methods, and existing advances in the ex ante process-simulation-based techno-environmental-economic (TEE) assessment of thermochemical waste or biomass to energy (W/BtE) technologies.
2. Thermochemical W/BtE technologies can be one of the most promising low-carbon technologies in the future, and numerous studies conducted at laboratory- and pilot-scale have been published. As the commercial application of most W/BtE technologies is still in the early stage, tools are needed to elucidate the coexisting risks and opportunities of newly proposed or ready-to-be-retrofitted W/BtE systems, which can be provided by ex ante TEE assessment.
3. Despite the fact that the existing studies provide references for many cases, basic methods and eventual results vary significantly, causing poor comparability and integrity. This study summarizes general and comprehensive TEE assessment structures and methods, providing guidelines, understanding and prospects to improve the accuracy and credibility of future work.

1 Introduction

With the expansion of the global population, it is estimated that >2 billion tonnes of municipal solid waste (MSW) is generated annually, and about 38% of it is under uncontrolled management.[1] In this case, waste to energy (WtE) technology, as one of the most important waste utilization methods, has attracted increasing attention to meet the goals of the present carbon neutrality policy and achieve a circular economy.

[a]School of Electric Power Engineering, South China University of Technology, Guangzhou 510640, China. E-mail: eptangyt@scut.edu.cn
[b]Guangdong Province Key Laboratory of Efficient and Clean Energy Utilization, Guangzhou 510640, China
[c]Guangzhou Institute of Energy Conversion, Chinese Academy of Sciences, Guangzhou 510640, China

† Electronic supplementary information (ESI) available. See DOI: https://doi.org/10.1039/d4gc06016d

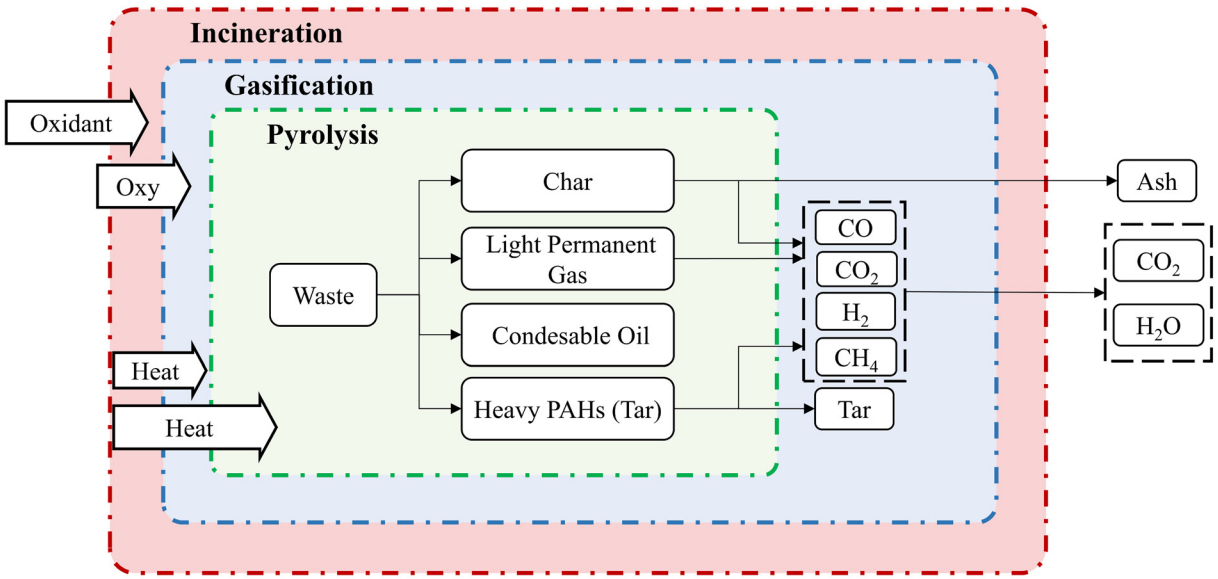

Fig. 1 Schematic flow sheet of thermochemical W/BtE technology (redrawn from Urena[13]).

Initially, the utilization of waste can substitute the mining of fossil fuel-resources, reducing fossil-based carbon emission.[2,3] Furthermore, the application of WtE technology has lower environmental risks compared with traditional landfill treatment.[4] High organic-content waste (MSW, biomass waste, *etc.*) has high utilization value in the application of WtE technology,[5,6] and its considerable generation makes it a dependable feedstock source.[7] The organic-content in MSW is a mixture of food residue, wood, paper, textile, plastic, rubber, and other components. Besides plant-based agricultural waste, animal-based wastewater, sludge and animal manure are also important components of the organic content in biomass.[8] Generally, plant-based organic content mainly includes cellulose, hemicellulose and lignin, while animal-based content basically consists of sugars, lipids and proteins.[9] Polymers are the main component of the manufactured organic content in textiles, plastic and rubber.[10] Thus, the concept of WtE can be expanded to waste or biomass to energy (W/BtE). W/BtE technology mainly includes thermochemical, biochemical, and chemical routes.[11] This review mainly focuses on the thermochemical route.

Thermochemical W/BtE technology refers to the power generation or value-added chemical production based on pyrolysis, gasification, and incineration processes,[12] and the main scheme for the three processes is shown in Fig. 1.[13] Pyrolysis is conducted in an oxidant-free atmosphere with an external heat supply.[14] Pyrogas mainly consists of CO, CO_2, H_2, CH_4 and noncondensable hydrocarbons.[15,16] Condensable oil product includes acids, alcohols, aldehydes, ketones, phenols, esters, sugars, furans, complex oxygenates and hydrocarbons.[9] Moreover, a considerable carbon content still exists in the generated char.[17] The reported yield of gas, liquid and char during MSW pyrolysis is about 37 wt%, 27 wt%, and 46 wt%, respectively.[18] To maximize the production of high-value fuel

Jiehong Tang

Jiehong Tang is currently a Ph.D. student at South China University of Technology under the supervision of A.P. Yuting Tang and obtained his B.E. degree from the same university in 2020. His research focuses on the global design and optimization of waste-to-energy systems and the high-resolution prediction of municipal solid waste generation.

Yuting Tang

Yuting Tang received her Ph.D. at South China University of Technology in 2014. From December 2016 to January 2018, she carried out research as a visiting scholar at Cornell University. She is currently an Associate Professor at South China University of Technology. Her research interests include product-targeted conversion, combustion and emission control and techno-environment-economic assessment during the waste-to-energy process.

gas *via* thermochemical conversion, an atmosphere with an inadequate amount of oxidant (air, oxygen, steam, *etc.*) for complete combustion is employed during the gasification process.[19] Due to the simultaneous occurrence of partial oxidation and thermal decomposition, the combustible content of waste or biomass is mostly converted into the gas phase, leaving a minor content of ash and tar.[13] With an increase in the supplied amount of oxidant, the gasification process can realize auto-thermal at the expense of a reduction in the temperature for gas production.[20,21] Common gasification agents include air, steam, and O_2. Among them, air is the most conveniently available, steam promotes the H_2 yield in the syngas, and O_2 is the ideal option to prevent the dilution of N_2, which reduces the potential formation of NO_x. Regarding the gaseous product of pyrolysis and gasification, after removal of pollutants (H_2S, HCl, COS, NH_3, HCN, tar, and particulate),[22,23] it can be further processed for the manufacture of value-added fuel.[24,25] Incineration is the process employed for the complete oxidation of waste or biomass with an adequate or excessive supply of oxygen or air, generating high-temperature flue gas (mainly CO_2 and steam).[8] In the Rankine cycle (RC), massive heat transfer occurs from the flue gas to generate steam, which propels the power generator. An air pollution control (APC) section is necessary in the incineration facility to ensure that the content of SO_2, NO_x, HCl, dioxin, and particulate in the flue gas satisfies the local emissions standards.[26–28]

To date, incineration is most widely applied method for the treatment of waste worldwide owing to its advantages of rapid treatment and reduction in the volume of residues.[29] Since the 1970s, lots of studies and programs have been conducted on waste pyrolysis and gasification technology to avoid the environmental risks of dioxin and heavy metal emission during waste incineration,[30,31] but its commercial application is still in its infancy.[32] Recently, both existing and proposed W/BtE facilities have encountered challenges. Firstly, the synergistic disposal of multiple waste and biomass has become the mainstream trend, and thus the characteristics of the feedstock will fluctuate, introducing uncertain factors in the optimized operation of the facility.[33] Secondly, with the implementation of the carbon neutrality policy, low-energy efficiency and high-environmental-risk equipment and techniques need to be replaced by more advanced ones,[34] and new sections need to be added to the original system, such as carbon capture and storage (CCS) units.[35] This requires guidance in the aspects of equipment section and technique suitability. Finally, for the assessment of the long-term environmental and economic performance of the facility operations, it is a significant requirement to provide guidance to avoid the potential risks associated with sensible factors in advance of the improvement or construction of facilities.[36]

The concept of ex ante techno-environmental-economic (TEE) assessment has been well developed with time.[37] However, although there are plenty of lab-scale and pilot-scale experimental data and real operational data as a foundation, a more credible and adjustable calculation model is still required.[38] Obviously, the process simulation method can be employed, given that it can acquire credible data of various operating conditions based on existing data using rigorous chemical, hydrodynamic, and thermodynamic theories.[39]

According to previous studies, the classification of the assessment boundary and process simulation completeness is shown in Fig. 2. From the perspectives of process simulation, tier I only focuses on the core sections of the W/BtE system, including the thermochemical conversion section and power generation or product synthesis section. Then, tier II further considers the quality control sections, such as pollution control section, product purification section, and by-product utilization section. Tier III includes the complete process of the W/BtE system, given that the simulation of auxiliary sections (heat recovery network, pipeline transportation network, utilities network, *etc.*) is added into the flowsheet. From the perspectives of assessment boundary, tier I concentrates on the direct emissions, regardless of the indirect emissions caused by chemicals, energy and utilities, and tier II completes the scope, which basically covers the W/BtE system. Furthermore, tier III considers the influence of upstream and downstream processes, such as raw material collection, product transport and storage, and residue treatment.

Hongyu Liu

Hongyu Liu is currently a Ph.D. student at South China University of Technology under the supervision of Prof. Xiaoqian Ma and obtained his B.E. degree from Wuhan Textile University in 2021. His research focuses on catalytic-targeted conversion and carbon capture and utilization during biomass gasification and pyrolysis processes.

Xinfei Chen

Xinfei Chen received his Ph.D. at South China University of Technology in 2022. He is currently an Associate Professor at Guangzhou Institute of Energy Conversion, Chinese Academy of Sciences (GIEC, CAS). His research interests include clean and highly efficient utilization of organic solid waste.

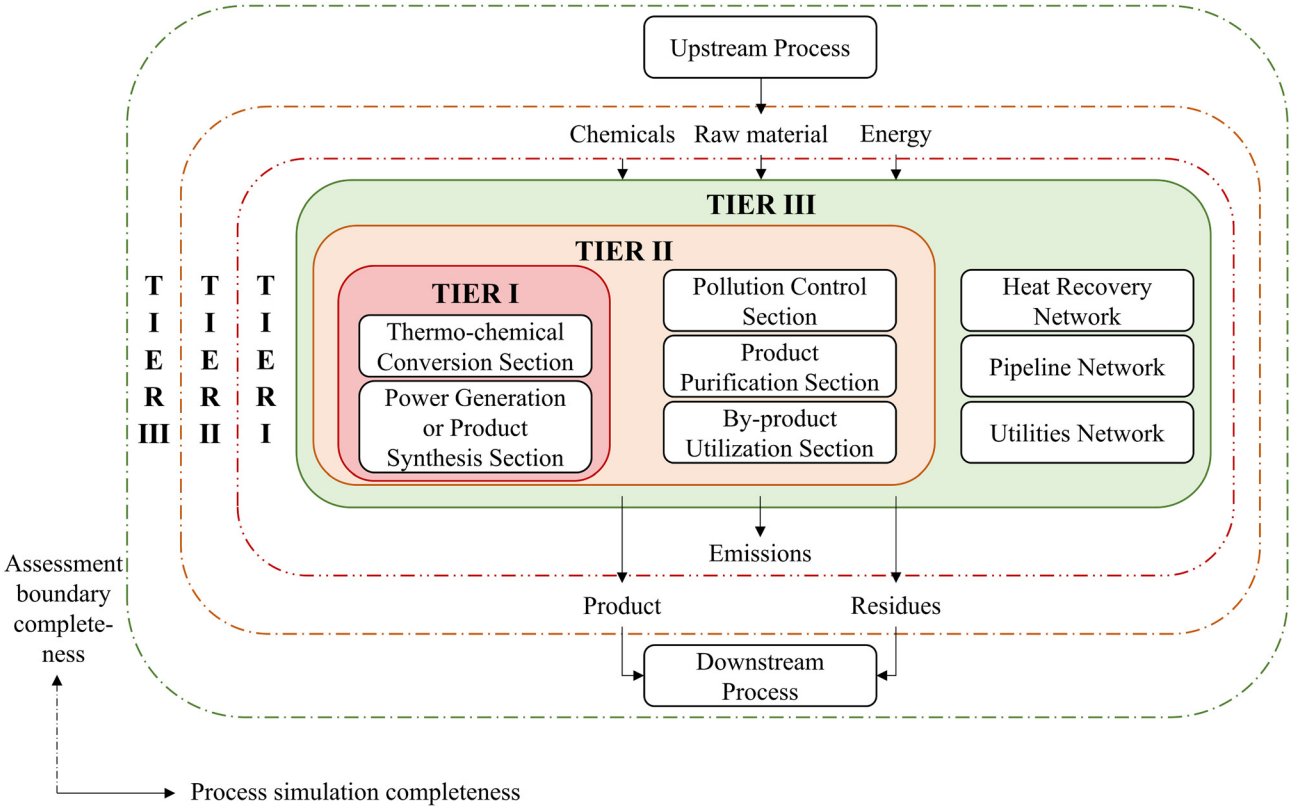

Fig. 2 Classification of assessment boundary and process simulation completeness.

Consequently, tier III covers the complete life cycle of the W/BtE system.

This review is organized as follows: section 2 introduces the progress in the establishment of a process simulation model; section 3 introduces the calculation methods for TEE assessment; section 4 compares the TEE performance of the different hybrid W/BtE systems reported in recent years; section 5 illustrates the prospects and shortcomings in this field; and section 6 concludes this review.

Xiaoqian Ma

Xiaoqian Ma is currently a Professor at South China University of Technology. He is also the chairman Chairman of the Guangdong Technical Innovation Association of Energy Conversation Engineering and Guangzhou Energy Association. He received his Ph.D. at Huazhong University of Science and Technology in 1995. His research interests include combustion and pollution control theory, waste-to-energy technology, and renewable-energy-involved complementary system operation.

2 Model establishment for process simulation

Process simulation plays a vital role in ex ante TEE assessment, given that it not only generates the life cycle inventory of W/BtE systems as foreground data, but also enables the solving of flow equilibrium formulations as the foundation of techno analysis, as shown in Fig. 3. The establishment of the model for process simulation is mainly determined by the selection of modelling approaches based on the feedstock properties, operational parameters, and reactions mechanisms.

In the case of thermochemical processes, the main model approaches are summarized at the molecular level, particle level, and rector level.[40,41] The main model approaches at various levels of the thermochemical W/BtE process are shown in Fig. 4. The kinetic model is a multi-level approach, given that it can participate in the simulation of different levels. In this review, as shown in Fig. 3, the role of process simulation is to provide the foreground data, which reflects the product yield and composition influenced by the feedstock characteristics and operational parameters at the reactor level, as the reference for the following TEE assessment. Thus, this review emphasizes the reactor-level modeling approaches. A detailed introduction

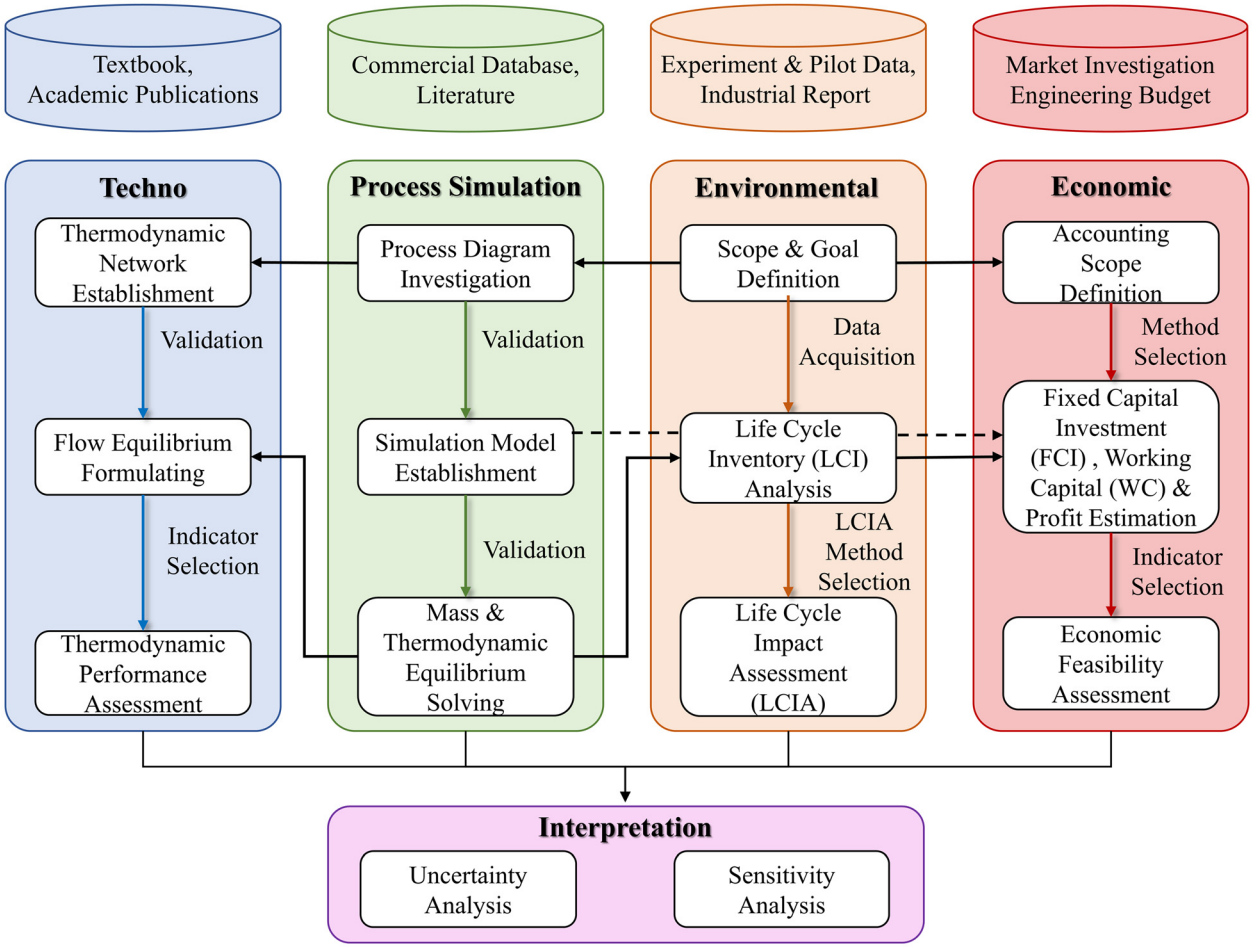

Fig. 3 Basic flowsheet of the ex ante techno-environmental-economic assessment based on process simulation.

on the mechanistic models and network models can be obtained by referring to Vikram *et al.*[40] and Hameed, *et al.*[41]

2.1 Kinetic model

The kinetic model is often integrated with other models to precisely predict the non-equilibrium product distribution, gas composition and temperature profiles within a finite time or volume at various levels of simulation. The participation of the kinetic model in modelling can be summarized as follows.

At the molecular level, employing the force field method (or molecular mechanics) and electronic structure calculation (or first-principles or *ab initio* method), the mechanistic model establishes the detailed reaction mechanism, which includes the potential reaction paths and the intermediate and final products.[40] However, the pyrolysis of the organic content in waste or biomass involves millions of interconnected reactions, including the decomposition of the feedstock and secondary reactions among intermediate products. Furthermore, in the case of the classical organic contents in waste or biomass, the understanding of their pyrolysis molecular mechanism is still limited. Thus, it is impossible to provide precise descriptions of every reaction with sufficient experimental data as validation, and a detailed and complicated reaction mechanism may cause extensive calculation cost. Accordingly, to simplify the calculation process with acceptable accuracy, the focus of future research is the establishment of an universally applicable kinetic model, which aggregates multiple reactions, sets up a concise mechanism of representative elementary reactions, and clarifies the expression of the reaction rate equations of each elementary reaction with limited experimental data.[48] Fig. 5(a) shows the different reaction schemes in the kinetic model, which include one-step, parallel, independent, competitive, interaction, and detailed lumped schemes.

At the particle level, the network model (mainly includes Bio-FG-DVC, Bio-FLASHCHAIN, and Bio-CPD models) and the heat and mass transport model are usually applied to study thermochemical processes.[41] The kinetic model can serve as the source item of heat and mass transport equations to simulate the occurrence of the interface heterogeneous reactions, and consequently the yield and composition of the product can be predicted.[52]

At the reactor level, the kinetic model is further integrated with the hydrodynamics and geometry of the reactors to

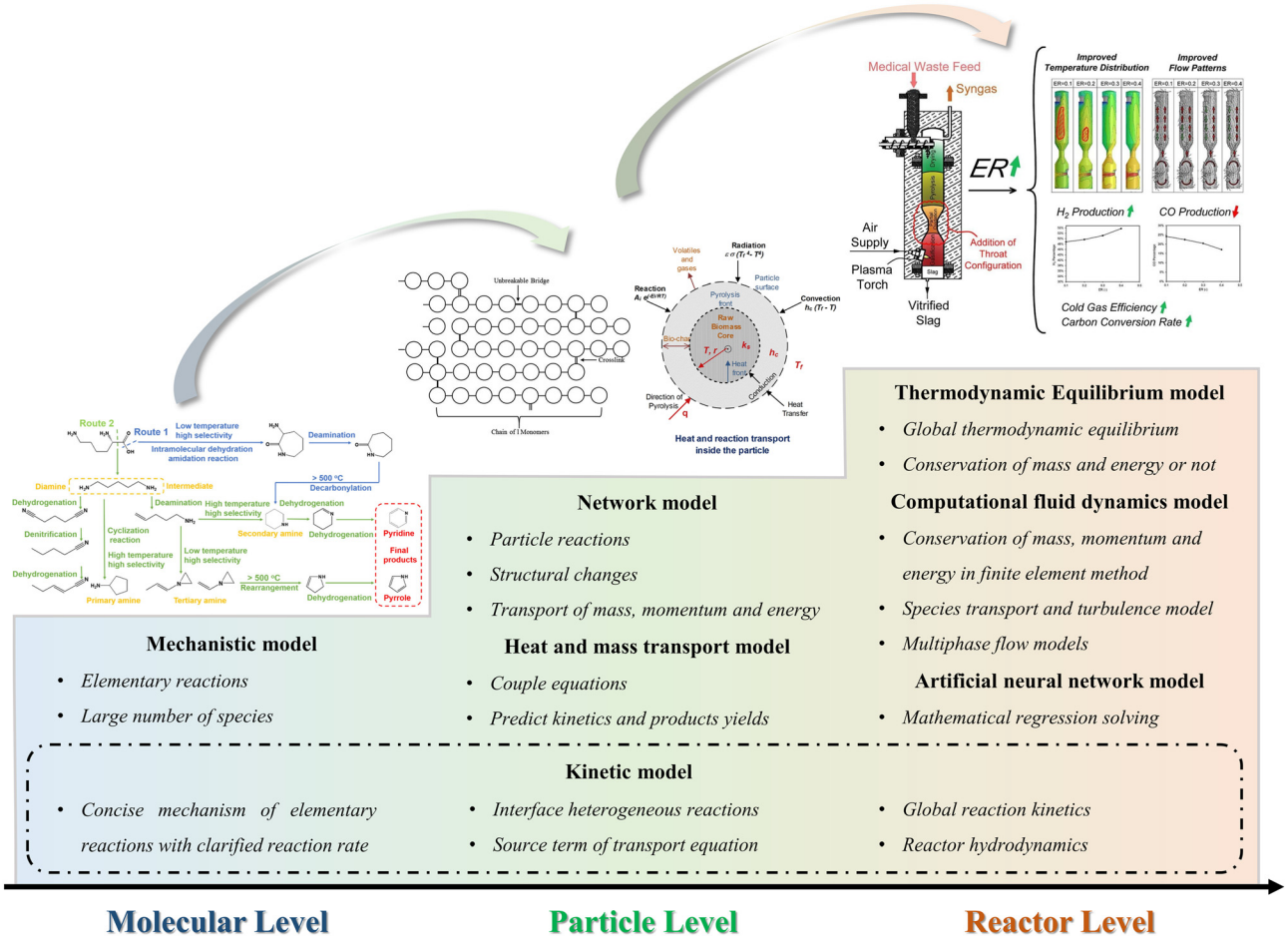

Fig. 4 Approaches for the modelling of the thermochemical W/BtE process at various levels[40–44] (reprinted with the permission.[45] Copyright 2022, the American Chemical Society; reprinted with permission.[41,46,47] Copyright 2019, 2020, and 2023, Elsevier Ltd).

provide results ranging from zero-dimensional (stirred tank) to one- (plug flow), two-, and three-dimensional. When the finite element or volume method is introduced to solve the set of multiphase flow equations, hydrodynamics, heat and mass transport, and the reaction mechanism problems, the model is developed into the computational fluid dynamics (CFD) model. The integration of multi-step reaction mechanisms and coupling cross-scale modelling provides broader possibilities in the directed conversion of products, reaction condition optimization and ex ante reactor design.

Over the decades, thermogravimetry analysis under different operating conditions has provided sufficient data to build a mathematical model of the solid fuel thermochemical process, and the description of the model is listed in Table 1. The goal of model establishment is to give the analytical, numerical, or approximate solution of the "kinetic triplet", which refers to the activation energy (E), pre-exponential factor (A), and mathematical translation of the reaction progression mechanism ($f(\alpha)$).[9] The solution for $f(\alpha)$ and $g(\alpha)$ in the common kinetic models can be obtained from the study by Mostafa, *et al.*[53] In the case of common homogeneous and heterogeneous reactions (as shown in Fig. 5(a)), the kinetic model varied in previous studies due to the difference in feedstock characteristics, reactor design, type of W/BtE technology, catalyst selection, *etc.*[43,44,47,54–56] The reaction rate of common homogeneous and heterogeneous reactions can be shown by different mechanisms, such as the Arrhenius, Langmuir–Rideal, Langmuir–Hinshelwood, Langmuir–Hinshelwood–Hougen–Watson, and Eley–Rideal mechanisms. The applicable model can be obtained and modified by experimental data fitting or referring to the model under similar operation conditions.

2.2 Thermodynamic equilibrium model

The thermodynamic equilibrium (TE) model includes two subcategories, *i.e.*, the stochiometric method and non-stochiometric method, which can be employed to calculate the production yield and composition at the equilibrium state of an entire zero-dimensional reactor. The detailed mathematical models are listed in Table 1. Based on the acquisition of thermochemical properties of the considered species (such as standard molar enthalpy of formation, standard entropy, and heat capacity), the key to the stochiometric method and non-stochiometric method is the calculation of the equilibrium con-

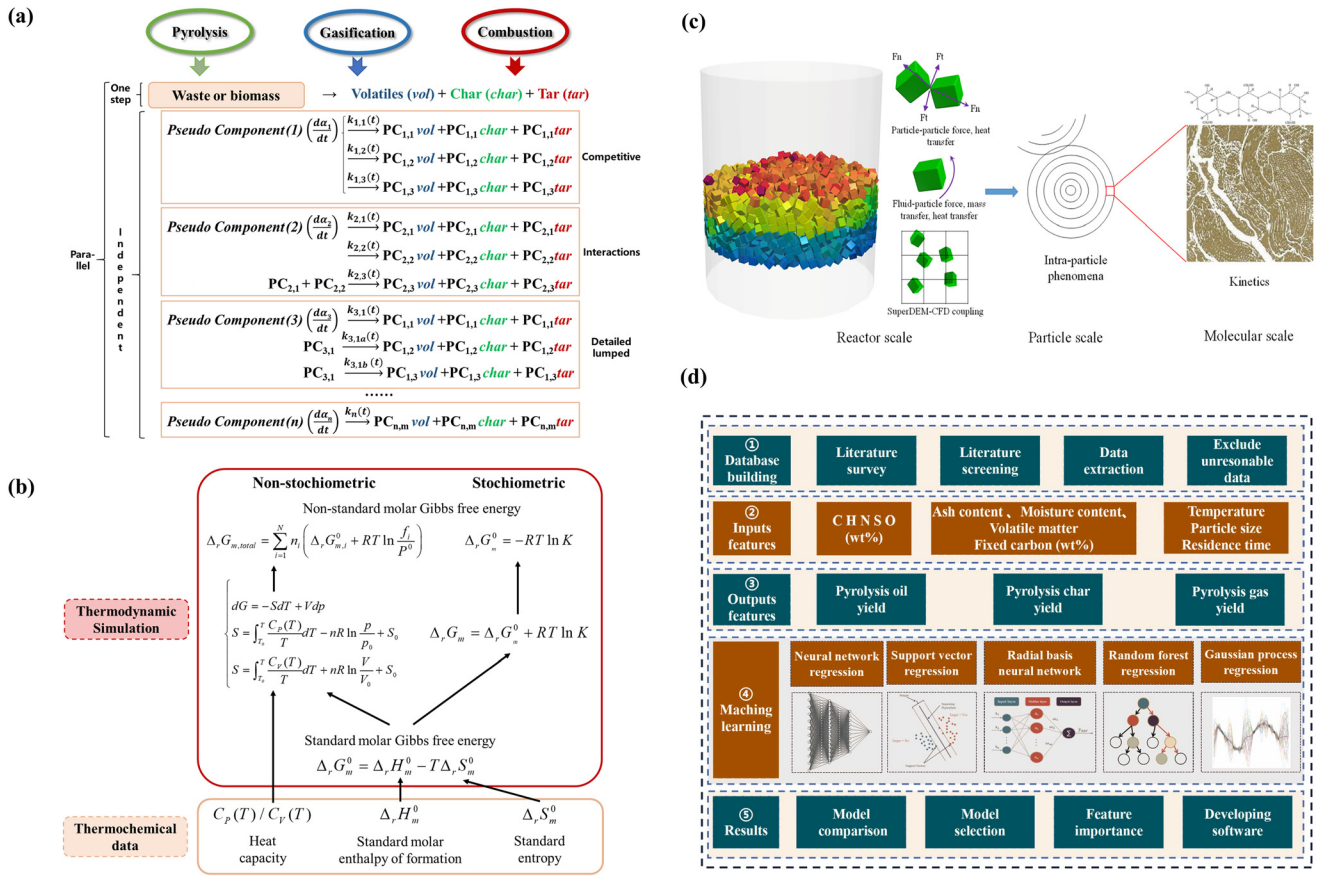

Fig. 5 Schematic examples of different simulation models. (a) Kinetic model;[41] (b) TE model;[49] and (c) CFD model. Reprinted with permission.[50] Copyright 2021, AIChE. (d) ML model. Reprinted with permission.[51] Copyright 2023, Elsevier, Ltd.

stants of reactions and the minimization of the Gibbs free energy, respectively (see Fig. 5(b)).

In the case of the stochiometric method, all the relevant species and reactions are considered in the simulation.[43] Due the numerous potential uncharacterized species and reactions during the thermochemical conversion of waste or biomass, the applied reaction mechanism needs to be simplified after rigorous consideration.[42] Thus, the first step of the stochiometric method is to clarify the chemical coefficients in the selected dominant reactions. Then, in the second step, the equilibrium constants of these reactions are calculated at the given state (the coefficients for functions of equilibrium constants of common gaseous reactions as a function of temperature are presented in Table S1†). Eventually, the overall product yield and composition can be calculated with chemical and energy equilibrium under the given feedstocks and operation parameters.

In the case of the non-stochiometric method, specific reactions do not need to be considered, only requiring the selection of the potential product species under effective feed-in (the actual feed after excluding the component of ash and unreacted char).[57] Furthermore, after computing the minimum Gibbs energy distribution, the product yield and composition under given circumstances can be obtained. It is worth noting that the non-stochiometric method is more convenient than the stochiometric method. Consequently, the stochiometric method is less preferable when handling complex processes compared with the non-stochiometric method.[57]

The fundamental of the TE model is the thermochemical data. Modification the thermodynamic equilibrium model has been conducted with the accumulation of experimental results and the improvement of measurement equipment. Firstly, in terms of the model structure, researchers discovered that a multi-stage equilibrium model is more accurate when considering realistic conditions, given that the integrated model provides the chance to exclude certain reactions from full equilibrium.[57] Secondly, when handling the complicated generation of char and tar, researchers constrain the composition and yield of char and tar by using a group of empirical functions related to the operation parameters.[58,59] Furthermore, correction factors or functions are used to adjust the equilibrium constant in the stochiometric method,[60,61] while the chemical equilibrium is constrained by the heat capacity and the temperature difference in the non-stochiometric method.[62,63] However, although the accuracy of the TE model has been fully developed, it still has certain deviation between the predicted results and experiment data. Zhang *et al.*[49] pointed out that the main challenges in the application of the TE model are the

Table 1 Mathematical description of kinetic and thermodynamic equilibrium models[41–43]

	Equilibrium model	
Kinetic model	Stochiometric approach	Non-stochiometric approach
1. The conversion rate α definition: $\alpha = (w_{start} - w_t)/(w_{start} - w_{end})$, where w_{start}, w_{end} and w_t are the weight of the sample at the start, end, and time t or temperature T, respectively	1. The global reaction of a basic thermochemical process is as follows: $CH_aO_bN_cS_dCl_e + wH_2O + rO_2 + r\theta N_2 \xrightarrow{\text{pyro/gasi}} n_1H_2 + n_2H_2O + n_3CO + n_4CO_2 + n_5CH_4 + n_6N_2 + n_7NH_3 + n_8H_2S + n_9HCl + n_{10}C(\text{char}) + n_{11}CH_pO_q(\text{tar}) \xrightarrow{\text{combust}} n_{12}H_2O + n_{13}CO + n_{14}CO_2 + n_{15}CH_4 + n_{16}N_2 + n_{17}NO_2 + n_{18}SO_2 + n_{19}HCl + n_{20}C(\text{char})$	1. Calculation of global Gibbs free energy ($\Delta_rG_{m,total}$) with selected species at the given state: $\Delta_rG_{m,total} = \sum_{i=1}^{N} n_i\left(\Delta_rG^0_{m,i} + RT\ln\frac{f_i}{P^0}\right)$ $f_i = \frac{n_i}{n_{total}}\varphi P$, where n_i is the molar content of species i; $\Delta_rG^0_{m,i}$ is the standard Gibbs free energy of species i at the standard state; f_i is the fugacity of species i; φ is the fugacity coefficient; P and P^0 are the pressure in the given and standard state, respectively
2. The conversion process of waste or biomass: $\frac{d\alpha}{dt} = kf(\alpha)$ $k = A\exp\left(-\frac{E}{RT}\right)$	2. The element balance: $A_j = \sum_{i=1}^{N} a_{i,j}n_i, \quad j = 1, 2, 3, 4, \ldots, k$, where A_j is total atomic mass of the j^{th} element; $a_{i,j}$ is atom of j^{th} element present in each molecule of the species	2. The element balance (same as the stochiometric method): $A_j = \sum_{i=1}^{N} a_{i,j}n_i, j = 1, 2, 3, 4, \ldots, k$
	3. Calculation of the equilibrium constants of the selected reactions (*e.g.*), as follows: $K = \prod_i (x_i)^{y_i}\left(\frac{P}{P_0}\right)^{\sum_i y_i}$	3. The LaGrange multiplier method is used to minimize G_{total}, for ideal gas: $\frac{\partial L}{\partial n_i} = \frac{\Delta_rG^0_{m,i}}{RT} + \sum_{i=1}^{N}\ln\left(\frac{n_i}{n_{total}}\right) + \frac{1}{RT}\sum_{j=1}^{k}\lambda_i\left(\sum_{i=1}^{N} a_{i,j}n_i\right) = 0,$ where L is the Lagrange function; λ_i is the LaGrange multiplier; the total atomic mass of the j^{th} element; and $a_{i,j}$ is atom of j^{th} element present in each molecule of the species
$\beta = \frac{dT}{dt}$ $\frac{d\alpha}{dT} = \frac{A}{\beta}\exp\left(-\frac{E}{RT}\right)f(\alpha)$ $g(\alpha) = \int_0^\alpha \frac{d\alpha}{f(\alpha)} = \int_0^T \frac{A}{\beta}\exp\left(-\frac{E}{RT}\right)dT \approx \frac{AE}{\beta R}P(u)$	$\Delta G^0_T = -RT\ln K$ $\Delta G^0_T = \sum_i \nu_i \Delta g^0_{f,T,i}$ $\Delta g^0_{f,T,i} = h^0_f - a'T\ln T - b'T^2 - \left(\frac{c'}{2}\right)T^3 - \left(\frac{d'}{3}\right)T^4 + \frac{e'}{2T} + f' + g'T$, where K is the equilibrium constant; x_i is molar fraction of species i; ν_i is the stochiometric coefficient of species i; P and P^0 are the pressure in the given and standard state, respectively; ΔG^0_T is the standard Gibbs function of reaction; $\Delta g^0_{f,T,i}$ is the formation standard Gibbs function at temperature T of species i; and h^0_f and a'–g' are empirical coefficients	
$P(u) = \int_0^u \frac{\exp(-u)}{u^2}$, where k is the reaction rate, min^{-1}; A is the pre-exponential factor, min^{-1}; E is the activation energy, kJ mol^{-1}; R is the gas constant, which equals 8.314 J mol^{-1} K^{-1}; β is the heating rate, K min^{-1}; $f(\alpha)$ is the reaction model; $g(\alpha)$ is the integrated form of $f(\alpha)$; and $P(u)$ is the temperature integral, $u = E/RT$	4. Calculation of energy balance: $\sum_{\text{reactant}} n_i(h^0_{f,i} + \Delta h^T_{298\,K}) = \sum_{\text{product}} n_i(h^0_{f,i} + \Delta h^T_{298\,K})$, $\Delta h^T_{298\,K} = \int_{298\,K}^{T} C_p(T)dt$, where Δh^T_{298K} is the enthalpy difference between the given state and the standard state and $C_p(T)$ is the heat capacity at constant pressure	

improvement of the accuracy in the thermochemical data prediction of complex waste and biomass feedstocks and the combination of kinetic and TE models to reduce the deviation caused by simplified assumptions of microscopic information and insufficient reaction time.

2.3 Computational fluid dynamic (CFD) model

The CFD model provides a vital option for researchers to obtain the detailed distribution of the target parameters (such as velocity, temperature, pressure, and substance concentration) and geometry of tracer particle trajectories inside the reactor. The application of the CFD model is essentially the process of solving the discrete governing function group with specific initial and boundary conditions inside the computational domain. Its general step can be summarized as follows:[64] 1. establishment of the governing equations; 2. clarification of the initial and boundary conditions; 3. discretization of the computational domain (also called grid generation); 4. CFD solver setting; 5. satisfaction of grid independence test and model validation (if the results are out of the acceptable error range, the simulation will restart at step 1); and 6. interpretation.

The conservation equations in the aspects of mass, momentum, and energy build the foundation of the governing equations group. In the typical thermochemical process, the phenomena of turbulence, heat transfer, chemical reaction, interphase interaction, and multi-phase flow need extra governing equations for their expression.[44,54,64] In the case of turbulence, various forms of the RANS (Reynolds averaged Navier–Stokes) method-based k–ε model have been considered as mature and cost-effective choices.[44] The convection heat transfer process is expressed in Newton's law of cooling with different experiment-fitted equations for the Nusselt number, and the homogeneous radiation heat transfer process can mainly apply the discrete ordinates (DO) and P1 model.[65] The species transport model is universal for chemical-involved processes, and validated kinetic models of homogeneous and heterogeneous reactions can be introduced with various turbulence-chemical interaction methods. The descriptive equations of forces exerted on a particle (including gravitational force, particle–particle/particle–wall contact force, drag force, pressure gradient force, and cohesive force) are vital in the calculation of interphase interaction.[66] The multi-flow model has been developed comprehensively, and recently the distinguished performance of the CFD-DEM (discrete element method)/SuperDEM (superquadric discrete element method) models has proven their significant potential[50,66,67] in the further development of particle models of thermochemical and hydrodynamic behavior.[66,68–70]

2.4 Machine learning model

The machine learning (ML) model is a data-driven model, which involves adjusting the node parameters inside the algorithm network to correlate the input and output. Unlike the kinetic, thermodynamic equilibrium and CFD models, the establishment of an ML model is a purely mathematical process without the expression of physical and chemical mechanisms. Thus, ML cannot provide analytical results and understanding of the reaction mechanism.

Database establishment is the foundation of ML models. In the case of the thermochemical W/BtE process, the feedstock characteristics, operational parameters, and reaction patterns are commonly selected as the input data, and the yield and composition of the products are the expected output.[51] After data acquisition and processing, the collection of sufficient, correct, and validated data is split into the training set (about 80%) and the test set (about 20%).[71] Hyperparameter optimization and cross-validation are conducted based on the principle of various ML algorithms to acquire the trained model with the expected performance.[10] ML models can be classified into supervised learning, unsupervised learning, and reinforcement learning models based on their learning behavior. Supervised learning models have been reported to be the most widely used given that they predict the output variables based on the input variables.[72,73] The common categories of supervised learning models include artificial neutral network (ANN), gradient boosting (GB), support vector machine (SVM), decision tree (DT) and Gaussian process (GP).[71]

2.5 Model comparison and mainstream software application

Each simulation model has advantages and disadvantages based on its methodical mechanism and calculation cost. The kinetic model simulates the overall reaction rate with parameters from experimental data, and as the product is accumulated with time, this model can accurately give non-equilibrium predictions with finite time and volume, making it very suitable for reactions occurring at a low temperature and in a fluidized reactor.[42] The kinetic model can provide analytical results, but has limited application due to its difficult parameter acquisition and high calculation cost when coupled with hydrodynamics.[43] Also, the kinetic model shows weakness in the simultaneous prediction of gas–solid reaction.[57]

The CFD model is an improved calculation of the kinetic model, and due to its integration of rigorous governing equation groups and the reactor geometry, this model can provide detailed results inside the reactor in both the steady and non-steady states. Thus, the CFD model gives reliable and practical reference in reactor design and operation optimization, especially in the case of fluidized reactors.[65] However, the CFD model requires considerable computing power and potential software expenses, and the validity of the results significantly depends on the selection of physical and chemical models.[64]

The TE model is known for its rapid response capability, convenient model establishment without considering the reactor geometry, and low computing cost.[49] This model can provide the maximum product yield in the equilibrium state with simple modifications and has high accuracy at high reaction temperatures.[57] However, the main limitation of the thermodynamic equilibrium model is its deviation between the assumption of global equilibrium and infinite reaction

time or volume with the realistic situation, and the lack of geographical distribution of zero-dimensional results.[74]

The ML model has good applicability under equilibrium and non-equilibrium conditions, and it can handle data with a complex non-linear relationship.[51] However, despite its outstanding accuracy, the ML model lacks knowledge on the reaction mechanism, and it has high requirements of quantity and quality of the training data.[73] Also, the ML model does not perform well with input under diverse backgrounds.[75]

The application of software has witnessed great progress with the development of simulation models. The mainstream CFD software includes ANSYS Fluent, COMSOL Multiphysics, OpenFOAM, ANSYS CFX, Star CCM, and PHOENICS.[64,75] The application of these software greatly improves the intuitive understanding of the thermochemical process inside the furnace based on the visualization of the results, but CFD simulation mainly focuses on the reactor furnace due to the limited computing power. Given that the W/BtE process can extend to the further utilization of the products of thermochemical process, process simulation software, such as Aspen Plus, Aspen HYSYS, Engineering Equation Solver, UniSim Design, gPROMS, CHEMCAD, and GAMS, has been widely used to assess the performance of the whole W/BtE system.[75–77] Among these categories of software, the advantages of Aspen Plus and Aspen HYSYS have been recognized by researchers, given that they both have an extensive database, ripe computational models, and convenient prepackaged modules.[9,78,79] However, the source code of their simulation package is not available, and their cost is also considerable.[80] MATLAB provides an open-source platform for researchers to customize individual simulation functions. Technically, the four above-mentioned models can all be established in MATLAB by self-programming or invoking modules from open source code hosting platforms, such as GitHub. Similar software or programming platforms such as Scilab, PyCharm, Jupyter Notebook can also play the same role, but certain programming skills are required for their operation, especially when dealing with unestablished modules.[80]

3 Techno-environmental-economic assessment methods

The common techno-environmental-economic assessment methods mainly include the 7Es, *i.e.*, energy, exergy, advanced exergy, environmental, economic, exergoenvironmental, and exergoeconomic analysis. Their relationship is both deepening and interdisciplinary, as shown in Fig. 6.

3.1 Techno assessment method

3.1.1 Energy analysis. The components of the total energy are shown in eqn (1).[81] In chemical or thermal systems, the kinetic energy and potential energy can be neglected, and eqn (1) is reduced to eqn (2), which is expressed as follows:[82]

$$\mathrm{En} = \mathrm{En_{ph}} + \mathrm{En_{ch}} + \mathrm{En_{kl}} + \mathrm{En_{po}} \quad (1)$$

$$\mathrm{En} = \mathrm{En_{ph}} + \mathrm{En_{ch}} \quad (2)$$

where En is the total energy, kJ; $\mathrm{En_{ph}}$ is the physical energy, kJ; $\mathrm{En_{ch}}$ is the chemical energy, kJ; $\mathrm{En_{ki}}$ is the kinetic energy, kJ; and $\mathrm{En_{po}}$ is the potential energy, kJ. Generally, for biomass and waste:[83]

$$\dot{\mathrm{En}}_{\mathrm{biomass/waste}} = \dot{m}_{\mathrm{biomass/waste}} \mathrm{HHV}_{\mathrm{biomass/waste}} \quad (3)$$

where $\dot{\mathrm{En}}_{\mathrm{biomass/waste}}$ is the energy flow rate of the biomass or waste, kW; $\dot{m}_{\mathrm{biomass/waste}}$ is the mass flow rate of the biomass or waste, kg s^{-1}; and HHV is the higher heat value, kJ kg^{-1}. Similarly, the $\dot{\mathrm{En}}$ of char and tar can also be calculated using the same method.[84] In the case of a gas mixture:[81]

$$\dot{\mathrm{En}}_{\mathrm{gas}} = \sum \dot{m}_{\mathrm{gas},i}(h_{\mathrm{gas},i} + \mathrm{HHV}_{\mathrm{gas},i}) \quad (4)$$

where $\dot{\mathrm{En}}_{\mathrm{gas}}$ is the energy flow rate of the biomass or waste, kW; $\dot{m}_{\mathrm{gas},i}$ is the mass flow rate of component i in the gas mixture, kg s^{-1}; $h_{\mathrm{gas},i}$ is the enthalpy of component i in the gas mixture, kJ kg^{-1}; and $\mathrm{HHV}_{\mathrm{gas},i}$ is the HHV component i in the mixture gas kJ kg^{-1}. The entropy of a single component can be calculated as follows:[81]

$$h_{\mathrm{gas}} = h_{\mathrm{gas},0} + \int_{T_0}^{T} c_{\mathrm{p}} \mathrm{d}T \quad (5)$$

$$c_{\mathrm{p}} = a' + b'T + c'T^2 + d'T^3 \quad (6)$$

where h_{gas} and $h_{\mathrm{gas},0}$ represent the specific enthalpy of component i at the specified temperature T and T_0, kJ kg^{-1} and c_{p} is the constant pressure specific heat capacity, K $(\mathrm{kg\ kJ})^{-1}$. Eqn (6) shows its empirical equation.

In the case of a unit or system, the energy efficiency η_{en} (%) is defined as the ratio of the useful energy outputs to the energy inputs. The exergy efficiency η_{en} (%) of the system is calculated as follows:

$$\eta_{\mathrm{en}} = \frac{\sum \dot{\mathrm{En}}_{\mathrm{out}}}{\sum \dot{\mathrm{En}}_{\mathrm{in}}} \quad (7)$$

where $\sum \dot{\mathrm{En}}_{\mathrm{out}}$ and $\sum \dot{\mathrm{En}}_{\mathrm{in}}$ denote the sum of the energy flow rate of the useful products and all input streams, respectively, kW.

Energy analysis is based on the first law of thermodynamics. By analyzing the energy flow, the energy saving potential can be discovered, the key for process optimization can be verified, and the basis for energy cost estimation can be founded. However, energy analysis has certain limitations, considering that it focuses on the total amount of energy, not the availability of energy in the given external environment. Thus, the concept of exergy is defined for a deeper and more comprehensive analysis of energy availability.

3.1.2 Exergy analysis. Considering the comparison between the state of the studied system and the external environment, the amount of energy can be divided in to exergy and anergy, as expressed in eqn (8):

$$\mathrm{En} = \mathrm{Ex} + \mathrm{An} \quad (8)$$

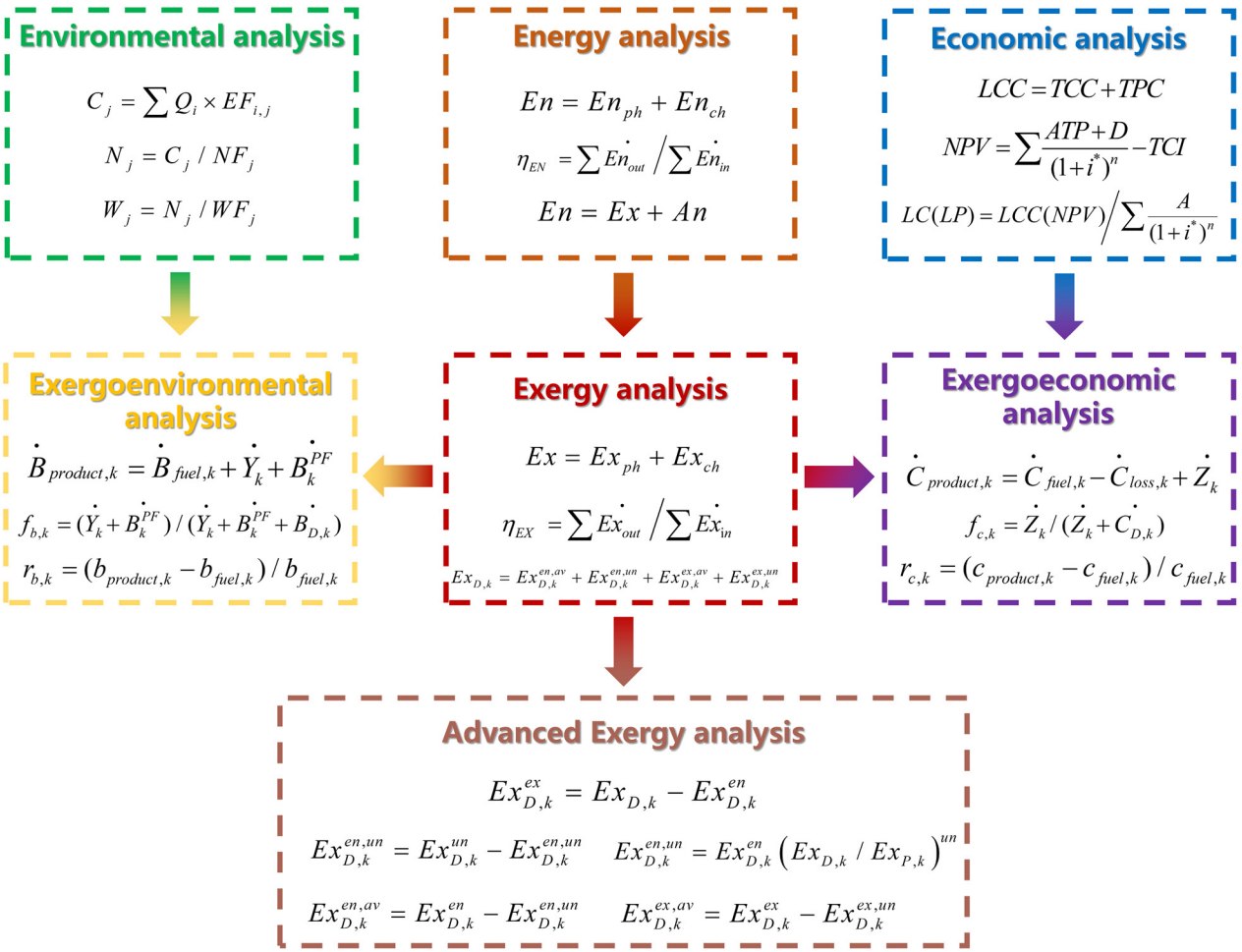

Fig. 6 Relationship among common techno-environmental-economic assessment methods.

where Ex and An is exergy and anergy in the state of the given external environment, respectively, in units of kJ. When a system is considered in thermal and chemical equilibrium with its surroundings, exergy is the part of energy that can be converted into other forms of energy without limits and anergy is the part of energy that can be not utilized without further operation.

Similar to the explanation in the energy analysis, the exergy in the study involves exergy Ex^{ph} and chemical exergy Ex^{ch}, given that the kinetic exergy and potential exergy can be neglected. The physical exergy per unit can be expressed as follows:[85]

$$Ex^{ph} = (H - H_0) - T_0(S - S_0) \quad (9)$$

where T_0 is 298.15 K; H_0 and S_0 are the basic enthalpy (kJ kg^{-1}) and entropy (J (mol K)$^{-1}$) at the environmental state (298.15 K and 0.1013 MPa) and H and S denote the enthalpy (kJ kg^{-1}) and entropy (J (mol K)$^{-1}$) at a given state, respectively. The chemical exergy Ex^{ch} per unit mass is defined as follows:[86]

$$Ex^{ch} = \sum x_i e_{x_i}^{ch} \quad (10)$$

In the case of a gas mixture, the chemical exergy per unit mass is as follows:[87]

$$Ex^{ch} = RT_0 \sum x_i \ln x_i + \sum x_i e_{x_i}^{ch} \quad (11)$$

where R denotes the gas constant with a value of 8.3145 kJ (kmol K)$^{-1}$ and x_i and $e_{x_i}^{ch}$ refer to the molar fraction (%) and standard chemical exergy (kJ kg^{-1}) of component i, respectively. The standard chemical exergy of component i can be obtained from the study by Morris and Szargut.[88] The exergy of MSW or biomass per unit mass can be can be obtained in the reports by Silva *et al.*[42] and Shahbeig *et al.*[89]

In the case of a unit or system, the exergy efficiency η_{ex} (%) is defined as the ratio of the useful exergy outputs to the exergy inputs. The exergy efficiency η_{ex} of the system is calculated as follows:

$$\eta_{ex} = \frac{\sum \dot{Ex}_{out}}{\sum \dot{Ex}_{in}} \quad (12)$$

where $\sum \dot{E}x_{out}$ and $\sum \dot{E}x_{in}$ denote the sum of the exergy flow rates of the useful products and all input streams, respectively.

Exergy analysis can accurately reveal the utilization of the available part of the total energy by excluding the distraction of the anergy. In this way, sections destructing more exergy can be considered more significant than those mainly destructing anergy or low-grade exergy (such as the condenser in the Rankine cycle). However, not all exergy constructions can be recovered through technological improvement.[90] To clarify the reasons for the exergy destruction more comprehensively from the perspectives of avoidability and the forcing source, the advanced exergy analysis method has been proposed.

3.1.3 Advanced exergy analysis. The level and source of irreversibility can be identified by conducting advanced exergy analyses.[91] Exergy destruction can be divided into endogenous and exogenous based on the aspects of the forcing sources and unavoidable and avoidable parts based on the aspects of avoidability.[92] Regarding the exergy destruction for component k in the system, endogenous and exogenous exergy destruction refer to the part of destruction due to the internal irreversibility of component k in the system and the external irreversibility from other components influencing component k in the system, respectively. Then, avoidable exergy destruction is destined to occur regardless of the technological improvement and the design optimization, and the unavoidable exergy destruction can be reduced through the above-mentioned measures. The relationship between various types of exergy destruction is shown in eqn (13)–(17), as follows:[90]

$$Ex_{D,k} = Ex_{D,k}^{en,av} + Ex_{D,k}^{en,un} + Ex_{D,k}^{ex,av} + Ex_{D,k}^{ex,un} \quad (13)$$

$$Ex_{D,k}^{en} = Ex_{D,k}^{en,av} + Ex_{D,k}^{en,un} \quad (14)$$

$$Ex_{D,k}^{ex} = Ex_{D,k}^{ex,av} + Ex_{D,k}^{ex,un} \quad (15)$$

$$Ex_{D,k}^{av} = Ex_{D,k}^{en,av} + Ex_{D,k}^{ex,av} \quad (16)$$

$$Ex_{D,k}^{un} = Ex_{D,k}^{en,un} + Ex_{D,k}^{ex,un} \quad (17)$$

where $Ex_{D,k}$ is the exergy destruction of component k in the system, kJ; and the superscripts en, ex, av and un represent endogenous, exogenous, avoidable, and unavoidable parts of the exergy destruction, respectively.

The endogenous exergy destruction can be obtained when the studied component is under real operational conditions, while the other components operate without irreversibility theoretically. Kelly *et al.*[93] described the methods to split the endogenous and exogenous exergy destruction, which are thermodynamic-cycle-based approach and engineering approach, respectively. Given that the thermodynamic-cycle-based approach is not applicable when the ideal theoretical cycle of the system cannot be established (such as combustion), most studies apply the engineering approach. Briefly, for an ideal system, if irreversibility is only introduced in component k, the exergy balance can be expressed as follows:[94]

$$\dot{E}x_{fuel,total} - \dot{E}x_{loss,total} - \dot{E}x_{product,total} = \dot{E}x_{D,k} + \dot{E}x_{D,others} \quad (18)$$

where $\dot{E}x_{fuel,total}$, $\dot{E}x_{loss,total}$, and $\dot{E}x_{product,total}$ are the total systematic exergy flow rate of fuel, loss, and product, kW, and $\dot{E}x_{D,k}$ and $\dot{E}x_{D,others}$ are the exergy destruction flow rate of component k in the system and other components, kW, respectively. When $\lim \dot{E}x_{D,others} \to 0$, $\lim \dot{E}x_{fuel,total} - \dot{E}x_{loss,total} - \dot{E}x_{product,total} \to \dot{E}x_{D,k}^{en}$.

$\dot{E}x_{D,k}^{un}$ of each component is separately calculated from the system under the assumed operational conditions with minimum exergy destruction.[95]

After obtaining the value of $\dot{E}x_{D,k}^{en}$ and $\dot{E}x_{D,k}^{un}$, the calculation can be completed, as shown by eqn (19)–eqn (23), as follows:[96]

$$Ex_{D,k}^{ex} = Ex_{D,k} - Ex_{D,k}^{en} \quad (19)$$

$$Ex_{D,k}^{ex,un} = Ex_{D,k}^{en}(Ex_{D,k}/Ex_{P,k})^{un} \quad (20)$$

$$Ex_{D,k}^{en,un} = Ex_{D,k}^{un} - Ex_{D,k}^{en,un} \quad (21)$$

$$Ex_{D,k}^{en,av} = Ex_{D,k}^{en} - Ex_{D,k}^{en,un} \quad (22)$$

$$Ex_{D,k}^{ex,av} = Ex_{D,k}^{ex} - Ex_{D,k}^{ex,un} \quad (23)$$

The energy, exergy, and advanced exergy analyses can all facilitate the understanding of the principle of energy conversion inside the system. However, when discussing the energy, exergy, and advanced exergy performance between different systems, it has been suggested to conduct a comparison of systems with the same products (or shared products in the coproduction). For instance, in the comparison of system A, which generates electricity, and system B, which produces chemicals, given that the boundary often ends up with the production being manufactured but does not include the end-of-life utilization processes, system B producing chemicals would have a better performance. The reason for this is that the energy/exergy destruction during the end-of-life utilization to produce electricity or power is not included in the boundary of the system, but it actually occurs and is considered in the electricity-generating system. Also, the level of irreversibility of different products varies significantly. Thus, it is recommended that the results of the energy, exergy, and advanced exergy analyses be employed as a reference to judge the performance of technological improvement and design optimization of similar systems.

3.2 Environmental analysis method

The methodological framework of life cycle assessment (LCA) includes goal and scope definition, life cycle inventory (LCI) analysis, life cycle impact analysis (LCIA), and interpretation. In the process-simulation-based environmental analysis, the framework is modified to fit the situation in various tiers, as shown in Fig. 7(a).

3.2.1 Goal and scope definition. In this step, the goal of the study should be clarified, mainly deciding the functional unit of the environmental analysis method (per unit mass and volume of the feedstock or product or per unit time period of

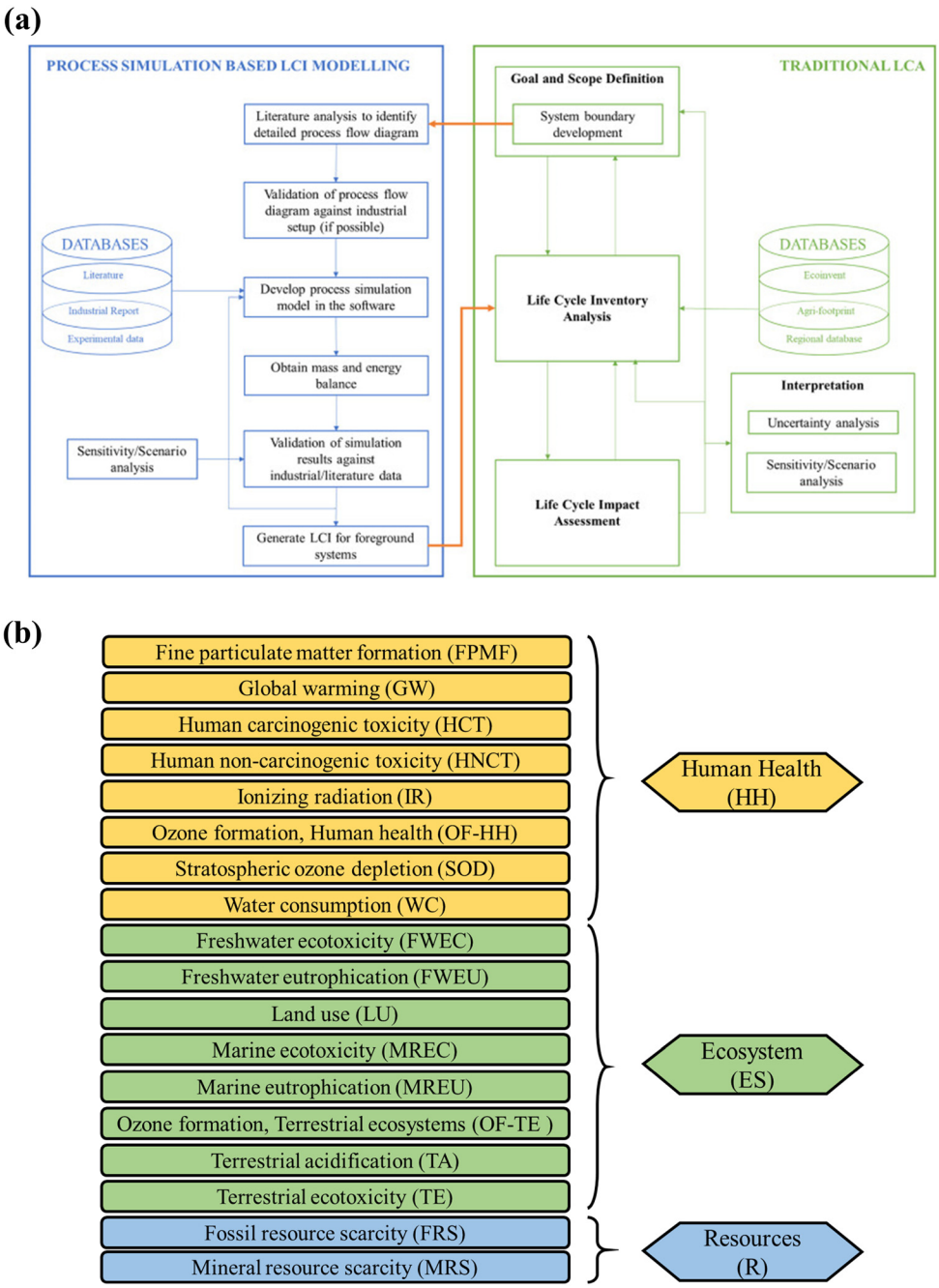

Fig. 7 Process-simulation-based LCA. (a) Generic methodology. Reprinted with permission.[97] Copyright 2024, Elsevier Ltd. (b) Midpoint and end-point indicators (*e.g.*, ReCiPe 2016).

the system operation). The boundary (or tier of the assessment completeness) of the system should be chosen. Also, the process simulation model should be established, developed, and validated in this step. If the environmental analysis has been conducted in tier III (a complete LCA system), the potential data source should be identified.

3.2.2 Life cycle inventory analysis. The data collection of LCI based on the chosen functional unit and system boundary is fundamental in LCA. A complete LCI includes a mass and energy flow of various inputs and outputs. The input flow includes the consumption of feedstock, chemicals, utilities, energy, catalysts, solvents, *etc*. The output flow includes the generation of products, direct emissions, residues, *etc*. In process-simulation-based environmental analysis, the foreground LCI can be directly obtained from the simulation results. When the level of environmental analysis reaches tier II, the indirect impacts of the production or treatment of various inputs and outputs are considered, and the background LCI can be obtained from commercial databases (such as ecoinvent, CLCD, Gabi, and ELCD), the literature, industrial

operation data, published reports, *etc*. If a tier-III analysis is conducted, the LCI of upstream and downstream processes can also be obtained from the above-mentioned sources.

3.2.3 Life cycle impact analysis. Given that various LCIA methods have different purposes and preferences, the selection of LCIA methods directly decides the number of sub-categories and the numerical figure of environmental analysis.[98] Generally, then sub-categories of impact can be divided into midpoint and endpoint categories, and the impacts of several midpoint category finally total the impact on one endpoint category (see Fig. 7(b), taken ReCiPe 2016 LCIA method as an example). The midpoint of global warming potential (GWP) is the indicator with the most attention in recent studies.

The framework of LCIA has 4 steps including classification, characterization, normalization, and weighting. The classification step classifies emissions into various impacts.[99] In the characterization step, for emitted substance i and environmental impact category j, the environmental impact potential of j (EP_j) equals the amount of i (Q_i) multiplied by the equivalency factor ($EF_{i,j}$), as expressed in eqn (24), as follows:

$$EP_j = \sum Q_i \times EF_{i,j} \quad (24)$$

The normalization step combines the characterized environmental impacts in different units, and consequently the magnitude of these impacts can be comparable with the total effect of the given ref. 100. The calculation of normalization step is as follows:

$$N_j = EP_j/NF_j \quad (25)$$

where N_j is the normalized result of category j, pts; and NF_j is the normalization factor, which is related to the referenced year and region.

The weighting step can summarize the characterization results into reduced impact categories or even a single score based on different value choices, but it is not recommended to singly apply weighted results in the comparison due to the potential subjective judgment.[101] The calculation of the normalization step is as follows:

$$W_j = N_j/WF_j \quad (26)$$

where W_j is the weighting result of category j; and WF_j is the weighting factor, which relates to the values choices.

3.2.4 Interpretation. Interpretation is the last step in LCA. It consists of the goal and scope of the study, an interpretation is aimed to recognize significant issues, form conclusions based on the results, and give suggestions for improvement of the W/BtE systems. A sensitivity analysis of operational parameters can provide more in-depth advice. Regarding the uncertainty of the final results due to the measurement methods, the data sources, and the mathematical algorithms, the application of a pedigree matrix and Monte Carlo simulation can give the statistical indicators of the results conveniently.

Environmental analysis conducted at different tiers can focus on the local, regional, and total environmental impact of W/BtE systems. Given that the normalization and weighting factors can significantly differ due to the chosen LCIA methods and values choices, it is suggested to compare the results based on the sane choice of assessment methods. Also, with the inevitable implementation of stricter policies for environmental protection and carbon taxes, the results of environmental analysis can assist W/BtE systems to obtain accurate and comprehensive environmental performances in daily operations and technological improvement.

3.3 Economic analysis method

Economic analysis aims to reveal feasibility of the W/BtE systems within their lifespan. The estimation of cost and profit is the basic aspects of economic analysis.

3.3.1 Cost estimation model. After development over the last few decades, a mature system estimation theory of the life cycle cost (LCC) has been established, which can be divided into fixed capital investment (FCI) and working capital (WC). FCI (also called fixed costs) is the total cost of designing, construing, installing of equipment and auxiliary facilities, and the preparation of the plant site at the beginning of the program.[102,103] WC (also called variable cost) is the cost to maintain the common operation in the aspects of manufacturing, marketing, management and administration.[102,104,105] Although the name of the concepts may differ, their detailed definition remains consistent in various studies (Fig. 8).

3.3.1.1 FCI estimation. FCI consists of direct cost (mainly related to purchase and installation of equipment and auxiliary facilities) and indirect cost (related to financial investment, contingency, engineering and supervision expenses).[102,103] The basis of the FCI estimation is the source of equipment purchase cost (EPC). The potential of purchased equipment cost in order of priority is quoted offer from the vendor, budgeted prices, in-house data from other projects, commercial databases, books, and the Internet.[107] Cost estimation starts with the estimation of the purchased equipment. For design engineers who lack access to reliable cost data or estimating software, the refined exponential estimating method is often used,[102–105] as shown in eqn (27).

$$EI_{estimate} = EI_{ref} \times \left(\frac{Q_{estimate}}{Q_{ref}}\right)^n \times \frac{INDEX_{estimate}}{INDEX_{ref}} \times f_{location} \quad (27)$$

where EI is the equipment investment, M$; Q is the benchmark (usually the size or capacity); INDEX is index, which reflects the fluctuation in the chemical equipment with time, such as Marshall and Swift index (M&S), and chemical engineering plant cost index (CEPCI); and $f_{location}$ is the location factor. The subscripts estimate and ref represent the estimated and referred data, respectively.

Ali *et al.*[39] concluded the capital cost estimation methods and relative accuracy in previous studies. Based on the variation in the chosen method, the capital cost estimation can be conducted at different accuracy. For the convenient and prompt estimation of FCI, the existing studies tend to use the factorial method for cost estimation, such Lang factors, detailed factorial estimates, module costing technique, and

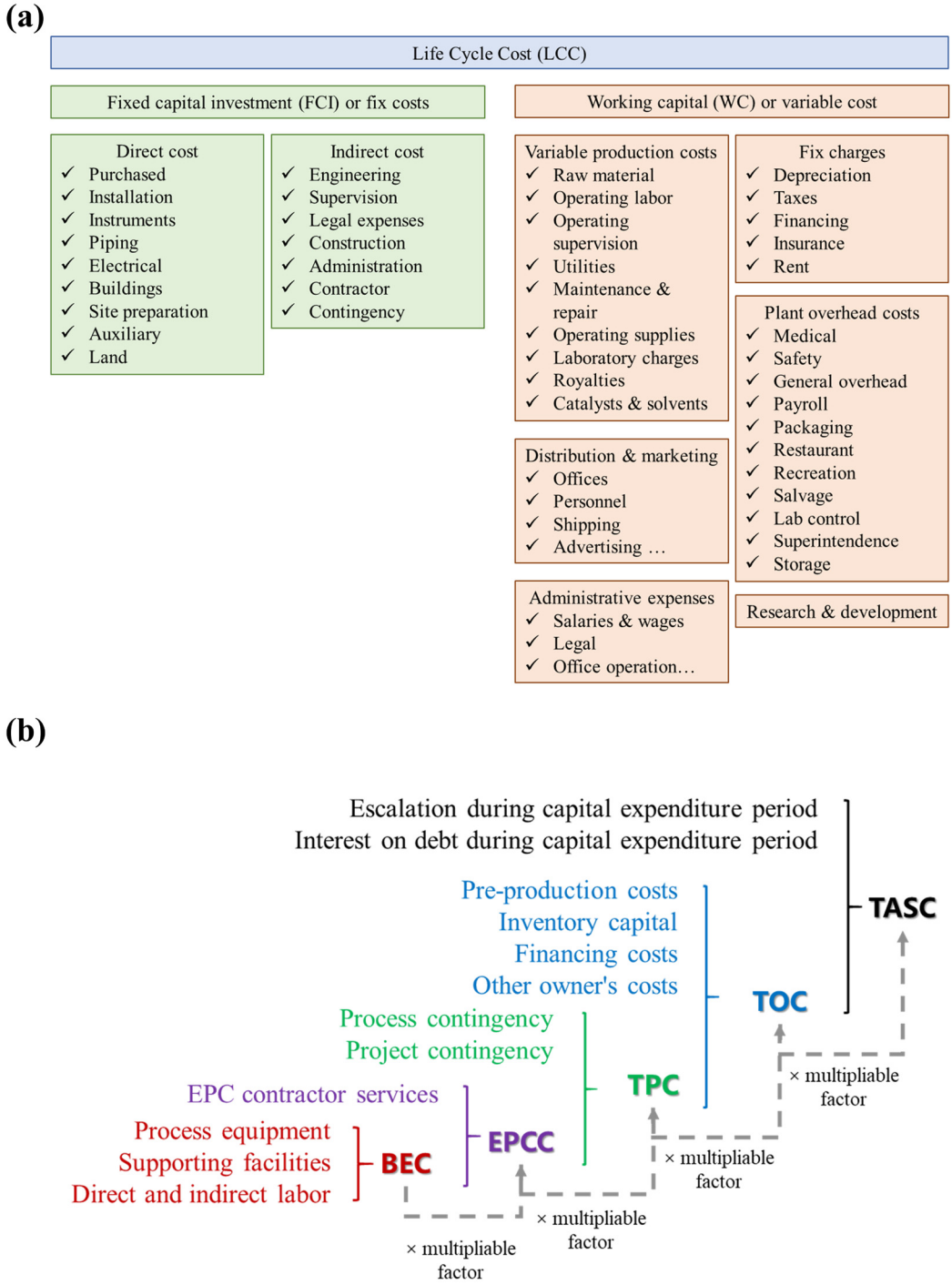

Fig. 8 (a) Components and (b) NETL estimation model of TCI.[103,106]

percentage of delivered-equipment cost method.[108] Lang factors are used to evaluate the FCI based on eqn (28),[102] as follows:

$$C = F\left(\sum C_i\right) \tag{28}$$

where C is the total fixed capital cost, M$; $\sum C_i$ is the total purchased cost of all the major equipment items including reactors, tanks, columns, heat exchangers, furnaces, M$; and F is the Lang factor, which is 3.1, 4.74, and 3.63 for solids, fluids, and mixed fluids-solids processing plant, respectively.[109]

Based on the Lang factors, the detailed factorial estimates method gives factors for each individual equipment,[102] and the calculation of FCI changes as follows:

$$C = \sum F_{e,i} C_{e,i} \tag{29}$$

where $C_{e,i}$ is the purchased cost of equipment item i, M$; and $F_{e,i}$ is the factor for detail equipment, such as Hand factors.[110]

The module costing technique is a more precise method given that it evaluates the detailed factor of each part of the FCI in the cost estimation of each module, which can be described as follows:[105]

$$C = \sum C_{e,i}(1 + \theta_L + \theta_{FIT} + \theta_O\theta_L + \theta_E)(1 + \theta_M)(1 + \theta_{CONT\ \&\ FEE}) \quad (30)$$

where $C_{e,i}$ is the purchased cost of equipment i, M$; θ is the cost factor, and subscripts L, FIT, O, E, M, CONT & FEE represent the aspects of labor, freight, overhead, engineering, material, and contingency and fee, respectively.

The percentage of delivered-equipment cost method can be seen as a simplification and deformation of the module costing technique. It gives the range of the proportion of each component in FCI to the EPC. Based on the given examples of 3 types of facilities, the chosen proportion can be adjusted with the recommended range according to the studied case. Table 2 lists the details of the percentage of delivered-equipment cost method.

Detailed program data provide solid references to adjust the theoretical model. Rubin *et al.* concluded the cost estimation data of reports published by the National Energy Technology Laboratory (NETL), Electric Power Research Institute, International Energy Agency Greenhouse Gas Program, Zero Emissions Platform and Global CCS Institute.[111] However, besides the publications by NETL, which can still be assessable and remains updated,[106,112] the other documents cannot be found in the official channel. Lots of research applied the factorial model modified by data from NETL. The summarized NETL model gives the definition and scope of the bare erected cost (BEC), engineering procurement and construction cost (EPCC), total plant cost (TPC), total overnight cost (TOC) and total as-spent cost (TASC), and multipliable factors are used in the calculation between the above-mentioned definitions.[106] It should be mentioned that the reported multipliable factors differ in the literature published in various years,[113–117] and as the reports by NETL keep updating, the multipliable factors may also be updated by researchers when applying this model.

3.3.1.2 WC estimation. WC estimation is an essential part in evaluating the cash flow of a program. In the reports by Turton *et al.*[102] and Peters *et al.*,[103] a similar estimation model was established, and the reported NETL model is very neat. A comparison of these three models is listed in Table 3. Compared with the other two models, obviously the NETL model has more simplified assumptions, posing the risk of underestimating the WC. Carbon tax is a very important cost in the current implementation of carbon tax. Based on the estimated boundary of CO_2 emission regulated by local authorities, the cost of carbon tax can be calculated as the product of the amount of CO_2 emission and the tax per unit CO_2 emission. Given that the cost of carbon tax relies on the production of the program, it suggests that the carbon tax should be listed as an item of variable production costs.

Depreciation, the invisible cost in the cashflow, can play a significant role in assessing the economic feasibility. The common methods for the calculation of depreciation are straight line method (SLM), sum of the years digits method (SYDM), double declining balance method (DDBM), and modified accelerated cost recovery system (MACRS). The MACRS method uses a double declining balance method and switches to a straight-line method at a point. The SLM, SYDM, and DDBM can be calculated as follows:

$$D_k^{SLM} = \frac{FCI_L - S_n}{n} \quad (31)$$

$$D_k^{SYDM} = \frac{2[(n+1) - k]FCI_L - S_n}{n(n+1)} \quad (32)$$

$$D_k^{DDBM} = \frac{2}{n}\left[FCI_L - \sum_{j=0}^{j=k-1} D_j\right] \quad (33)$$

Table 2 Recommended range of components of FCI and three examples[103]

	Range of FCI, %			
Component	Recommended	Solid processing	Solid-fluid processing	Fluid processing
Direct costs				
Equipment	15–40	25.19	23.36	19.84
Installation	6–14	11.34	9.11	9.33
Instrumentation & controls	2–12	4.53	6.07	7.14
Piping	4–17	4.03	7.24	13.49
Electric	2–10	2.52	2.34	2.18
Buildings	2–18	6.30	6.78	3.57
Site preparation	2–5	3.78	2.80	1.98
Auxiliary	8–30	10.08	12.85	13.89
Land	1–2	—	—	—
Indirect costs				
Engineering & supervision	4–20	8.31	7.48	6.55
Construction	4–17	9.82	7.94	8.13
Legal	1–3	1.01	0.93	0.79
Contractors	2–6	4.28	4.44	4.37
Contingency	5–15	8.82	8.64	8.73

Table 3 WC estimation method reported in the literature

Item	Turton *et al.*[102]	Peters *et al.*[103]	NETL (reported by Moosazadeh *et al.*[117])
1. Variable production costs[a] (or direct manufacturing costs)			
a. Raw material	Inventory based	Inventory based	Inventory based
b. Utilities[b]	Inventory based	Inventory based	Inventory based
c. Catalysts and solvents	Inventory based	Inventory based	Inventory based
d. Operation labor (C_L)	—[c]	—[c]	—
e. Operating supervision	0.1–0.25 of C_{OL}	0.15 of C_{OL}	
f. Maintenance and repairs	0.02–0.1 of FCI	0.07 of FCI	0.025[d]
g. Operating supplies	0.1–0.2 of 1.f	0.15 of 1.f	—
h. Laboratory charges	0.1–0.2 of C_{OL}	0.15 of C_{OL}	—
i. Patents and royalties	0–0.06 of WC[e]	0.04 of WC[e]	—
2. Fix charges			
a. Depreciation[f]	—	—	—
b. Taxes and insurance	0.014–0.05 of FCI	0.02 of FCI	0.02[d]
c. Overhead cost	0.5–0.7 of (C_{OL} + 1.e + 1.f)	0.5–0.7 of (C_{OL} + 1.e + 1.f)	—
d. Rent	—	—[g]	—
e. Interest	—	—[h]	—
3. General expenses			
a. Administration	0.15 of (C_{OL} + 1.e + 1.f)	0.15–0.25 of C_{OL}	—
b. Distribution and marketing	0.02–0.2 of TPC	0.02–0.2 of TPC[i]	—
c. Research and development	0.05 of TPC	0.05 of TPC	—

[a] Direct manufacturing costs in the study by Turton *et al.*,[102] and annual operating and maintenance cost in the study by Moosazadeh *et al.*[117] [b] Includes water, electricity, fuel, refrigeration, steam, and waste treatment and disposal. Turton *et al.*[102] lists waste treatment and disposal as a single item of variable production costs. [c] Labor cost = labor number × annual operating hours × salary per hour of each labor. [d] The NETL model only includes the fixed operation and maintenance costs and the insurance cost besides the cost of raw material, utilities, catalysts and solvents. [e] Without depreciation. [f] Calculated separately. [g] 0.08–0.12 of the value of rented property. [h] 0.05–0.1 of the total value of the borrowed capital. [i] The higher figure is applied to selling in small quantities, and *vice versa*.

where D_k^{SLM}, D_k^{SYDM}, and D_k^{DDBM} represent the annual depreciation in the k^{th} year applying SLM, SYDM and DDBM, respectively, M$ per year; n is the depreciation period, year; FCI_L represents the depreciable fixed capital investment, M$; and S_n is the salvage value after n years, which is usually assumed to be zero, M$.

3.3.2 Profit estimation model. The first step of profit estimation is to evaluate the income. In the case of W/BtE systems, the income mainly includes the selling of the products and by-product, and the subsidy when treating specific waste. Also, if the W/BtE systems have effective carbon emission control, the excess carbon quota can be traded as profit. Thus, the annual production income (API) can be expressed as follows:

$$\mathrm{API} = \sum B_{\mathrm{product}} \times P_{\mathrm{product}} + \sum B_{\mathrm{waste}} \times \mathrm{Sub}_{\mathrm{waste}} + \mathrm{others} \quad (34)$$

where $B_{product}$ is the annual production capacity of products or by products, M$; $P_{product}$ is the selling prices of products or by products, M$; B_{waste} is the annual treatment capacity of waste, t per year; Sub_{waste} is the financial subsidy for waste treatment, M$ per t; and others is the potential profit in other fields.

Then, the after tax profit (ATP) is calculated using eqn (35), as follows:[118]

$$\mathrm{ATP} = (\mathrm{API} - \mathrm{APC}) \times (1 - \text{tax rate}) \quad (35)$$

The net present value (NPV), dynamic payback period (DPP) and internal rate of return (IRR) are chosen to evaluate the economic feasibility of the project. NPV (M$) is the present value of current and future profits minus the present value of the current and future cost over a period. A positive NPV refers to foreseeable profitability. DPP (year) is the time that NPV can realize the balance of income and outcome, which reflects the time needed to recover the initial investment. IRR (%) is the discount rate when NPV equals zero over the lifespan, and it refers to the expected annual growth rate of the initial investment.

NPV, DPP, and IRR can be calculated using eqn (36)–(38), resprectively.[85,119]

$$\mathrm{NPV} = \sum \frac{\mathrm{ATP} + D}{(1 + i^*)^n} - \mathrm{TCI} \quad (36)$$

$$\sum_{1}^{\mathrm{DPP}} \frac{\mathrm{ATP} + D}{(1 + i^*)^n} - \mathrm{TCI} = 0 \quad (37)$$

$$\sum \frac{\mathrm{ATP} + D}{(1 + \mathrm{IRR})^n} - \mathrm{TCI} = 0 \quad (38)$$

where i^* is the real interest rate, %.

Levelized cost (LC, M$) (see eqn (39)[120]) and levelized profit (LP, M$) (see eqn (40)[87]) are used to show the breakeven price and the actual profit of the calculated benchmark (B) considering the time value of capital, respectively.

$$\mathrm{LC} = \frac{\mathrm{LCC}}{\sum \frac{B}{(1 + i^*)^n}} \quad (39)$$

$$\mathrm{LP} = \frac{\mathrm{NPV}}{\sum \frac{B}{(1+i^*)^n}} \tag{40}$$

Based on the estimation of cost and profit, the economic feasibility of W/BtE systems can be evaluated. However, given that the estimation is based on several simplified assumptions, the inaccuracy between the estimation results and actual situation is unavoidable. Thus, it is recommended to considered the results as the reference to clarify the key economic factors and the distribution of capital investment.[37] When discussing the possible economic performance, it is suggested to further modify the results by engineering data and conduct a comprehensive sensitivity analysis. Besides, differences in the application of the estimate methods and the assumed parameters in the literature also cause errors when comparing the performance among various facilities. To ensure the comparability of different studies, the discussion of the results should be based on similar method applications and parameter assumptions.

3.4 Exergoenvironment and exergoeconomic assessment

Exergoenvironmental and exergoeconomic assessment integrates environmental analysis (based on LCA) and economic analysis with exergy analysis to identify the environmental impact mitigation priority and the cost-effectiveness of the components in the system, respectively.

The F–P principles are often applied in the exergoenvironmental and exergoeconomic assessment, which are described as follows:[121] 1. the specific cost and environmental impacts of the exergy flow, which are extracted from the fuel stream and equal to the average specific cost and environmental impacts of the same fuel stream supplied by upstream components and 2. the specific cost and environmental impacts of the co-products from the same component are the same.

In the exergoenvironmental analysis, the environmental impact flow balance can be expressed as follows:[122,123]

$$\dot{B}_{\mathrm{product},k} = \dot{B}_{\mathrm{fuel},k} + \dot{Y}_k + \dot{B}_k^{\mathrm{PF}} \tag{41}$$

$$\dot{B}_k^{\mathrm{BF}} = \sum b_{\mathrm{BF}}(m_{\mathrm{pollutant,in}} - m_{\mathrm{pollutant,out}}) \tag{42}$$

$$\dot{B}_i = b_i \dot{\mathrm{E}}\mathrm{x}_i \tag{43}$$

where $\dot{B}_{\mathrm{product},k}$ is the environmental impact rate of the product of component k, pts per s; $\dot{B}_{\mathrm{fuel},k}$ is the environmental impact rate of fuel to component k, pts per s; $\dot{Y}_k$ is the environmental impact rate of component k; $\dot{B}_k^{\mathrm{PF}}$ is the environmental impact rate of pollutant to component k, pts per s; $\dot{B}_i$ is the environmental impact rate of stream i, pts per s; and b_i is the environmental impact per exergy unit of stream I, pts per kJ.

$\dot{Y}_k$ can be obtained by decomposing the total environmental impact of the component (Y_k^{total}) into daily operation, and Y_k^{total} includes the environmental impact of the component in the phases of construction (Y_k^{CO}), operation & maintenance (Y_k^{OM}), and disposal phase (Y_k^{DI}). $\dot{Y}_k$ and Y_k^{total} can be calculated using eqn (44) and (45), as follows:

$$\dot{Y}_k = \frac{Y_k^{\mathrm{total}}}{n \cdot N} \tag{44}$$

$$Y_k^{\mathrm{total}} = Y_k^{\mathrm{CO}} + Y_k^{\mathrm{OM}} + Y_k^{\mathrm{DI}} = Y_k^{\mathrm{total}} \cdot w_k \tag{45}$$

where Y_k^{total} is the environmental impact per mass unit of component k, pts per t; w_k is the mass weight of component k, t; and N is the annual operation hours.

The relative specific environmental impact difference between the product and fuel ($r_{\mathrm{b},k}$) is applied to judge the environmental quality of the component (see eqn (46)). The smaller the value of $r_{\mathrm{b},k}$, the less effort needed for environmental performance improvement. Besides, the exergoenvironmental factor ($f_{\mathrm{b},k}$) can facilitate the understanding of the dominant environmental factor. $\dot{Y}_k$ is the main contributor when $f_{\mathrm{b},k}$ is higher than 0.7, whereas the main contributor is the environmental impact flow of exergy destruction ($\dot{B}_{\mathrm{D},k}$) when $f_{b,k}$ is lower than 0.3.[124]

$$r_{\mathrm{b},k} = (b_{\mathrm{product},k} - b_{\mathrm{fuel},k})/b_{\mathrm{fuel},k} \tag{46}$$

$$f_{\mathrm{b},k} = \left(\dot{Y}_k + \dot{B}_k^{\mathrm{PF}}\right)\left(\dot{Y}_k + \dot{B}_k^{\mathrm{PF}} + \dot{B}_{\mathrm{D},k}\right) \tag{47}$$

The exergoeconomic analysis has a similar cost flow balance, as follows:[91,123,125]

$$\dot{C}_{\mathrm{product},k} = \dot{C}_{\mathrm{fuel},k} - \dot{C}_{\mathrm{loss},k} + \dot{Z}_k \tag{48}$$

$$\sum \dot{C}_{\mathrm{in},k} + \dot{C}_{\mathrm{W},k} = \sum \dot{C}_{\mathrm{out},k} + \dot{C}_{\mathrm{Q},k} + \dot{Z}_k \tag{49}$$

$$\dot{C}_i = c_i \dot{\mathrm{E}}\mathrm{x}_i \tag{50}$$

$$\dot{Z}_k = \frac{\Phi_k \times \mathrm{FCI}_k \times \mathrm{CRF}}{3600N} \tag{51}$$

$$\mathrm{CRF} = \frac{i^*(1+i^*)^n}{(1+i^*)^n - 1} \tag{52}$$

where $\dot{C}_{\mathrm{product},k}$ is the cost rate of the product stream of component k, \$ per h; $\dot{C}_{\mathrm{fuel},k}$ is the cost rate of the fuel stream to component k, \$ per h; $\dot{C}_{\mathrm{loss},k}$ is the cost rate of the loss stream to component k, \$ per h; $\dot{Z}_k$ is the cost rate of component k, \$ per h; $\dot{C}_{\mathrm{in},k}$ and $\dot{C}_{\mathrm{out},k}$ are the cost rate of the inlet and outlet stream to component k, respectively, \$ per h; $\dot{C}_{\mathrm{W},k}$ and $\dot{C}_{\mathrm{Q},k}$ are the cost rate of net input power and net output heat to component k, respectively, \$ per h; $\dot{C}_i$ is the cost rate of stream i, \$ per h; c_i is the cost per exergy unit of stream i, \$ per kJ; and CRF is the capital recovery factor of the W/BtE system.

The cost effeteness of the component can be reflected by the relative specific cost difference between the product and fuel ($r_{\mathrm{c},k}$). A small $r_{\mathrm{c},k}$ indicates a slight loss in cost-effectiveness in the component. The exergoeconomic factor ($f_{\mathrm{c},k}$) can help distinguish the main contributor in the loss of cost-effectiveness, similar to the application of $f_{\mathrm{b},k}$, and the explanation of the values $f_{\mathrm{c},k}$ can refer to $f_{\mathrm{b},k}$.

$$r_{\mathrm{c},k} = (c_{\mathrm{product},k} - c_{\mathrm{fuel},k})/c_{\mathrm{fuel},k} \tag{53}$$

$$f_{\mathrm{c},k} = \dot{Z}_k/(\dot{Z}_k + \dot{C}_{\mathrm{D},k}) \tag{54}$$

where $\dot{C}_{D,k}$ is the cost rate of exergy destruction, $ per h.

As mentioned above, the results of exergoenvironment and exergoeconomic analysis strongly rely on the selection of the LCIA method and economic assumptions (price of fuel and product, annual operation year, lifespan, interest rate, *etc.*), suggesting that a similar selection of the above-mentioned two aspects is the foundation for the comparison among various reports in the literature.

4 Techno-environmental-economic performance of various W/BtE systems

In the previous reviews, researchers mainly concentrated on the advances in W/BtE simulation models and their principles and modifications have been summarized in the literature, as mentioned in section 2. Given that the modelling approaches have been fully developed, the research hotspot has shifted to the TEE assessment of thermochemical W/BtE technologies. In this section, the TEE performances of hybrid W/BtE systems are investigated based on the survey of the published literature since 2020.

4.1 Optimization of the primary thermochemical process

The primary production of syngas (flue gas), char and oil during the thermochemical process is the core and foundation of the W/BtE system. Process simulation, as an excellent complementary tool for data acquisition besides experiments, can provide sufficient, informative, and reliable results with low time cost and financial expense after validation. Numerous studies have been conducted to investigate the results distribution of thermochemically processed waste or biomass, and similar product generation patterns reported with the experimental data. The most important usage of the process simulation is to acquire results of newly proposed processes based on the data of the existing processes, and if the process simulation cannot provide specific parametric guidance aimed at targeted performance indicators, the significance of process simulation will be remarkably weakened.

Table 4 lists the optimized conditions for the targeted performance indicators. The targeted performance indicators include the aspects of the product quality and the process performance. In terms of product quality, the targeted indicators include fraction designated species (H_2, CO_2, CO, CH_4, pollutants, *etc.*), LHV, and HHV. Also, researchers focused on the product yield of various phases, carbon conversion efficiency, cold gas efficiency, and energy/exergy efficiency in the aspects of process performance. In the kinetic, TE and ML models, the influence of global control parameters based on the specific feed-in are investigated, such as temperature, pressure, equivalence ratio (ER), steam ratio (SR), agent composition, blending ratio, and residue time. The optimization can be targeted for the maximum of single indicators or the poly-optimization of a group of indicators. The carbon conversion efficiency (CCE) is used to evaluate the degree of carbon content in the feedstock to be converted into products. Besides, most studies tend to use the cold gasification efficiency (CGE, which equals the ratio between the product and the feedstock) to reflect the energy utilization efficiency of the process. In the absence of a distinction in the aspects of an allothermal or autothermal reactor, the figure of CGE may not represent the true situation of the energy efficiency. If certain extra heat requirement is supplied, the difference between CGE and η_{en} can be significant. Zaman *et al.*[126] reported the thermodynamic performance of the steam biomass gasification process, and the CGE, $\eta_{ex,syngas}$, and $\eta_{ex,total}$ were 87.1%, 76.12%, and 77%, respectively. These results remarkably emphasized the consideration of extra heat supply when assessing the thermodynamic performance of a thermochemical process. Besides performance optimization, some researchers provided parametric guidance for adjusting the H_2/CO ratio to satisfy the requirement for further chemical synthesis applications. Vikram *et al.*[127] reported the optimized range of temperature and CO_2 to biomass ratio (CBR) in wood residue gasification under atmospheric pressure. For the synthesis of dimethyl ether (DME) (H_2/CO = 1), methyl formate (H_2/CO = 2), and synthetic natural gas (SNG) (H_2/CO = 3), the recommended temperature and CBR were >800 °C and 0.15–0.3, 750–800 °C and 0.375–0.45, and 650 °C and 0.525–0.565, respectively. Yu *et al.*[128] also reported the optimal condition for adjustable H_2/CO syngas production based on dry/steam reforming of corncob pyrolysis gas. In the case of H_2/CO = 2, the condition was CO_2/C of 0.5, H_2O/C of 2, and the reforming temperature of 770 °C, and for H_2/CO = 3, it changed into CO_2/C of 0, H_2O/C of 2, and the reforming temperature of 770 °C.

The CFD model can investigate the detailed improvement of the operational conditions and process performance under the given global control parameters. Thus, researchers tend to apply the CFD model rather than the other models in the investigation of the combustion process. Fig. S6–S9† show the recently reported concentrations of the operational conditions in various reactors. The combustion process in the moving grate combustor is a hot topic in CFD simulation. Given that combustion is a process for the complete oxidation of combustible species, the targeted indicators are commonly the pollutant fraction and the burnout rate, which strongly relies on the local field distribution. Also, the temperature distribution is of great concern, given that it is directly related to the operation safety issues, such as corrosion, coking and blasting. The optimization of in-bed combustion is usually related to the coordination of the grate speed, primary air (PA) distribution and temperature, and employing the optimized conditions, both the char burnout ratio and the pollutant generation can be improved. Hoang *et al.*[159] and Tang *et al.*[160] both reported that a decrease in the grate speed helped improve the complete combustion in the MSW grate incinerator. Su *et al.*[161] proposed a refined-staged PA distribution method in a 130 t h^{-1} biomass-fired grate boiler to adjust the air supply to the real combustion demand, which promoted the char burnout ratio from 76.5% to 95.5% and decreased the NO_x emission from 172 mg m^{-3} to 156 mg m^{-3} compared with a reasonable PA distribution. Yan *et al.*[162] studied the effects of primary air pre-

Table 4 Thermochemical performance of various types of waste and biomass based on optimized conditions

Feedstock	Scene	Approach	Optimized conditions	Optimized performance	Ref.
MSW	Gasification	TE	Temperature, SR, and steam temperature: 698.7 °C, 0.897, and 120.7 °C, respectively	LHV: 10.84 MJ Nm^{-3}, H_2 fraction: 64.13 vol%, CGE 92.4%	129
MSW	Gasification	ML	Temperature, ER, residence time, and loading weight: 900 °C, 0.2, 30 min, and 6 g, respectively	Gas yield: 72.5 wt%, tar yield: 8.3 wt%, char 19 wt%, LHV 11.2 MJ Nm^{-3}, H_2 fraction: 42.1 vol%	130
MSW	Gasification	TE	ER, SR and O_2% in the agent: 0.04, 0.28, 84.31%, respectively	CCE: 86.52%, CGE: 57.64%, H_2 fraction: 50.66 vol%, CO fraction: 44.67 vol%	131
Sewage sludge	Gasification	TE-kinetic	Temperature, pressure, ER, SR, and residence time: 950 °C, 0.2, 1, 2 min, respectively	Sum of H_2 and CO fraction: 54.63%	132
Sewage sludge	Gasification	TE	Temperature, moisture content, pressure, and oxidation coefficient: 450 °C, 87 wt%, 25 MPa, and 0, respectively	Gas yield: 30.32 mol kg^{-1}, CCE: 100%, LHV: 17.1 MJ Nm^{-3}, composition: 43.56% CH_4, 11.41% H_2, 39.11% CO_2	133
Sewage sludge	Gasification plasma	TE	Temperature, ER, SR: (1) 926.85 °C, 0.2, and 0; (2) 926.85 °C, 0, and 0.1, respectively	CGE, energy efficiency, and composition: (1) 83.94%, 56.82%, 8.22% CO, 20.26% CO_2, 44.57% H_2, and 27.57% N_2; (2) 105.82%, 63.60%, 10.59% CO, 21.81% CO_2, 65.74% H_2, and 1.96% N_2, respectively	134
Poultry litter	Gasification	TE	Temperature, pressure, and biomass to air ratio: 765 °C, 1 bar, and 0.59, respectively	LHV: 6.36 MJ Nm^{-3}, H_2 fraction: 24 vol%, net heat: 442.37 kW	135
Poultry litter	Gasification	TE	Temperature, ER, and moisture content: 830 °C, 0.2, and 16.36%, respectively	LHV: 5.71 MJ Nm^{-3}, H_2 fraction: 21.80 vol%, CGE: 57.68%	136
Corn stock	Gasification	TE	ER 0.25	LHV: 6.8 MJ Nm^{-3}, CCE 99%, CGE 92%, H_2 fraction: 20 vol%	137
Date palm waste leave	Gasification	ML	Temperature: 738.39 °C	LHV: 11.10 MJ Nm^{-3}, composition: 34.03% CO, 4.07% CH_4, 49.03% H_2, 11.30% CO_2	138
Medical waste	Gasification	TE	Temperature, SR, and steam temperature: 1560 °C, 0.1, and 0.99 °C, respectively	LHV: 7.50 MJ Nm^{-3}, CGE 89.95%, H_2 fraction: 43.88 vol%	139
PP, PVC, HDPE, PS, PET	Gasification	TE	Temperature, ER, and pressure PP: 850 °C, 0.15, and 1 bar PVC: 850 °C, 0.15, and 1 bar HDPE: 850 °C, 0.15, and 1 bar PS: 850 °C, 0.15, and 1 bar PET: 850 °C, 0.1, and 1 bar, respectively	LHV and CGE PP: 6.4 MJ Nm^{-3} and 39% PVC: 5.12 MJ Nm^{-3} and 29% HDPE: 6.2 MJ Nm^{-3} and 39% PS: 5.56 MJ Nm^{-3} and 33% PET: 6.46 MJ Nm^{-3} and 33%, respectively	140
Sawdust	Gasification	Kinetic	Temperature, ER, SR, and agent composition: 1000 °C, 0.28, 1, and 40% O_2-air/steam, respectively	LHV: 6.48 MJ Nm^{-3} Gas yield: 1.54 Nm^3 kg^{-1} Tar yield: 6.01 g Nm^{-3} H_2 fraction: 20.46 vol% CGE: 94.1%	141
Waste tire	Gasification	ML	Agent composition: (1) SR = 0.3 (2) SR = 0.1 (3) Steam/air = 0.6	(1) H_2 fraction = 50 vol% (2) LHV = 15.8 MJ Nm^{-3} (3) Energy conversion efficiency: 57%, gas yield = 6.2 Nm^3 kg^{-1}	142
Rice straw & MSW	Gasification	Kinetic	Temperature, SR, and biomass blending ratio: 1099.95 °C, 0.79, and 10.02%, respectively	Gas yield: 2.672 Nm^3 kg^{-1}, CO_2 fraction: 8.05 vol%, tar yield: 17.06 g Nm^{-3}	143
Tree bark & RSW	Gasification	TE	ER and biomass blending ratio: 0.45 and 20%, respectively	Temperature: 799 °C, CGE 57.17%	144
Pine & HDPE	Gasification	TE	Temperature, SR, and plastic/biomass: 921 °C, 1.186, and 74.99%, respectively	LHV: 10.46 MJ m^{-3}, composition: 27.15% CO, 0.4% CH_4, 65.40% H_2, 4.05% CO_2	145
Shiitake substrate & PE	Gasification	Kinetic	Temperature, ER, PE blending ratio, and agent composition: (1) 750 °C, 0.1, 80%, and pure steam (2) 950 °C, 0.1, 80%, and pure CO_2 (3) 950 °C, 0.3, 0%, and pure CO_2 (4) 950 °C, 0.2, 0%, and pure CO_2, respectively	(1) HHV = 21.96 MJ kg^{-1} (2) H_2/CO = 1.58 (3) CCE = 54.55% (4) CGE = 48.93%	146
Casuarina wood & plastics	Gasification	TE	ER, plastic blending ratio, SR, and steam temperature: 0.185, 30%, 0.75, and 150, respectively	HEE: 33.44%, GEE: 68.48%, LHV: 10.99 MJ Nm^{-3}	147
Casuarina wood & plastic waste	Gasification	TE	ER, plastic blending ratio, moisture content, and O_2 content in the agent: 0.2495, 30%, 8%, and 50%, respectively	LHV: 8.65 MJ Nm^{-3}, CGE: 71.04%	148
Biomass	Gasification	ML	Temperature and SR: 800.3 °C and 0.8, respectively	LHV: 12.13 MJ Nm^{-3}, CGE: 87.1%, syngas exergy efficiency: 76.12%, total exergy efficiency: 77%.	126

Table 4 *(Contd.)*

Feedstock	Scene	Approach	Optimized conditions	Optimized performance	Ref.
Biomass waste	Gasification	CFD	ER: 0.25	LHV: 5.57 MJ m^{-3}, CGE: 67.50%, composition: 22.00% CO, 3.99% CH_4, 12.50% H_2, 7.95% CO_2, 0.82% C_mH_n Gas yield: 2.01 m^3 kg^{-1}	149
Rice husk	Pyrolysis	Kinetic	Temperature and residence time: (1) 588 °C and 0.25 s (2) 450 °C and 43.66 s (3) 798.8 °C and 15.47 s, respectively	Bio-oil, char, and gas yield (wt%): (1) 36.72%, 41.88%, and 21.16% (2) 30.93%, 38.36%, and 27.10% (3) 0.77%, 26.07%, and 73.25%, respectively	150
Pine sawdust	Pyrolysis	TE	Temperature and pressure: 550 °C and 1 atm, respectively	Bio-oil, char, and gas yield (wt%) 65.80%, 8.65%, and 25.55%, respectively	151
Olive pomace	Pyrolysis	Kinetic	Temperature and residence time: (1) 650 °C and 0.1 s (2) 675 °C and 15 s, respectively	Bio-oil, char, and gas yield (wt%): (1) 23.72%, 66.96%, and 9.32% (2) 0.74%, 58.09%, and 41.17%, respectively	152
Empty fruit bunch	Pyrolysis	Kinetic	Particle size, temperature, and residence time 0.3 mm, 500 °C, and 1 s, respectively	Bio-oil, char, and gas yield (wt%): (1) 52.05%, 25.49%, and 22.46%, respectively	153
Wood residue	Pyrolysis	TE	Particle size and temperature: 1 cm and 480 °C, respectively	Bio-oil, char, and gas yield (kg kg^{-1}): (1) 0.38 kg kg^{-1}, 0.22 kg kg^{-1}, and 0.4 kg kg^{-1}, respectively	154
Pine needles	Pyrolysis	ML	Temperature, heating rate, and inert flow rate: 552.06 °C, 50 °C min^{-1}, 164.40 mL min^{-1}, respectively	Bio-oil, char, and gas yield (wt%): (1) 51.72%, 17.73%, and 30.55%, respectively, bio-oil HHV: 22.52 MJ kg^{-1}, biochar HHV: 27.51 MJ kg^{-1}, gas HHV: 10.69 MJ kg^{-1}, gas composition: 31.58 vol% CO, 45.10 vol% CO_2, 9.49 vol% H_2, and 13.73 vol% CH_4	155
Pine wood sawdust	Pyrolysis	Kinetic	Temperature and residence time: 415 °C and 1 s, respectively	Bio-oil, char, and gas yield (wt%) (1) 53.9%, 25.4%, and 20.6%, respectively	156
Argan pulp, argan fruit layer, argan nut shell	Pyrolysis	Kinetic	Temperature and temperature holding time: 471.86 °C, 475.42 °C, and 487.58 °C and 0 s, respectively	Bio-oil, char, and gas yield (wt%): (1) 25.45%, 37.99%, and 36.56%; (2) 23.40%, 36.33%, and 40.27%; (3) 19.19%, 38.97%, and 41.85%, respectively	157
Flax straw	Pyrolysis	Kinetic	Temperature and heating rate: (1) slow pyrolysis: 500 °C and 30 °C min^{-1}; (2) fast pyrolysis: 500 °C and 1 s to setting temperature, respectively.	Bio-oil, char, gas yield (wt%), energy efficiency, and exergy efficiency: (1) 39.76%, 35.51%, 25.61%, 95.68%, and 94.90%; (2) 43.57%, 33.56%, 22.95%, 98.22%, and 97.90%, respectively.	158

heating in a 500 t d^{-1} MSW incinerator and reported that a higher PA temperature increased the boiler thermal efficiency, but it also brought the risks of intensified thermal NO_x formation and grate damage. Considering the pros and cons, the optimal PA temperature was 453 K. The injection of secondary air (SA) is beneficial for the complete combustion inside the furnace. Regarding the inlet parameters of SA, Zheng *et al.*[163] reported the optimal temperature, velocity, and inlet angle of SA in a waste incinerator, and their influence on NO_x generation and thermal efficiency followed the order of angle > velocity > temperature, and angle > temperature > velocity, respectively. Zeng *et al.*[164] further comprehensively considered the interacting effect of grate speed, PA temperature and SA arrangement. In the case of the PA temperature of 463 K and 483 K, the SA volume ratio of the front and rear arches was 1.59 : 1 and the SA direction of the front arch was 40° and 60°, with the same SA direction of the rear arch of 0°, respectively. Deep air-staged technology with an increase in the over-fired air (OFA) ratio is economical and efficient technology to further reduce the NO_x emission. Yang *et al.*[165] studied the effects of the ratio of PA/SA/OA in an MSW grate incinerator, and the results showed that the air supply optimization suppressed the initial generation of NO_x and promoted the NO_x removal efficiency of the selective non-catalytic reduction (SNCR) process from 38.85% to 62.81% with the NO_x emission of less than 100 mg m^{-3} (PA/SA/OA = 65%/25%/10%).

The application of flue gas recirculation (FGR) can suppress thermal NO_x emission and partially improve the boiler thermal efficiency. Yang *et al.*[166] reported that with an increase in the FGR ratio from 13% to 20%, the boiler efficiency increased gradually from 80.16% to 83.78%, and about 16% of the initial NO_x emission was reduced. With the coupled application of OFA, FGR, and SNCR, the total NO_x removal efficiency reached 76.48%. Co-disposal of different categories of biomass and waste is often seen. Thus, Zhou *et al.*[167] compared the co-combustion behavior of low and high ash biomass in a moving grate incinerator, and reported that low ash fuel blending enhanced the stability of high ash fuel grate-firing. The optimal blending ratios of anaerobic food digestate, sludge with 40% moisture, and sludge with 60% moisture with MSW were reported to be 15%,[168] 13%[169] and 7%,[170] respectively. Fluidized bed reactors can be used in the combustion process. In this case, Huang *et al.*[171] evaluated the effects of the SA angle and ER on the tri-combustion of coal, biomass

and oil sludge in a 130 t h^{-1} circulating fluidized bed boiler, and the results showed that the mole fraction of NO_x had a positive correlation with ER, while that of SO_2 was negative. Also, the outlet NO_x mole fraction decreased from 4.17×10^{-5} to 3.99×10^{-5} with an increase in the SA angle from 15° to 30°. Liu *et al.*[172] not only discovered a similar positive correlation between ER and outlet NO_x concentration in a 130 t h^{-1} biomass circulating fluidized bed, but also reported the negative correlation between ER and outlet KCl concentration, and the optimal PA/SA for minimum NO generation was 4 : 6. Deep air-staged technology can be also applied in a bubbling fluidized bed (BFB). Karlström *et al.*[173] reported that with PA/SA/OA = 50%/25%/25%, the total NO + HCN + NH_3 concentration decreased from 1169 ppm to 76 ppm.

Regarding the application of the CFD model in the gasification process, similar results were reported for the effects of gasifying agent composition, blending ratio, pressure, and temperature on the reactor-level performance when applying the TE model. Wan *et al.*[174] investigated the effects of ER and SR on the syngas composition and thermochemical performance in a pilot-scale circulating fluidized bed. An increase in SR elevated the H_2 yield, but had the opposite effect on the concentration of C_2H_4, CH_4, CO and CO_2, and the value of LHV. Also, an increase in ER above 0.3 would dramatically reduce CGE. Yang *et al.*[175] located the optimal SR = 0.5 of a 100 kW dual fluidized bed (DFB) gasifier, and reported that the yields of H_2 and CO_2 and the ratio of H_2/CO first increased, and then decreased with an increase in SR. Erdogan *et al.*[47] compared the performance of a laboratory-scale updraft plasma gasifier with ER = 0.1–0.4, and found that optimum conditions for the PG of medical waste were obtained for ER = 0.4, which yielded 54.7% H_2, 17.1% CO, 11.8% CH_4 and 2.5% H_2S in the syngas with CCR of 29.1% and CGE of 28.5%. Wang *et al.*[176] reported that the optimal conditions for sawdust gasification in a two-stage entrained flow gasifier was S/B = 0.1 and ER = 0.16, given that a higher ER contributed to the conversion of char, but it decreased the effective constituent of gas produced.

The CFD model shows the highest sensitivity to a change in the particle parameters and the structural design. A larger particle diameter can prolong the residue time, together with limited reaction and heat transfer rates, while a smaller particle diameter leads to sufficient contact between the reactants, with the potential risks of coagulation, restricted fluidization of the bed, and incomplete conversion.[177–180] Therefore, it is essential to locate the optimal particle diameter with the consideration of the reactor geometry and operating parameters. Wang *et al.*[69] proposed a multiple thermally thick particle model and revealed that the temperature difference inside the particle could be significantly reduced by decreasing the particle size from the centimeter- to millimeter-level, which was beneficial for the in-bed reaction rates. The structural design optimization includes two aspects. The first aspect is the geometry of the reactor, such as the furnace arch structure in the moving grate incinerator,[181] coating thickness and heat arrangement in a rotary kiln incinerator,[182,183] and the throat size in a fixed bed gasifier.[184] The second aspect is the use of auxiliary devices. In a conical spouted bed pyrolizer, Sun *et al.*[185] reported that the use of a fountain confiner could significantly extend the biomass residence time, and Yu *et al.*[186] found that the use of a draft tube enhanced the stability of the bed within a wider range of operating gas velocities. Moreover, in a fluidized bed gasifier, Bello *et al.*[187] reported that the use of an air distributor could enhance the particle recirculation. Raza *et al.*[188] further compared the performance when using static and rotating air distributor plates, and the results revealed that using rotating air distributor plates reduced 88% of the pressure fluctuations within the fluidized bed.

In summary, the primary thermochemical process is the basis of W/BtE systems. With the given goal and boundary, the simulation results of the thermochemical process provide input data for the following subsystems. Therefore, it is of great significance to choose appropriate models according to the background and assumptions of the studied W/BtE system. Given that the CFD model often requires high computing power and solving time, most studies adapt the other three models for the quick TEE assessment of integrated W/BtE systems.

4.2 Production of power, heat, and cooling

The main topics when discussing W/BtP systems are as follows: 1. the performance variation with and without CCS subsystem; 2. the improvement by the application of advanced thermochemical technology, such as chemical looping gasification/combustion (CLG/CLC), fuel cells (FC), and calcium looping (CaL); 3. the performance improvement due to cascade heat utilization (CHU) and product cogeneration, which includes combined heat and power (CHP) production systems and combined cooling, heat, and power (CCHP) systems; and 4. assistance from solar energy and the strategy of energy storage.

Fig. 9 shows the configurations of W/BtP systems. According to the number of the application of the heat utilization sub-systems, the whole system can be defined as X-stage W/BtP, -CHP, and -CCHP system. Commonly, combustion and gasification are the first steps to produce power. In the combustion (COMB)- and CLC-based route, waste or biomass is complete oxidized in the combustor to generate high-temperature flue gas. In the pyrolysis-(PY) gasification-(GSF), and CLG-based route, combustible syngas is produced and sent to a gas turbine or fuel cell for primary power production, and the outlet gas of fuel cell can be further combusted and sent to a gas turbine to be fully utilized. The CHU process occurs in the downstream section of the thermochemical section. The common power cycles include the Rankine cycle (RC), organic Rankine cycle (ORC), and supercritical CO_2 cycle (sCO_2). The heat production, which refers to the generation of steam and hot water, can be realized by cooling the flue gas in a heat exchanger (HE) or the condensation of an agent in the power cycle. Technically, the multi-effect distillation (MED) of sea water also involves a temperature raising process, which can be also seen as a type of heat production. The cooling pro-

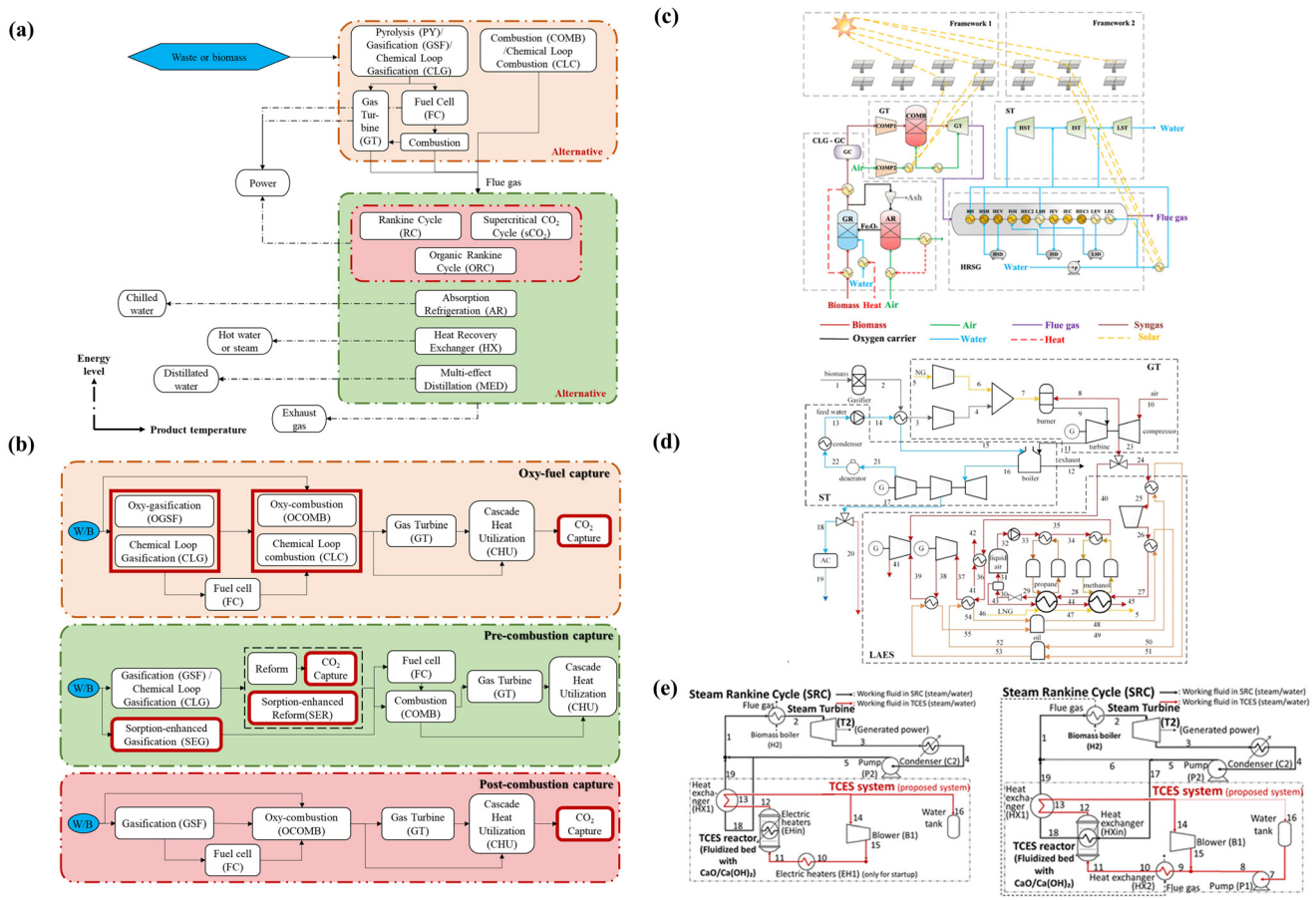

Fig. 9 Application of various technical routes in WtP systems. (a) Cascade heat utilization (CHU) subsystem; (b) carbon capture and storage (CCS) subsystem; (c) compressed air energy storage (CAES) subsystem. Reprinted with the permission.[189] Copyright 2021, the American Chemical Society. (d) Thermochemical energy storage (TCES) subsystem. Reprinted with the permission.[190] Copyright 2023, Elsevier Ltd. (e) Solar-assisted heating scheme. Reprinted with the permission.[191] Copyright 2023, the American Chemical Society.

duction is also satisfied by the production of chilled water in the absorption refrigeration (AR) subsystem. In some cases, a natural gas regasification (NGR) subsystem is integrated to use the waste heat to convert the natural gas from the liquid state to gas state.

4.2.1 Systematic variation due to carbon capture and storage. Carbon capture during the production of power can be divided into three ways, as follows: pre-combustion capture, post-combustion capture, and oxy-fuel capture. Pre-combustion capture technology is applied with the steam reforming of the syngas to remove CO_2 and obtain a high H_2-content product gas. Post-combustion capture technology is the most widely applied, given that it captures the CO_2 in the flue gas at the end of the production process and can be added to the existing facilities. Oxy-fuel capture technology provides a high-purity oxidant in the combustion process to avoid the dilution of N_2 and maintains a high CO_2 content in the flue gas, and the flue gas can be directly compressed to realize carbon capture.

In the case of COMB-RC-based systems, post-combustion capture is the most convenient option, but a decrease in the tier-I GWP also induces an extra energy penalty ($(\eta_{en,without\ CCS} - \eta_{en,with\ CCS})/\eta_{en,without\ CCS}$). Conventional post-combustion capture mainly applies solvents based on physical absorption (DEPG, low-temperature MeOH, *etc.*) and chemical-absorption (MEA, MDEA, *etc.*). The CO_2 capture rate (CCR) is a decisive indicator for the CCS subsystem, given that the more CO_2 captured, the more energy is consumed. Bore *et al.*[192] investigated the influence of CCR on the performance of a COMB-RC-CCS (MEA)-based WtP system, and found that the energy penalty was 13.17%, 14.85% and 16.56%, with the CCR of 85%, 90%, and 95%, respectively. The optimal CCR was suggested to be 90%, with the carbon captured cost (CCC) of 57.67 € per ton_{CO_2}, carbon avoided cost (CAC) of 187.80 € per ton_{CO_2}, and tier-I GWP emission of 0.19 $kg_{CO_2,eq}$ kW^{-1} h^{-1}. Zhang *et al.*[193] also discovered that in a GSF-SOFC-GT-HE-CCS(MEA)-based BtCHP system with CCR of 100%, the energy penalty can be almost twice that with the CCR of 90%, together with a higher tier-III GWP. Moreover, the energy penalty in $\eta_{en,CHP}$ (~50%) was much larger than $\eta_{en,P}$ (~25%), indicating that the for the application of solvent-based post-combustion capture, the low-cost supply of heat consumption during the solvent regener-

ation process was the key. Similarly, Saharudin *et al.*[194] pointed out that in a COMB-RC-CCS(MEA)-based WtP system with the CCR of 90%, the ratio between heat and power consumption was approximately 2.75. Although the application of post-combustion capture is beneficial to GWP reduction (from 0.06–0.12 $kg_{CO_2,eq}$ kW^{-1} h^{-1} to −1.27–1.41 $kg_{CO_2,eq}$ kW^{-1} h^{-1}, with carbon credit created by biogenic CO_2 emission capture), it was reported that the other LCA indicators and LCOE increased from 13% to 217% and 360% to 410%, respectively. Averagely, in the CCS subsystem, per ton of CO_2 captured, there is an extra tier-III GWP of 175–183 $kg_{CO_2,eq}$ and CCC of 50–53 $. CaL can be applied as another choice for post-combustion capture. Ortiz *et al.*[195] reported the performance of the application of CaL in a COMB-RC-CCS-based WtP system. Using MSW as the fuel in the calciner, they reported the CCC of 111.87 € per kg_{CO_2}, LCOE of 207.48 € per MW per h, and tier-I GWP of 0.31 $kg_{CO_2,eq}$ kW^{-1} h^{-1}. If oxy-combustion is further applied in the calciner, the energy penalty would decrease from 25.85% to 21.70%, and the tier-I GWP also dropped to 0.15 $kg_{CO_2,eq}$ kW^{-1} h^{-1}, while the CCC and LCOE increased to 177.75 € per kg_{CO_2} and 308.53 € per MW per h, respectively. Recovering waste heat in the calciner played a vital role in maintaining the η_{en} of the WtP system.

GSF-based systems have more flexible options, and thus Zang *et al.*[196] compared the performance of a GSF-GT-RC-based BtP system with pre-(used Selexol) and post-combustion (using MEA) capture, and the results showed that the post-combustion capture had a lower tier-III GWP (~0.43 $kg_{CO_2,eq}$ kW^{-1} h^{-1} to ~0.35 $kg_{CO_2,eq}/kW^{-1}$ h^{-1}, without carbon credit created by biomass cultivation) due to its higher CCR. However, post-combustion capture lacks an advantage in terms of LCA indicators and energy penalty. Technically, the low CCR of conventional pre-combustion capture is due to the limited chemical equilibrium of the reforming reaction, and in this case the application of CaL technology can promote both the H_2 yield and CCR (~90% to ~98%).[197] Han *et al.*[198] reported that with the similar CCR of ~91%, the SEG-GT-RC-based BtP system (η_{en} of 42.42% and η_{ex} of 38.87%) had better performance than the GSF-CCS-GT-RC-MEA-based system (η_{en} of 37.18% and η_{ex} of 33.99%).

Oxy-combustion (OCOMB) is the most conventional oxy-fuel capture method, including the direct oxy-combustion of the feedstock itself and the indirect oxy-combustion of the syngas from oxy/steam-gasification (OGSF/SGSF). Ling *et al.*[199] proposed an OCOMB-sCO_2-CCS-based BtP system, which directly captured and compressed ~99% of CO_2 from the outlet with the consumption of ~10% net energy output, and the tier-I GWP, CAC and CCC were ~0.58 $kg_{CO_2,eq}$ kW^{-1} h^{-1}, 24.05 $ per ton_{CO_2}, and 18.78 $ per ton_{CO_2}, respectively. Xiang *et al.*[200] proposed an OGASF-OCOMB-RC-CCS-based BtP system, which exhibited the η_{en} of 35.41%, η_{ex} of 31.21%, and CCR of ~96.7%. The direct CO_2 capture and compression subsystem could operate at a high η_{en} and η_{ex} of over 95%. Furthermore, with the application of flue gas circulation, the η_{en} of the OGASF-internal combustion engine (ICE)-CCS-based BtP system showed an improvement up to 10%.[201] The application of CL can provide the same effect as OCOMB. Saqline *et al.*[202] compared the OGSF-CLC-GT-RC-CCS-based and CLC-RC-CCS-based BtP systems with the conventional OGSF-GT-RC-based and COMB-RC-based BtP systems. The results revealed that both systems applying CLC exhibited the η_{en} of ~44% and η_{ex} of ~32.0%, and they achieved a CCR of over 99% with the energy penalty of ~5%. The η_{en} and η_{ex} followed the order of OGSF-CLC-GT-RC-based > CLC-RC-CCS-based > OGSF-GT-RC-based > COMB-RC-based, indicating the advantages of CL in high-efficiency operation and low-cost CO_2 capture.

Emenike *et al.*[203] compared the performance of the application of three capture technologies in a BtP system. The OGSF-CCS-GT-RC-based system had the highest η_{en}, lowest LCOE, and modest tier-III GWP (~35%, ~0.17 £ per kW per h, and ~0.14 $kg_{CO_2,eq}$ kW^{-1} h^{-1}) compared to the COMB-RC-CCS-based (~26%, ~0.18 £ per kW per h, and ~0.17 $kg_{CO_2,eq}$ kW^{-1} h^{-1}) and OCOMB-RC-CCS-based systems (~29%, 0.20 £ per kW per h, and ~0.09 $kg_{CO_2,eq}$ kW^{-1} h^{-1}), respectively. The energy penalty for the application of oxy-combustion, post-combustion, and pre-combustion was ~20%, ~28%, and 13%, respectively. However, the energy penalty results can vary depending on the technical assumptions and the calculation references. Zheng *et al.*[204] reported that the ranking of carbon capture technologies in energy penalty was post-combustion (8–14%), oxy-fuel combustion (8–12%), pre-combustion (6–10%), and CLC (<3%). Overall, post-combustion capture has the greatest adaptability, but it also causes a high energy penalty and economic cost. Pre-combustion capture has comprehensive advantages in energy and economic aspects, but its application scenarios are restricted, and its modest CCR needs to be further improved by process innovations. Oxy-fuel combustion capture is attractive owing to its high CCR and convenient carbon capture subsystem design, especially in the advanced concept of CLC. However, its feasibility still needs to be proven in large-scale commercial facilities considering the high construction costs and potential safe operation issues.[205,206]

Several assumptions have a significant effect on the results between different studies. Statistically, in the case of W/BtP systems without CCS, their tier-I GWP is about 1–1.5 $kg_{CO_2,eq}$ kW^{-1} h^{-1}, with a CCR above 90%, which can be reduced to under 0.15 $kg_{CO_2,eq}$ kW^{-1} h^{-1}. Regarding the tier-III GWP, the consideration of biogenic CO_2 and biomass cultivation can cause a significant difference. Firstly, some studies considered the CO_2 stored during biomass cultivation as a type of negative emission, generating −0.8 to −1.5 $kg_{CO_2,eq}$ kW^{-1} h^{-1}.[196,207] Moreover, given that the biogenic CO_2 emission can be excluded from the calculation owing to its carbon neutrality, the negative GWP varies due to the biogenic carbon fraction in different waste. Liu *et al.*[2] measured the biogenic carbon fraction of printed paper, textiles, plastics and synthetic textiles, rubber and leather and reported the biogenic carbon fraction of ~96.80%, ~67.52%, ~6.20%, and ~92.55%, respectively. Regarding MSW, the reported biogenic CO_2 fraction is in the range of ~40% to 80%.[208–210] Thus, the basic assumptions of biogenic CO_2 storage and emission should be uniform before a comparison is performed. In the case of post-combustion

capture using MEA and pre-combustion capture using Selexol, the tier-III GWP was reported to be approximately 0.5 and 0.6 $kg_{CO_2,eq}$ kW^{-1} h^{-1} for power production, respectively.[194,196] The tier-III GWP of oxy-fuel combustion is about 0.1 $kg_{CO_2,eq}$ kW^{-1} h^{-1} for power production.[207,211] In the case of economic performance, the difference in plant size, feedstock cost, and other aspects can cause a great effect. Mohamed *et al.*[212] reported that with an increase in the plant size of a CLG-CCS-GT-RC-based BtP system from 50 to 800 MW, the LCOE could have a reduction of ~45%. Biomass is always seen as the merchant, and thus the buyer needs to pay for biomass acquisition. Meanwhile, the treatment of MSW is profitable due to the subsidy, tipping fee, and grate fee. In this case, it is better to compare different technologies quantitatively under the same framework. Yan *et al.*[207] calculated the LCOE of COMB-RC-CCS-based, GSF-CCS-GT-RC-based, and OGSF-SOFC-RC-CCS-based BtP systems, which was 0.06 $ per kW per h, 0.05 $ per kW per h and 0.05 $ per kW per h with the biomass price of 44.52 $ per $ton_{biomass}$, respectively. Xu *et al.*[213] investigated a COMB-ORC-MED-HE-AR-NGR-based BtCCHP system, with the biomass price and carbon tax of 49 $ per $ton_{biomass}$ and 24 $ per ton_{CO_2}, and the cost of biomass purchasing and CO_2 emission was responsible for 31.06% and 15.67% of the total cost, respectively.

4.2.2 Multi-stage cascade heat utilization for P, CHP & CCHP production. The theoretical principle of multi-stage CHU is the matching of the heat source temperature with the application temperature window of the subsystem. In the case of the RC and sCO_2 cycle, it has been reported that a heat source temperature of approximately 300 °C and 450 °C realized a high efficiency operation, respectively.[214] In the case of a heat source with a temperature below 300 °C, the ORC cycle is a good choice, given that it can adapt to the temperature of the heat source in a wide range from 40 °C to over 300 °C.[215] Besides, the HE can also be used to generate hot water or low-level steam for district heat supply.[216] Finally, the application of AR and MED can further recover the heat from <100 °C heat source to produce chilled water and fresh water, respectively.[217,218]

The choice of the sub-systems can cause a variation in the performance of the entire system. In the case of the thermochemical process, the GSF-GT-RC-based BtP system had a slightly advantageous thermodynamic efficiency (~3–10%) than the COMB-RC-based BtP system in a specific case.[202] The η_{en} and η_{ex} were ~35% for the GSF-GT-RC-based and ~30% for the COMB-RC-based systems. As the gasifying agent of GSF-GT-RC-based systems, Cvetinović *et al.*[134] suggested that steam was a better choice than air in terms of thermodynamic and economic performance. When choosing PY as the thermochemical process, higher η_{en} and η_{ex} are often reported than applying GSF and COMB because of the cogeneration of oil and char. Liu *et al.*[219] proposed a PY-SOFC-GT-ORC-based WtP system for the cogeneration of power, oil and char, exhibiting the η_{en} and η_{ex} of 70.11% and 69.65%, respectively. However, its $\eta_{en,P}$ and $\eta_{ex,P}$ were ~23%. Considering that some of the pyrolysis product is utilized in the same system, the contribution of electric output to the systematic output is promoted. Lampropoulos *et al.*[220] used char as the feedstock of the secondary GSF in a PY-GSF-SOFC-RC-based BtCHP system, reporting that the electrical output contributed ~60% of the systematic output. Li *et al.*[221] also found similar conclusions in a PY + GSF-GT-RC system for the same cogeneration, with sludge and medical waste as the feedstock for PY and GSF, respectively. The $\eta_{en,P}$, η_{en}, $\eta_{ex,P}$, and η_{ex} were 55.02%, 66.31%, 40.96% and 66.30%, respectively. Although the input of sludge only contributed ~8% of the total energy and exergy, the output of char and oil accounted for ~20% of energy and ~33% of exergy, respectively. When applying PY in the first step, the high η_{en} and η_{ex} do not mean that PY is the most advantageous thermochemical technology, given that it exhibits a relatively low $\eta_{en,P}$ and $\eta_{ex,P}$ with the pyrolysis products not being completely utilized inside the system boundary. Thus, the following utilization of the pyrolysis products is worth more attention, given that Su *et al.*[222] noticed that the cogeneration of power and char reduced ~50% of the DPP than the single generation of power with the biochar selling price of ~200 $ per $ton_{biochar}$. Given that the chemical and physical properties of the biochar products remarkably vary depending on the realistic operational conditions, to reflect the real elementary composition of biochar, prediction models of biochar yield and composition at different formation temperatures have been developed.[223,224] With the application of these models, the output of product and heat during the further utilization of biochar can be specified. In terms of the power cycle, Kong *et al.*[225] also claimed that the application of FC could improve the systematic performance than GT, especially integrated with oxy-combustion capture. Exergoeconomic results showed that the with a closed r_k of ~20%, the f_k of SOFC (~98%)[220,226,227] was remarkably higher than that of GT (~20%).[90,228] Biancini *et al.*[229] found that in the GSF-COMB-RC/ORC/sCO_2-HE/AR WtCCP/CHP system, RC and sCO_2 were prior to the power generation and CHP/CCP, respectively. Also, ORC showed flexibility for varying MSW compositions and temperature levels. Zare *et al.*[230] reported that the use of a closed Brayton cycle GT (with He as the agent) yielded a higher net power output by 13.5% instead of an open Brayton cycle GT (with air as the agent). This indicates that researchers need to select the subsystems based on the feedstock characteristics, cogeneration types, and energy level of heat to be utilized.

The construction of a multi-stage CHU subsystem can improve the systematic thermodynamic performance. Table 5 lists the performance of W/BtCHP and W/BtCCHP systems. Compared to the fundamental $\eta_{en,P}$, with the application of CHP and CCHP, $\eta_{en,CHP}$ and $\eta_{en,CCHP}$ showed an improvement of approximately 10–30% and 15–50%, respectively. However, the improvement in $\eta_{ex,CHP}$ and $\eta_{ex,CCHP}$ is not significant as that for $\eta_{en,CHP}$ and $\eta_{en,CCHP}$. The 1% increase in η_{en} only results in an average of about 0.15% increase in η_{ex} due the production of heat, and this figure for the production of cooling further decreased to 0.035%. This is because the production of heat and cooling mostly recovers the low-temperature waste heat from flue gas after power production, where

Table 5 Recent representative studies on W/BtCHP and W/BtCCHP systems

System description	Thermodynamic performance	GWP performance	Economic performance	Ref.
GSF-HE-PEMFC-ORC-based WtCHP	$\eta_{ex,P}$= 19.03%, $\eta_{ex,CHP}$= 34.41%, $\eta_{en,P}$= 19.14%, $\eta_{en,CHP}$= 34.61%	—	—	232
GF-SOFT-GT-RC-based BtCHP	$\eta_{ex,P}$= 47.7%, $\eta_{ex,CHP}$= 51%, $\eta_{en,P}$= 54%, $\eta_{en,CHP}$= 68%	Tier-I GWP_{CHP} = 0.45 kg kW^{-1} h^{-1}		233
GF-SOFT-GT-HE-based BtCHP	$\eta_{ex,P}$= 60.16%, $\eta_{ex,CHP}$= 62.3%, $\eta_{en,P}$= 46.2%, $\eta_{en,CHP}$= 73.6%	Tier-III GWP_P = 0.52 kg kW^{-1} h^{-1}		193
GF-GT-sCO_2-HE-based BtCHP	$\eta_{ex,P}$= 38.12%, $\eta_{ex,CHP}$= 39.09%, $\eta_{en,P}$= 41.75%, $\eta_{en,CHP}$= 75.89%	Tier-I GWP_{CHP} = 0.52 kg kW^{-1} h^{-1}		235
GSF-SOFC-GT-sCO_2-HE-based WtCHP	$\eta_{ex,P}$= 56.40%, $\eta_{ex,CHP}$= 57.56%, $\eta_{en,P}$= 59.30%, $\eta_{en,CHP}$= 87.81%			236
GF-SOFC-GT-RC-HE-NGR-based BtCHP	$\eta_{ex,P}$= 55.29%, $\eta_{ex,CHP}$= 55.59%, $\eta_{en,P}$= 60.28%, $\eta_{en,CHP}$= 66.20%		LCOE = 0.104 $ per kW h	237
GF-SOEC-GT-RC-ORC-HE-based BtCHP	$\eta_{ex,P}$= 53.24%, $\eta_{ex,CHP}$= 58.22%, $\eta_{en,P}$= 51.43%, $\eta_{en,CHP}$= 81.13%			238
GF-SOFC-ICE-HE-AR-based BtCCHP	$\eta_{ex,P}$= 40.17%, $\eta_{ex,CHP}$= 44.34%, $\eta_{ex,CCHP}$= 45.7%, $\eta_{en,P}$= 50%, $\eta_{en,CHP}$= 62.5%, $\eta_{en,CCHP}$= 67.5%			239
CLG-GT-AR-ORC-HE-based BtCCHP	$\eta_{ex,P}$= 31.19%, $\eta_{ex,CHP}$= 32.44%, $\eta_{ex,CCHP}$= 33.82%, $\eta_{en,P}$= 35.14%, $\eta_{en,CHP}$= 58.26%, $\eta_{en,CCHP}$= 90.92%			240
GSF-SOFC-GT-sCO_2-AR-HE-CCS(MEA)-based WtCCHP	$\eta_{ex,P}$= 49.21%, $\eta_{ex,CHP}$= 50.88%, $\eta_{ex,CCHP}$= 51.15%, $\eta_{en,P}$= 54.60%, $\eta_{en,CHP}$= 78.37%, $\eta_{en,CCHP}$= 84.22%			241
GF-SOFC-HCCI-AR-HE-based BtCCHP with solar assistance	$\eta_{ex,P}$= 35.42%, $\eta_{ex,CHP}$= 35.95%, $\eta_{ex,CCHP}$= 36.58%, $\eta_{en,P}$= 35.56%, $\eta_{en,CHP}$= 45.22%, $\eta_{en,CCHP}$= 57.50%	Tier-I GWP_P = 0.44 kg kW^{-1} h^{-1}, GWP_{CHP} = 0.27 kg kW^{-1} h^{-1}, GWP_{CCHP} = 0.26 kg kW^{-1} h^{-1}		242
GSF-HE-(a)SOFC-ORC&(b)PEMFC-AR-based BtCCHP	$\eta_{ex,P}$= 23.92%, $\eta_{ex,CHP}$= 24.73%, $\eta_{ex,CCHP}$= 25.06%, $\eta_{en,P}$= 27.29%, $\eta_{en,CHP}$= 40.97%, $\eta_{en,CCHP}$= 49.48%	Tier-I GWP_P = 1.22 kg kW^{-1} h^{-1}, GWP_{CCHP} = 0.67 kg kW^{-1} h^{-1}	LCOE = 0.13 $ per kW h, $LCOP_{CCHP}$ = 0.07 $ per kW h	243
COMB-ORC&AR-CCS(MEA)-NGR-based BtCCHP	$\eta_{ex,P}$= 10.94%, $\eta_{ex,CHP}$= 11.84%, $\eta_{ex,CCHP}$= 17.09%, $\eta_{en,P}$= 10.09%, $\eta_{en,CHP}$= 35.55%, $\eta_{en,CCHP}$= 58.4%	Tier-I GWP_P = 0.24 kg kW^{-1} h^{-1}, GWP_{CHP} = 0.07 kg kW^{-1} h^{-1}, GWP_{CCHP} = 0.04 kg kW^{-1} h^{-1}	LCOE = 1.34 $ per kW h, $LCOP_{CCHP}$ = 0.25 $ per kW h	244
COMB-sCO_2-AR-MED-based BtCCHP	$\eta_{ex,P}$= 37.16%, $\eta_{ex,CHP}$= 38.71%, $\eta_{ex,CCHP}$= 38.78%, $\eta_{en,P}$= 38.56%, $\eta_{en,CHP}$= 47%, $\eta_{en,CCHP}$= 51.93%	Tier-I GWP_{CCHP} = 0.29 kg kW^{-1} h^{-1}	LCOE = 15.57 $ per GJ	245
COMB-RC-ORC-AR-MED-based BtCCHP	$\eta_{ex,P}$= 19.38%, $\eta_{ex,CHP}$= 28.87%, $\eta_{ex,CCHP}$= 29.14%, $\eta_{en,P}$= 25.85%, $\eta_{en,CHP}$= 43.93%, $\eta_{en,CCHP}$= 54.26%	Tier-I GWP_P = 1.71 kg kW^{-1} h^{-1}, GWP_{CHP} = 0.78 kg kW^{-1} h^{-1}, GWP_{CCHP} = 0.65 kg kW^{-1} h^{-1}	LCOE = 10.28 $ per GJ	246
COMB-ORC-HE-AR-MED-based BtCCHP	$\eta_{ex,P}$= 36.42%, $\eta_{ex,CHP}$= 36.7%, $\eta_{ex,CCHP}$= 37.15%, $\eta_{en,P}$= 41.52%, $\eta_{en,CHP}$= 47.41%, $\eta_{en,CCHP}$= 67.1%	Tier-I GWP_P = 0.36 kg kW^{-1} h^{-1}, GWP_{CCHP} = 0.22 kg kW^{-1} h^{-1}		213
GSF-SOFC-GT-sCO_2-AR-HE-CCS(MEA)-based WtCCHP	$\eta_{ex,P}$= 45%, $\eta_{ex,CHP}$= 46.44%, $\eta_{ex,CCHP}$= 47.04%, $\eta_{en,P}$= 50%, $\eta_{en,CHP}$= 74.52%, $\eta_{en,CCHP}$= 87.59%			247

the recovery energy rate can be large but actually recovers limited exergy due to the low energy grade. For the improvement of the systematic thermodynamic performance, CHP and CCHP can be a good way to realize high-efficiency waste heat recovery, but the most practical way is to improve the η_{ex} of the power production process. Also, these studies reported a lower tier-I GWP of CHP and CCHP compared to that of power generation in the same system. It should be noted that without the application of CCS, neither CCHP nor CHP can reduce the total tier-I GWP of the system, but the decrease in tier-I unit GWP reflects the fact that more energy can be produced with the same total GWP. In essence, W/BtCHP and W/BtCCHP are not direct carbon reduction technologies, but they indirectly realize the same goal by improving η_{en}. Fu *et al.*[231] compared the TEE performance of 9 GSF-SOFC-GT-X BtP/CHP/CCHP systems, where X represents the possible combinations of ORC, AR, and HE from 1-stage to 3-stage. According to the results, the highest η_{en} (86.87%) and η_{ex} (50.80%) were found for the GSF-SOFC-GT-AR-HE-based BtCCHP system and GSF-SOFC-GT-ORC-based BtP system, but the η_{ex} of the former system was only 45.32% (second lowest) and the η_{en} of the latter system was 54.77% (the lowest). This indicated that for the multi-optimization of energy and exergy utilization, the key was to match the energy trade of the heat source to production. Generally, the results showed that with complexity of the increase in heat utilization, the investment cost, operation cost, and the tier-III systematic GWP also increased. Also, from the perspective of energy, the application of CHP and CCHP reported a lower LCOP than single power generation (0.102 $ per kW per h for electricity, 0.025$ for chilled water, 0.042 $ per kW per h for hot water, and 0.096 for all products), but from the perspective of exergy, the conclusion was completely opposite (0.102 $ per kW per h for electricity, 0.453 $ per kW per h for chilled water, 0.11 $ per kW per h for hot water, and 0.119 for all products). Thus, the benefit brought by W/BtP/CHP/CCHP was better using LPOW/B instead of LCOP/CHP/CCHP to avoid misunderstanding, or reporting the LC for each product separately.

As mentioned above, reducing the exergy loss in the power generation process is the key. Reactors with highly irreversible chemical reactions, heat exchangers with significant temperature differences, columns with significant pressure differences, and turbines with intensive non-isentropic flow are the main exergy destruction contributors. Consequently, the combustor, gasifier, and pyrolyzer are the main exergy destruction contributors. Given that gasification and pyrolysis are milder than combustion, some studies reported a higher η_{ex} for the gasifier and pyrolizer than the combustor (~70–80%[219,232,236] to ~55–65%[244,246,248]). FC is an electrochemical "combustor" of syngas, and a solid oxide fuel cell (SOFC) is the most popular one in the medium and large power sectors.[249] The $\eta_{ex,SOFC}$ can reach above 90%,[239,247,250] and for the complete combustion of the syngas, the SOFC is always integrated with GT or ICE, with the $\eta_{ex,SOFC\text{-}GT}$ and $\eta_{ex,SOFC\text{-}ICE}$ of around 90%.[226,236,239,247] HE between the high temperature flue gas and the agent of the power cycle is also a great source of exergy destruction due to the large temperature difference between the hot stream and cold stream. Normally, the systematic exergy destruction ratio of HE is ~10–20%.[219,232,239] When discussing GT, it always includes a subsystem from air and fuel compression to combustion and power generation. The reported $\eta_{ex,GT}$ is ~80%–85%.[198,251–253] Given that the product is high CO_2 content flue gas when applying CaL pre-combustion and oxy-combustion capture, the CCS subsystem is much simpler that of post-combustion capture. Thus, the systematic exergy destruction ratio of CCS in the oxy-combustion system can be as low as ~5%.[198,254] Alternatively, for post-combustion capture, the systematic exergy destruction ratio of CCS can be above 50% due to the temperature difference during heat exchange and pressure difference during gas–liquid separation.[198,244,255,256]

Exergoeconomic analysis results show that in the W/BtP/CHP/CCHP system, the main reactors (gasifier, combustor, and SOFC), turbines for power generation and compressors for fuel transportation, and heat exchangers with significant temperature difference (cooler, condenser, steam generator, and high-temperature recuperator) are the main exergo-cost contributors.[90,125,228,232,233,257] A consensus has been reached that for the combustion chambers of gaseous fuel, heat exchangers, turbines, and compressors as the main contributors, the $f_{c,k}$ is below 0.5, which means that for these equipment, the focus should be exergy improvement.[90,125,228,232,233,257] In the case of the gasifier, most studies reported that the $f_{c,k}$ was above 0.5, and even up to ~0.88, indicating that it is necessary to reduce the investment cost by the promotion of applications, maturation of the manufacturing process, and increased competition in the market for similar products.[90,125,228,233] The results of FC are the most questionable, with $f_{c,k}$ ranging from nearly 0.1 to 0.9809 reported, due to the lack of conducted studies as a reference, and thus it can only be suggested that further improving η_{ex} of the FC is as vital as reducing its unit cost.[125,232,233,257] Exergoenvironmental analysis indicated the same exergo-impact contributors as the exergoeconomic analysis, but the results are diverse. Yang *et al.*[258] proposed a solar-assisted GSF-ICE-ORC-AR-based BtCCHP system and reported that the $f_{b,k}$ of the main components was beyond 70%, and thus its environmental impact associated with the manufacturing, transportation, installation, operation, maintenance, retirement, and disposal processes must be reduced. Ren *et al.*[259] and Casas-Ledón *et al.*[260] further pointed out that for most components, basically the $B_{D,k}$ was the main contributor, but for the components that generated (such as gasifier, combustor for solid and gas fuel, and pyrolizer) or eventually emitted the pollutants (such as HRSG), $B_{P,k}$ could play a dominant role, causing the $f_{b,k}$ to reach above 0.5. Regarding these issues, extra effort should be paid to reduce the generation or emission of pollutants through the optimization of the reaction parameters and flue gas treatment.

Advanced exergy analysis clarifies the source and characteristics of the exergy loss. Fu *et al.*[261] investigated the effects of the gasifying agent on a GSF-OCMOB-RC-based BtP system, and reported that the gasifier, combustion chamber, and

HRSG were the main exergy destruction contributors, and the proportion of unavoidable exergy was larger than avoidable exergy. Khoshgoftar Manesh *et al.*[90] reported the advanced exergy distribution of a GSF-GT-RC-based BtP system, showing that for most components, $Ex^{en}_{D,k}$> $Ex^{ex}_{D,k}$, and $Ex^{un}_{D,k}$> $Ex^{av}_{D,k}$. Regarding the distribution of the sub-categories of advanced exergy, certain disagreements were found in the distribution of $Ex^{en,av}_{D,k}$ and $Ex^{ex,av}_{D,k}$. Hashemian *et al.*[262] proposed a solar-assisted COMB-RC-AR-MED-based BtP system with external proton exchange membrane electrolysis cell (PEMEC) to produce H_2. They showed that for the COMB, RC and MED sub-systems, $Ex^{av}_{D,k}$ was mostly $Ex^{en,av}_{D,k}$, and for the AR system, $Ex^{av}_{D,k}$ was mostly $Ex^{ex,av}_{D,k}$. The $Ex^{un}_{D,k}$ of the RC, AR and MED sub-systems was mostly cause by external factors, and the $Ex^{ex,un}_{D,k}$ and $Ex^{en,un}_{D,k}$ had similar shares in COMB sub-system. Xiao *et al.*[263] investigated the performance of a CCHP system using syngas as the fuel, and the system was based on the SOFC-GT-RC-ORC (with a steam ejector refrigerator, SER)-HE route. The results showed that for the SOFC and combustor, $Ex^{av}_{D,k}$ had a small share of ~3% of the component exergy destruction, and basically was $Ex^{en,av}_{D,k}$. In the case of turbines, HRSG and fuel/air compressors, $Ex^{en,av}_{D,k}$ was still larger than $Ex^{ex,av}_{D,k}$. Endogenous factors were responsible for the main part of $Ex^{un}_{D,k}$ in the SOFC, combustor, and turbines, while in HRSG, it was exogenous factors. Regarding the factors in RC and ORC, $Ex^{en,av}_{D,k}$ and $Ex^{ex,av}_{D,k}$ were closed. However, Ayub *et al.*[264] also proposed a GSF-SOFC-RC-CCS-based BtP system, and reported that except for torrefaction, almost all its components had a dominant $Ex^{ex,av}_{D,k}$ with a negative $Ex^{en,av}_{D,k}$, which needed further explanation. More studies on the advanced exergy analysis of W/BtE systems need to be conducted for a more in-depth and comprehensive understanding of the reason for exergy destruction, especially in the negative figure as potential results.

4.3.3 Assistance from solar energy and energy storage. Solar energy, a readily available source of renewable energy, has been a vital option as the energy input of distributed energy systems together with waste and biomass. The primary solar harnessing approaches include photovoltaic or photothermal devices, where the latter remains a more pragmatic choice.[265] Solar heat is basically utilized in the heating of the working mediums in the power cycles, and the preheating of the feedstock and gasifying agent.

Regarding the solar heating medium route, Khan *et al.*[234] found that for a COMB-RC-based WtP system with the overheating of primary steam by solar energy, although the improvement in η_{ex} from 26.74% to 37.08% brought the extra penalty of 11.76% in the total cost rate, the proposal of solar assistance was still economically feasible. Parvez *et al.*[266] also reported that for a GSF-GT-RC-SER-AR BtCCHP system, with the extra solar heat source for primary steam generation in HRSG, a considerable increase in direct normal irradiance resulted in slight gain of ~4% in η_{ex} and η_{en}, eventually reaching 62.10% and 27.71%, respectively. Moreover, about 59.18% of the exergy destruction occurred in the photothermal devices. Different passive and active efficiency enhancement configurations in a COMB-RC-based WtP system with a solar-preheated boiler feed were discussed by Behzadi *et al.*[267] They found that recovering the waste heat of flue gas and substituting the turbine extraction lines with solar collectors contributed to a considerable decrease in the GWP and LCOE, and the application of heat storage tank could promote the heat effectiveness by sacrificing the economic profit. In the case of the solar heating feedstock and agency way, Liu *et al.*[242] proposed a GSF-SOFC-ICE-AR-HE BtCCHP system, and the assistance of solar comprehensively promoted its systematic performance. It reduced the tier-I GWP_P and GWP_{CCHP} from 0.22 $ton_{CO_2,eq}$ per GJ to 0.12 $ton_{CO_2,eq}$ per GJ and 0.14 $ton_{CO_2,eq}$ per GJ to 0.09 $ton_{CO_2,eq}$ per GJ, and promoted η_{ex} and η_{en} from 34.50% to 36.60% and 54.08% to 57.50%, respectively. A similar improvement in η_{ex} of 3.17% and η_{en} of 2.11% was also observed in the CLG-GT-HE-based BtCHP system due to the solar assistance in heating the gasifying agent.[265] Mu *et al.*[189] compared the separate effect of two solar utilization ways in a CLG-GT-RC-based BtP system, and the results indicated that the use of solar energy for heating the gasifying agent was better. However, they also claimed that the coupling of solar energy was not positive in improving the systematic η_{ex} due to the lower η_{ex} of the solar collector subsystem, but it was much more meaningful in achieving comprehensive utilization of multiple energy sources and reducing greenhouse gas emissions. The utilization of solar energy could also satisfy the heat requirement of the post-combustion capture subsystem, which could avoid the interstage steam extraction from the steam turbine, without reducing the systematic power generation.[225]

The categories of photothermal devices are directly related to the thermodynamics performance. Biboum *et al.*[268] compared the application of a parabolic trough collector, linear Fresnel reflector, and solar tower in a solar-assisted COMB-RC BtP system, in which solar energy was used to generate part of the primary steam and reheat the inter-stage steam. The results showed that the application of a linear Fresnel reflector had the lowest LCOE of 0.14$ per kW per h compared to the other options (>0.2 $ per kW per h), while the application of a solar tower had the best exergo-economic and environmental performance. Consistent with the study by Qi *et al.*,[269] the cost rate and the environmental impact rate of the photothermal devices were mainly due to the life cycle of the equipment itself. Also, the photothermal devices had the profound endogenous optimization potential in exergy saving, which was also reported by Hashemian *et al.*[262] and Xiao *et al.*[263] in other solar-assisted CCHP systems.

The common energy storage systems include the compressed air energy storage (CAES) system and thermochemical energy storage (TCES) system. Cao *et al.*[190] proposed a GSF-GT-RC-AR-based BtCCHP system with CAES, and as LNG was introduced into the CAES to liquefy the compressed air, the CAES was promoted to liquid air energy storage (LAES). The proposal of LAES showed an improvement of 5.6% in $\eta_{electric}$, and an increase in η_{ex} by 6.5% could be realized by choosing a suitable liquid air storage pressure. The overall η_{ex} and η_{en} of the LAES system around the year was ~70% and

~90%, respectively. Razmi *et al.*[270] reported that the round trip efficiency (RTE) of CAES in a GSF-GT-RC-based BtCHP system was about 34% to 43% with different operational parameters. Hai *et al.*[271] further integrated an ORC subsystem to recover the waste heat in a hot air stream, and the generated power was transmitted to a PEMEC for hydrogen production, reporting an optimized η_{ex} of 39.22%.

The common CAES stores air for energy production, while Xue *et al.*[272] proposed a COMB(MSW)&GT(biogas)-RC-based WtP system with CAES system, which used stored air to meet the requirement of air during combustion and replaced the original compressor of GT, reporting an RTE of 69.55% and increase in η_{en} by 6.5%. Conventional TCES systems mainly utilize the hydration and dehydration process of $CaO/Ca(OH)_2$ to realize the storage and utilization of energy. Uchino *et al.*[273,274] investigated the performance when a TCES system was integrated with the COMB-ORC BtP system, reporting that utilizing the waste energy in the hot water or low temperature steam in the TCES could improve the η_{en}, and the fluctuation of biomass energy could be basically absorbed through the energy storage process, with an LC of storage of 0.92–2.37 $ per kW per h. Yasui *et al.*[191] further pointed out that integrating RC with TCES was more cost-effective than integrating ORC, given that its higher power generation efficiency ensured a higher power generation amount of unit stored heat, and then the levelized cost of storage could be reduced to 0.20–0.80 $ per kW per h. The stored energy efficiency and the RTE were 58.2% and 13.7%, respectively.

Utilizing part of electricity and thermal output in the waste or biomass to energy system for H_2 production can be seen as an energy storage way, which is reported in many CHP and CCHP systems.[122,275,276] However, the production of hydrogen brings extra exergy destruction and economic cost, and it was estimated that in a solar and geothermal-assisted GSF-GT-AR-HE BtCCHP system with PEMEC, the unit exergy cost of hydrogen fuel was almost 4-times higher than that of electricity (18.72 $ per GJ to 4.29 $ per GJ).[277] Ding *et al.*[278] also reported a similar conclusion for a biomass-methane-solar driven CCHP system with alkaline electrolysis cell (AEC). The RTE of hydrogen storage was reported to be around 45.5%, which consisted of PEMEC, PEMFC, H_2 storage tank, battery, and charging station.[279] Therefore, the design of the hydrogen production unit should be carefully considered according to the local consumption demands and the financial feasibility assessment.

4.3 Oriented production of commercial fuel

The production of commercial gaseous fuel from waste or biomass is attracting increasing attention. The section focuses on the comprehensive performance of waste or biomass to fuel (W/BtF) systems (Table 6). Fig. 10 shows the common technical routes of waste or biomass to H_2 (W/BtH), NH_3 (W/BtA), SNG (W/BtSNG), methanol (W/BtMeOH), and DME (W/BtDME) systems.

4.3.1 Hydrogen production. The main routes for H_2 production can be divided according to the following two aspects. Considering the initial thermochemical process, it includes GSF-based, PY-based, CLC-based, and CLG-based routes. Considering intermediate reaction, it includes water gas shift (WGS)-based, sorption-enhanced water gas shift (SEWGS)-based, and sorption-enhanced gasification (SEG)-based routes. In most cases, a fuel separation and purification (FSP) subsystem is necessary, where the pressure swing adsorption (PSA) facility is the most common one.

The GSF-WGS-based route is the most fundamental H_2 production route. Regarding the choice of gasification agent, Hosseingholilou *et al.*[280] reported that steam was the preferred choice, and the BtH system based on the GSF-WGS-PSA route yielded the highest η_{ex} of 48% and the lowest LCOH at 1.77 € per kg_{H_2} compared to air (28% and 3.88 € per kg_{H_2}) and CO_2 (46% and 3.83 € per kg_{H_2}) as the agent. Given that the maximum CO conversion efficiency was around 90–95% and the H_2 separation efficiency in FSP was around 80–90%. The residual gas still could be further utilized for heat or power production to recover the remaining exergy in the residual gas utilization (RGU) subsystem. Afzal *et al.*[24] investigated the performance of a WtH system based on the same route, reporting that the when MPW (mixed plastic waste) was the feedstock, the minimum selling price (MSP) was 0.70 $ per kg_{H_2}, and tier-III GWP was 10.80 $kg_{CO_2,eq}$ $kg_{H_2}^{-1}$. Compared to H_2 production based on SNG reforming, the MPW-based H_2 production needed more process fuel, and thus the systematic performance can be promoted by the introduction of renewable energy and technological refinements in gasification. If using MSW as the throughput, it gains an MSP of 0.55 $ per kg_{H_2} and tier-III GWP of 15.6 $kg_{CO_2,eq}$ $kg_{H_2}^{-1}$, and the tier-III GWP is reduced to 2.6 $kg_{CO_2,eq}$ $kg_{H_2}^{-1}$ with the carbon credit created by avoiding landfill. Recovering the exergy in the residual gas can play a significant role. Ma *et al.*[281] reported that η_{ex} of RC as the RGU subsystem reached about ~30%. Lümmen *et al.*[282] proposed that the generated heat from residual gas combustion can be used for regenerating the tar reformer catalyst and providing process heat.

For low-carbon H_2 production, the capture of CO_2 is always integrated in the acid gas removal (AGR) subsystems in the WGS-based route, and the results vary in a wide range. The research group of Wang *et al.*[283–286] conducted several studies on the food waste, sludge, and medical waste to H_2 system based on the GSF-WGS-AGR-GSP route, and the η_{ex} fluctuated in the range of 31.44% to 70.84% due to the difference in feedstock characteristics and the AGR subsystem operation. In the case of the WtH system based on the same route, Ren *et al.*[287] reported that η_{ex} and η_{en} were 39.34% and 46.39%, respectively. However, it is inconsistent that the promotion in GWP worsens the thermal and economic performance due to the extra energy consumption. With a high CCR, the tier-I GWP can be very small. Sun *et al.*[87] reported that the η_{ex} and tier-I GWP of an MSW to hydrogen system based on the GSF-WGS-AGR-PSA-RGU-based route were 46.70% and 0.91 $kg_{CO_2,eq}$ $kg_{H_2}^{-1}$, respectively. Zhou *et al.*[288] reported that the η_{en} and tier-III GWP of a WtH system based on a similar route were ~57% and 5.18 $kg_{CO_2,eq}$ $kg_{H_2}^{-1}$, respectively, and the indirect carbon emission due to the extra energy consumption

Table 6 Recent representative studies on W/BtF systems

System description	Thermodynamic performance	GWP performance	Economic performance	Ref.
H_2 production				
GSF-WGS-AGR-PSA	η_{ex}= 39.34–48.32%, η_{en}= 46.39–55.71		LCOH = 17.33–19.97 ¥ per kg_{H_2}	287
GSF-WGS-AGR-PSA	η_{ex}= 31.44%		LCOH = 2449.82 $ per t_{H_2}	283
GSF-WGS-AGR-PSA-RGU	η_{en}= 57%	Tier-III GWP = 5.18 $kg_{CO_2,eq}$ $kg_{H_2}^{-1}$		288
GSF-WGS-AGR-PSA-RGU	η_{ex}= 32.38%	Tier-III GWP = 3.93 $kg_{CO_2,eq}$ $kg_{H_2}^{-1}$	LCOH = 4.76 ¥ per kg_{H_2}	289
GSF-WGS-AGR-PSA-RGU		Tier-III GWP = −18.8–2.99 $kg_{CO_2,eq}$ $kg_{H_2}^{-1}$	MSP = ∼0.25–3 $ per kg_{H_2}	291
GSF-WGS-AGR-PSA-RGU	η_{en}= 44.35%	Tier-III GWP = 4.36 $kg_{CO_2,eq}$ $kg_{H_2}^{-1}$	DPP = 4.72	294
GSF-SEWGS	η_{ex}= 45.2%, η_{en}= 62.1	Tier-I GWP = 5.16 $kg_{CO_2,eq}$ $kg_{H_2}^{-1}$		303
SEG-PSA-RGU	η_{en}= 48.7%	Tier-I GWP = 1.4 $kg_{CO_2,eq}$ $kg_{H_2}^{-1}$	LCOH = 4.5–5.1 € per kg_{H_2}	210
GSF-SEWGS-PSA-RGU	η_{ex}= 57.5%		LCOH = 6.08 $ per kg_{H_2}	308
CLC (solar assisted)	η_{ex}= 41.0–52.1%, η_{en}= 41.1–49.1%		LCOH = 1.70 $ per kg_{H_2}	309
CLG-WGS-PSA	η_{en}= 57.66%	Tier-I GWP = 9.55 $kg_{CO_2,eq}$ $kg_{H_2}^{-1}$	LCOH = 2.94 $ per kg_{H_2}	310
SECLG-PSA	η_{ex}= 45.3%, η_{en}= 64.6%			311
GSF-CLC	η_{ex}= 32.72–49.89%		LCOH = 2.91–3.68 $ per kg_{H_2}	312
GSF-CLC	η_{ex}= 49.26%, η_{en}= 64.9%	Tier-I GWP = 38.1 $kg_{CO_2,eq}$ MW^{-1} h^{-1}	LCOH = 2.25 $ per kg_{H_2}	313
GSF-CLC-RGU-AGR	η_{en}= 66.6–72.2%	Tier-III GWP = 5.56–11.53 $kg_{CO_2,eq}$ $kg_{H_2}^{-1}$	LCOH = 2.82–3.05 $ per kg_{H_2}	314 and 315
NH_3 production				
GSF-WGS-AGR-FS with ASU (solar assisted)	η_{ex}= 36.7%, η_{en}= 44.6%			317
GSF-WGS-AGR-FS with ASU	η_{ex}= 53.5%			316
SEG-PSA-FS with ASU & RC	η_{en,NH_3}= 44.52%, $\eta_{en,total}$= 52.14%	Tier-III GWP = 0.73 $kg_{CO_2,eq}$ $kg_{NH_3}^{-1}$	LCOA = 0.42–0.69 $ per kg_{NH_3}	318
CLC-FS-RGU	η_{ex,NH_3}= 44.36%, $\eta_{ex,total}$= 46.09%		LCOA = 35.56 $ per GJ	319
GSF-SECLC-FS			LCOA = 0.49 $ per kg_{NH_3}	321
CLC-FS-RGU	η_{en}= ∼38–41%			320
SNG production				
GSF-FS-AGR	η_{ex}= 60.38%, η_{en}= 65.69%		LCOSNG = 15.17 $ per GJ	326
GSF-AGR-FS	η_{en}= 43.40%	Tier-II GWP = 48.65–92.64 $kg_{CO_2,eq}$ GJ^{-1}	LCOSNG = 17.5–21.8 $ per GJ	327
GSF-AGR-FS with SOEC	η_{ex}= 61–64%			328
COMB-FS with PEMEC		Tier-I GWP = 1.25 $kg_{CO_2,eq}$ Nm_{SNG}^{-3}	LCOSNG = 5 $ per MW per h	329
GSF-WGSR-AGR-FS	η_{ex}= 81%		LCOSNG = 10–28 $ per GJ	330
GSF-SOEC	η_{en}= 68%		LCOSNG = 23–30 $ per GJ	
GSF-WGSR-AGR + SOEC-FS	η_{ex}= 66%		LCOSNG = 26–32 $ per GJ	
MeOH production				
GSF-AGR-FS-FSP		Tier-II GWP = 2.32 $kg_{CO_2,eq}$ kg_{MeOH}^{-1}	LPOMeOH = 0.41 $ per kg_{MeOH}	333
GSF-AGR-FS-FSP		Tier-III GWP = 0.67 $kg_{CO_2,eq}$ kg_{MeOH}^{-1}	LCOMeOH = 502 $ per ton_{MeOH}	334
GSF-AGR-FS-FSP	η_{ex}= 37.92%	Tier-III GWP = 3.21 $kg_{CO_2,eq}$ kg_{MeOH}^{-1}	LCOMeOH = 0.58 $ per kg_{MeOH}	335
GSF-AGR-FS-FSP-RGU	η_{ex}= 48%, η_{ex}= 61% (solar assisted)		LCOMeOH = 632 $ per ton_{MeOH} LCOMeOH = 392 $ per ton_{MeOH} (solar assisted)	336
GSF-SEWGS-FS-FSP-RGU	η_{ex}= 64%	Tier-III GWP = 4.39 $kg_{CO_2,eq}$ kg_{MeOH}^{-1}		340
GSF-mPSA-FS-FSP	η_{ex}= 25.44%, η_{en}= 38.57%			341
GSF-mPSA-FS-FSP	η_{ex}= 50.93%, η_{en}= 54.08%		LCOMeOH = 41.09 $ per GJ	118
GSF-AGR-FS-FSP with WEV	η_{ex}= 71.63%, η_{en}= 78.13%	Tier-II GWP = 0.61 $kg_{CO_2,eq}$ kg_{MeOH}^{-1}	LCOMeOH = 103 $ per ton_{MeOH}	342
GSF-AGR-FS-FSP with AEC	η_{ex}= 64–69%, η_{en}= 67–68%			343 and 344
GSF-AGR-FS-FSP-RGU with AEC	$\eta_{en,MeOH}$= 59.5%, $\eta_{en,total}$= 85.8%		LCOMeOH = 511 € per ton_{MeOH}	345
GSF-FS-RGU with SOEC	η_{ex}= 68.98%		LCOMeOH = 529.02 € per ton_{MeOH}	348
GSF-SOEC-FS-RGU	η_{ex}= 68.76%, η_{en}= 79.86%		LCOMeOH = 526.49 € per ton_{MeOH}	348
GSF-AGR-SOEC-FS-RGU	η_{ex}= 67.04%, η_{en}= 77.53%		LCOMeOH = 582.43 € per ton_{MeOH}	348

Table 6 *(Contd.)*

System description	Thermodynamic performance	GWP performance	Economic performance	Ref.
GSF-AGR-FS	η_{ex} = 41.5%		LCOMeOH = 406.09 $ per ton_{MeOH}	353
GSF-FS with SOEC	η_{ex} = 60.8%		LCOMeOH = 355.89 $ per ton_{MeOH}	353
GSF-FS with SOEC	$\eta_{en,MeOH}$ = 60.42%, $\eta_{en,total}$ = 86.65%		LCOMeOH = 706 € per ton_{MeOH}	355
GSF-WGS-ARG-FS	η_{ex} = 38.5%	Tier-II GWP = 2.88 $kg_{CO_2,eq}$ kg_{MeOH}^{-1}	LCOMeOH = 2019.29 $ per ton_{MeOH}	356
GSF-FS with SOEC	η_{ex} = 53.58%	Tier-III GWP = 1.07 $kg_{CO_2,eq}$ kg_{MeOH}^{-1}	LCOMeOH = 2334.27 $ per ton_{MeOH}	356
GSF-FS with NG pyrolysis	η_{ex} = 63.95%	Tier-III GWP = 1.41 $kg_{CO_2,eq}$ kg_{MeOH}^{-1}	LCOMeOH = 1610 $ per ton_{MeOHv}	356
GSF-FS with NG CL reforming	η_{ex} = 55.35%	Tier-III GWP = 1.13 $kg_{CO_2,eq}$ kg_{MeOH}^{-1}	LCOMeOH = 1402.58 $ per ton_{MeOH}	356
GSF-AGR-FS with NG pyrolysis	η_{ex} = 49–56%	Tier-III GWP = −141–636 $kg_{CO_2,eq}$ per ton_{MeOH}	LCOMeOH = 440–470 $ per ton_{MeOH}	349
DME production				
GSF-sCO$_2$-WGS-AGR-FS	η_{ex} = 41.12%, η_{en} = 49.54%		LCODME = 286–686 $ per ton_{DME}	357
COMB-FS with SOEC	η_{ex} = 57.37%	Tier-II GWP = 4.38 $kg_{CO_2,eq}$ kg_{DME}^{-1}	LCODME = 653.9 $ per ton_{DME}	85
GSF-WGS-AGR-FS	η_{en} = 59.5%	Tier-II GWP = 1.45 $kg_{CO_2,eq}$ kg_{DME}^{-1}		359 and 360

of AGR was about a half of the captured CO_2. The effects of the CCR level were investigated by Ma *et al.*[289] In the BtH system based on the GSF-WGS-AGR-PSA-RGU-based route, the integration of an AGR subsystem (Rectisol) decreased the systematic η_{en} from 37.88% to 32.38%, and with the CCR of 0–95%, the changes in LCOH and tier-III GWP were in the range of 3.98 to 4.76 ¥ per kg_{H_2} and 5.39 to 3.93 $kg_{CO_2,eq}$ $kg_{H_2}^{-1}$, respectively. Furthermore, it should be also noted that the promotion in the GWP indicator does not represent the same situation as other LCA environmental indicators, given that the removal of CO_2 in the CCS subsystem reduced the GWP by 42–67%, but increased all the environmental impacts by 9–117%, which was attributed to the chemical and energy consumption.[290] According to the results from the above-mentioned studies, the exergy loss is mainly contributed by the GSF, AGR, and RGU subsystems. Process heat recovery can promote the thermal efficiency, especially when the heat consumption of AGR can be self-sustained, but Ayub *et al.*[91] reported that a heat exchanger with a significant temperature difference can be responsible for remarkable exergy loss and exergy cost. Also, the low CO conversion efficiency and H_2 separation efficiency can cause significant loss in the PSA subsystem due to the product loss in the residual gas.

Regarding the variation in economic performance, the feedstock purchasing price or treatment subsidy, and the carbon tax or credit have a remarkable effect. If the carbon tax is based on tier-I GWP, the economic fluctuation can be low, given that most of the CO_2 is captured. If it is based on tier-III GWP, Wu *et al.*[291] pointed out that the cost of biomass accounted for at least 30% of the TPC in a BtH system based on the GSF-WGS-AGR-PSA-RGU route, and a high carbon tax enhanced the advantages of BtH systems. Lan and Yao[290] also claimed that if the carbon tax was close to the CCS cost and the feedstock cost was low, the H_2 production from waste plastic could be more competitive. The above-mentioned two studies reported that an ideal minimum MSP is about 1 $ per kg_{H_2}.

In the WtH system, the waste treatment subsidy is a vital part of its income. Typically, for a system inputting high-moisture waste, the low H_2 yield does great harm to its systematic performance. Shi *et al.*[292] pointed out that for a WtH system, its LCOH was 6.66 $ per kg_{H_2} and its H_2 yield was 35.24 kg_{H_2} per ton_{waste}, and consequently a subsidy for waste treatment of 115.65 $ per ton_{waste} was necessary to ensure economic profit. Some hazardous waste can be a good feedstock choice owing to their foreseeable H_2 yield and high treatment subsidy. Regarding a WtH system using medical waste as feedstock, its H_2 yield was reported to be about 160 kg_{H_2} per ton_{waste}, and the waste treatment tipping fee contributed about 47% of its total income.[118]

The optimization of the upstream thermochemical process can be influential. For the pretreatment of the feedstock, Zhao *et al.*[293] reported that in the WtH system based on GSF-WGS-PSA-RGU route, the torrefaction of food waste before gasification increased the quality and yield of the syngas, which promoted η_{ex} and η_{en} from 57.2% to 59.6% and 56.8%

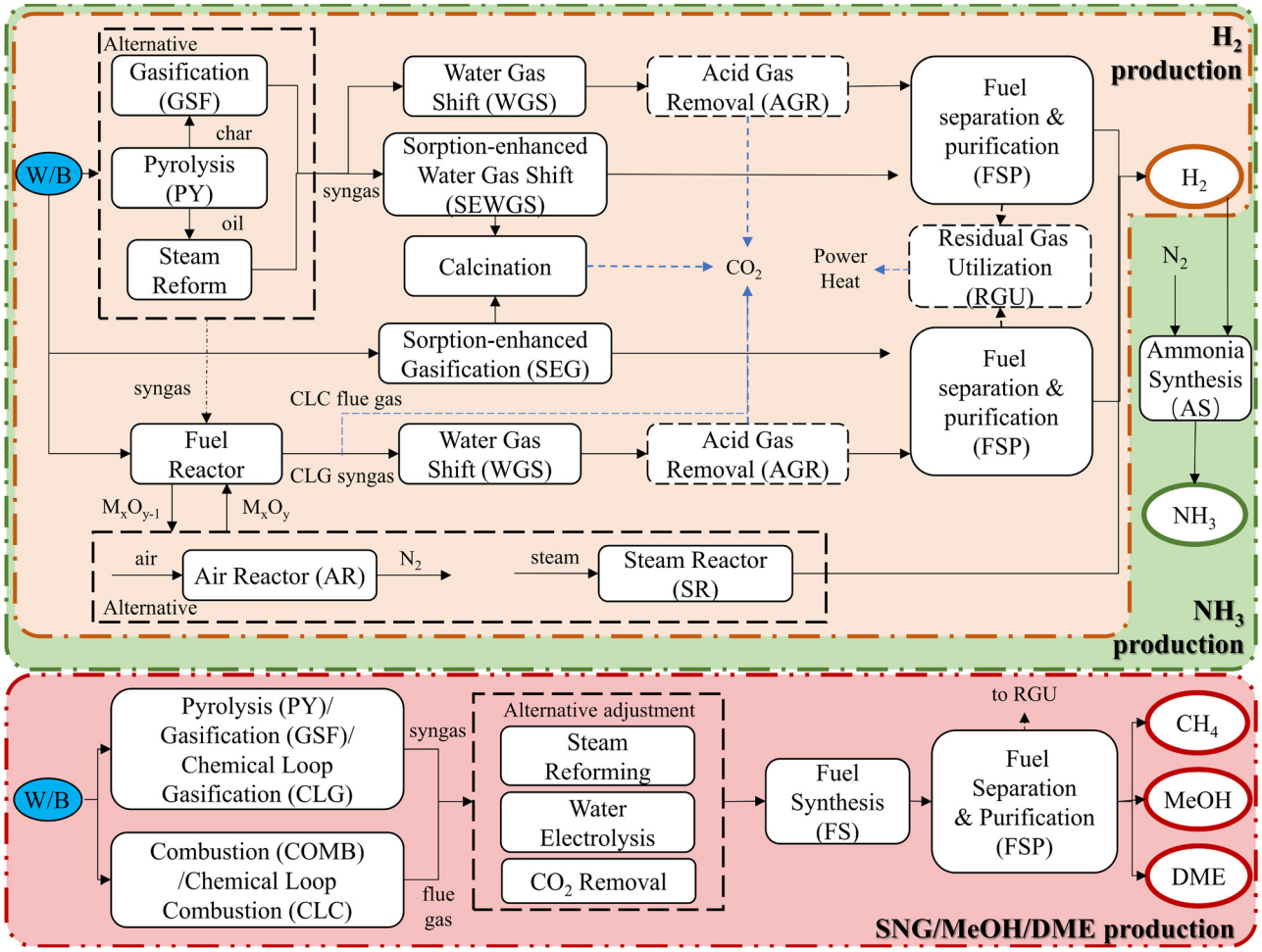

Fig. 10 Technical routes of W/BtH, W/BtA, W/BtSNG, W/BtMeOH, and W/BtDME systems.

to 58.9%, respectively. However, the MSP increased from 2.48 \$ per kg_{H_2} to 2.90 \$ per kg_{H_2}. Regarding the reforming of components not active in WGS subsystems, Li *et al.*[294] evaluated the application of methane tri-reforming in a BtH system based on the GSF-WGS-AGR-PSA-RGU route, reporting that η_{en} increased from 37.88% to 44.35%, and the tier-III GWP decreased from 5.39 to 4.36 kg_{CO_2} $kg_{H_2}^{-1}$, but the DPP increased from 4.5 to 4.72 years. If the gasification model considers the generation of tar, Shamsi *et al.*[295] noted that the reforming of tar in the syngas could promote the H_2 yield. In the thermal supply of the gasification process, Ren *et al.*[287] investigated the application of direct melting, and autothermal gasification in a WtH system based on the GSF-WGS-AGR-PSA route. The results showed that for autothermal reforming, although adding extra biochar resulted in a higher H_2 yield and thermal performance, utilizing self-generated syngas was a more economical option than adding extra biochar because of the remarkable decrease in the feedstock cost and the investment of ASU and AGR. Consequently, self-sustained autothermal gasification with direct melting was suggested to have the most promising potential with η_{ex} of 40.11%, η_{en} of 47.23%, and LCOH of 18.53 ¥ per kg_{H_2} compared to self-sustained autothermal gasification without direct melting (41.21%, 48.59%, and 17.33 ¥ per kg_{H_2}), and external energy sustained autothermal gasification with direct melting (48.32%, 55.71%, and 19.97 ¥ per kg_{H_2}). Wu *et al.*[291] also discussed the performance of a BtH system under fully self-sustained, partially self-sustained, and external supply electricity consumption conditions with the combustion of PSA residual gas or internal syngas. The results indicated that the case of fully self-sustained had the best tier-III environmental performance, and compared to the other two cases, its MSP was advantageous only with a carbon tax of over 70 \$ per ton_{CO_2}. The application of DFB separates the combustion and the gasification process in two reactors. Poluzzi *et al.*[296] evaluated the effect of the application of BFB and DFB in the BtH system based on the GSF-WGS-CCS-PSA-RGU-CCS route. The results showed that applying DFB resulted in a higher H_2 yield by 1.3%, but lacked advantages in the equivalent fuel efficiency (50.15% to 55.36%) and LCOH (4.51 € per ton_{H_2} to 4.33 € per ton_{H_2}).

The choice of initial thermochemical process has a great impact. Gasification can convert the carbon content into

syngas at the maximum level, while in the case of pyrolysis, carbon is converted to the multigeneration products of char, oil, and gas. If the pyrolysis multi-product in not fully utilized in H_2 production, the H_2 yield would decrease. Demol *et al.*[297] proposed a BtH system based on the autothermal GSF/PY-partial oxidation (POX)-GSP-RGU route. Oxygen was used as the gasification agent for self-sustained heating, and the oxidant for the POX of tar. The results showed that because of the extra production of char in the PY-based system, the GSF-based system showed higher H_2 yields (26 to 18 kg_{H_2} per $ton_{biomass}$) and higher heat efficiency due to the production of hot water (60% to 49%), but a slightly lower η_{en} (77.8% to 80.4%) than the PY-based route, given that the eventual utilization of char was not considered. In the PY-based system, the multi-products can be utilized by the combination of several chemical processes for the maximum H_2 production. Nouwe Edou *et al.*[298] proposed H_2 production systems with CCS based on the biomass gasification scheme, pyrolysis with bio-oil gasification scheme, and pyrolysis with bio-oil reforming scheme. In all the gasification subsystems, the char was combusted for heat supply. The results showed that the H_2 yield of the two PY-based systems (~92 kg_{H_2} per ton) was much higher than that of the GSF-based system (~30 kg_{H_2} per $ton_{biomass}$), which could be attributed to the increased contribution of hydrogen atoms in the reactant steam to eventual hydrogen gas product in the PY-based system. When considering the selling of captured CO_2 with the price of 120 $ per ton, the system based on fluidized bed gasification had the lowest MSP of 3.4 $ per kg_{H_2} compared to that based on pyrolysis with bio-oil gasification scheme (4.83 $ per kg_{H_2}) and pyrolysis with bio-oil reforming scheme (7.30 $ per kg_{H_2}). Situmorang *et al.*[299] proposed an PY-based BtH system. The hydrogen was produced from the WGS-PSA-RGU-based route fed by pyrogas and bio-oil and the CLC-based route fed by char. They claimed that the proposed system could increase the H_2 production efficiency from biomass by more than 50% than the direct CLC-based system. When the BtH system involved the utilization of multi-feedstocks, the application of GSF and PY could be based on the feedstock characteristics. Li *et al.*[300] proposed that the gasification of herbaceous biomass can provide heat to drive the fast pyrolysis of woody biomass, and the integration not only ensured the stability of the primary product, but also solved the problems of tar production and low efficiency caused by the high lignin content in woody biomass.

SEWGS and SEG are enhanced versions of the conventional GSF-WGS-based H_2 production, with the addition of a CO_2 sorbent. Most commonly, CaO is considered the optimal CO_2 sorbent due to its low cost and wide abundance, and consequently CaL is also the most promising form of SEWGS and SEG. Technically, based on *in situ* CO_2 capture, the reaction equilibrium of GSF and WGS is driven toward to the generation of H_2, which leads to a higher H_2 yield and purity.[301] However, given that the regeneration temperature of the common sorbents (MEA, MDEA, DPEG, methanol, *etc.*) in the AGR subsystem is much lower than that of Ca-based sorbents, more high-level energy is required in the SEWGS-based system. Therefore, unlike the thermal duty of the reboiler in the AGR subsystem, which can be satisfied by steam, the calcination of $CaCO_3$ usually needs fuel to be combusted or electrical heating, and the added fuel can be an external source or internal by-products (such as char, syngas, and residual gas). Chu *et al.*[302] proposed a PY-GSF-SEWGS-based WtH system, in which the pyrogas was combusted with external CH_4 to satisfy the heat requirements, and the char was gasified with the recirculated CO_2-rich flue gas. The proposed system exhibited a better performance in terms of H_2 yield, η_{ex}, and η_{en} with values of 30.6 kg_{H_2} per ton_{waste}, 31.83%, and 35.96% and the enhancement of 14.4 kg_{H_2} per ton_{waste}, 14.87%, and 11.27% compared to a similar system based on WGS without CCS. However, this was at the cost of an increase in CH_4 consumption from 64.57 to 114.78 kg_{CH_4} per ton_{waste}. Zhang *et al.*[303] reported that the η_{ex}, η_{en}, and tier-I GWP of a BtH system based on the GSF-SEWGS route with an external heat supply to the calcinatory was 45.20%, 62.10%, and 5.16 $kg_{CO_2,eq}$ $kg_{H_2}^{-1}$, respectively. Some studies discussed the integration of solar energy. Khosravi *et al.*[304] proposed a WtH system based on the SEG-PSA route, in which solar energy was introduced into the calciner through a heliostat field and solid storage, and the heat from SEG was recovered for power production. They reported the η_{ex} of 70.70% and η_{en} of 70.74% (8.55% contributed by power production). The introduction of solar energy substituted ~29% of the total energy input. Zhang *et al.*[305] investigated the integration of a solar-driven thermochemical heat storage (THS) subsystem into a PY-GSF-SEWGS-based B&CoaltH system. The THS subsystem was operating based on the reversible hydration/dehydration reactions of CaO. The results showed that the integration of THS enhanced the carbonation reactivity of CaO, and comprehensively improved the η_{ex}, η_{en}, and H_2 yield by 5.0%, 5.1%, and 17.4%, respectively.

The discussion on the energy self-sustaining situation of WGS-based and SEWGS-based systems is arguable. Santos *et al.*[210] compared WtH systems based on the GSF-WGS-PSA-RGU and SEG-PSA-RGU routes, reporting that both systems realize energy self-sustenance and the SEG-based system could promote the H_2 yield ($\eta_{en,H_2,SEG}$ = 48.7% and $\eta_{en,H_2,GSF}$ = 47.7%), with the cost of larger electricity requirements ($\eta_{en,total,SEG}$ = 49.3% and $\eta_{en,total,GSF}$ = 53.7%), respectively. The tier-I GWP decreased significantly from 21.7 to 1.4 $kg_{CO_2,eq}$ $kg_{H_2}^{-1}$ with the application of SEG. With the gate fee of 0–40 € per ton_{MSW} and carbon tax of 0–39.6 € per ton_{CO_2}, the LCOH was 2.1–3.2 € per kg_{H_2} and 4.5–5.1 € per kg_{H_2} for the GSF-based system without CCS and SEG-based system when 40% of the CO_2 emission was considered biogenic, respectively. The CAC was 114.9 € per ton_{CO_2}. Dziva *et al.*[306] also compared BtH systems based on the GSF-WGS-PSA-RGU and GSF-SEWGS-PSA-RGU routes, claiming that the GSF-based system needed an extra energy supply, while the SEWGS-based system was energy self-sufficient. The application of SEWGS promoted the η_{en,H_2} and $\eta_{en,total}$ from 50.71% to 51.86% and 48.47% to 51.96%, respectively. Furthermore, Dziva *et al.*[307] pointed out that the integration of SEG and SEWGS promoted η_{en} from 48.8% to 58.7% with an increase of 12% in H_2 yield

compared to the single SEG-based system, but the cost brought by the extra fuel to the calciner was not reported. Tang *et al.*[308] reported that both the GSF-SEWGS-PSA-RGU-based and GSF-WGS-AGR-PSA-RGU-based WtH systems needed an external energy supply. The results showed that the application of SEWGS *in situ* integrated the steam reforming and CO_2 capture processes and reduced the exergy loss of these two processes, which contributed to slight advantages in η_{ex} (~57.5% to ~54.0%). Given that the temperature for the calcination of the sorbent was much higher than the re-boiling of the DEPG sorbent, the recovery of the high-level energy from the SEWGS section was much more vital. Also, it showed a comprehensive advantageous environmental performance in all midpoint and endpoint LCA indicators compared to the conventional route, which could be mainly attributed to the higher H_2 yield (117 kg_{H_2} per ton_{waste} to 113 kg_{H_2} per ton_{waste}). Although the application of SEWGS resulted in a larger TPC, considering the improvement in total H_2 production, it still had preferable LCOH (~6.08 \$ per kg_{H_2} to ~6.20 \$ per kg_{H_2}). Overall, the SEG-based and SEWGS-based systems show remarkable application potential, typically when a cleaner energy source is available.

CL provides an innovative route to produce high-purity H_2 from SR without complex separation and purification, with an oxygen carrier (OC) acting as a heat and oxidant carrier at the same time. Firstly, CL can be an alternative to GSF and PY as the primary thermochemical process. Chen *et al.*[309] proposed a solar-assisted BtH system based on CLC, in which the heat in the high-temperature CO_2-rich flue gas and H_2-rich stream was recovered for power generation. The η_{ex} and η_{en} was in the range of 41.0%–52.1% and 41.1%–49.1% with a change in solar energy availability, respectively. The supplemental input of solar exergy avoided the splitting of exergy from FR, and the exergy from FR was directly sent to SR, which increased the H_2 yield. The LCOH of the proposed system was 1.70 \$ per kg_{H_2}.

CLG can be an alternative to GSF with the application of a DFB. Qi *et al.*[310] proposed a WtH system based on the CLG-WGS-PSA route, reporting the η_{en} of 57.66%, tier-I GWP of 9.55 $kg_{CO_2,eq}$ $kg_{H_2}^{-1}$, and LCOH of 2.94 \$ per kg_{H_2}. They claimed that the CLG-based η_{en} was higher than the GSF-based η_{en}, given that the existence of OC accelerated the heat transfer process from AR to SR. CaL can be also integrated with CL, which is called sorption enhanced chemical looping gasification (SECLG). Liu *et al.*[311] compared BtH systems based on the SEG-PSA and SECLG-PSA routes with waste heat recovery for power production, and under the optimized carbonator temperature (T_{car}) for autothermal operation, the SECLG-based system (η_{ex} of 45.3% and η_{en} of 64.6%, T_{car} = 740 °C) had a better performance than the SEG-based system (η_{ex} of 39.0% and η_{en} of 55.7%, T_{car} = 720 °C). They noted that the application of SECLG can lower the tar content and improve the H_2 concentration in the syngas, with the challenge of the extra cost and unsynchronized lifetime of OC and sorbent. Moreover, if oxyfuel combustion is further applied in the calciner, the higher calcination temperature would further harm the thermal performance.

Secondly, the gas product can be complete oxidized in the FR, and the production of H_2 is completely conducted in the SR. Rai *et al.*[312] proposed a GSF-CLC-based WtH system with direct CCS and HRSG. A printed circuit board (PCB) was gasified to produce syngas and OC, and a part of the syngas was sent to the CLC subsystem. They reported the $\eta_{en,PCB}$ of 32.72% and $LCOH_{PCB}$ of 3.68 \$ per kg_{H_2}, and if the waste polypropylene (PP) was co-disposed in the FR, both the $\eta_{en,PCB\ \&\ PP}$ and $LCOH_{PCB\ \&\ PP}$ improved to 49.89% and 2.91 \$ per kg_{H_2}, respectively. The co-disposal of e-waste and MSW can lead to a positive synergism for the effective production of value-added products. Mallick *et al.*[313] investigated the performance of a GSF-CLC-based WtH system with electrical switch waste (ESW) and computer keyboard plastic waste (CKPW). Under 100% H_2 production, they reported the $\eta_{ex,ESW}$ of 49.26%, $\eta_{en,ESW}$ of 64.92%, tier-I GWP of 38.1 $kg_{CO_2,eq}$ MW^{-1} h^{-1}, and $LCOH_{ESW}$ of 2.25 \$ per kg_{H_2}. In the case of CKPW with higher LHV, the $\eta_{ex,ESW}$, $\eta_{en,ESW}$, and $LCOH_{ESW}$ increased to 68.44%, 72.35%, and 1.30 \$ per kg_{H_2}, respectively. Also, it was strongly suggested to utilize the chemical energy content in H_2 than to use the sensible heat for power production to reduce the exergy loss. Wu *et al.*[314,315] proposed a GSF-CLC-based BtH system with CCS (MEA) and HRU subsystems, reporting the η_{en} of 66.6%, CCR of 92.8%, tier-III GWP of 5.65 $kg_{CO_2,eq}$ $kg_{H_2}^{-1}$, and LCOH of 3.05 \$ per kg_{H_2}, with air as the gasifying agent. When substituting air with O_2, the η_{en}, CCR, and LCOH improved to 72.2%, 9.15%, 2.82 \$ per kg_{H_2}, respectively, with a worse tier-III GWP to 11.53 $kg_{CO_2,eq}$ $kg_{H_2}^{-1}$ due to the increased energy consumption of ASU. If considering the carbon credit created by the captured CO_2, the O_2 case achieved more efficient *in situ* gas product separation, resulting in a greater tier-III GWP of −17.00 $kg_{CO_2,eq}$ $kg_{H_2}^{-1}$ than the air case (−15.13 $kg_{CO_2,eq}$ $kg_{H_2}^{-1}$). Xu *et al.*[283] compared the performance of WtH systems based on the GSF-WGS-AGR-GSP and GSF-CLC routes. The results showed that although the GSF-CLC-based system had a lower H_2 yield due to the successive oxidation of oxygen carriers in SR and AR, it still had a better performance in η_{ex} (54.31% to 31.44%), tier-I GWP, and LCOH (1.93 \$ per kg_{H_2} to 2.45 \$ per kg_{H_2}), given that the capturing of CO_2 in the GSF-CLC-based system did not require an extra separation process.

4.3.2 Ammonia production. The W/BtA process is an extension of the W/BtH process, given that the H_2 product of the W/BtH system is further utilized for the synthesis of NH_3, most commonly with N_2 from the internal source. The Haber–Bosch reaction ($N_2 + 3H_2 \leftrightarrow 2NH_3$) is the best known NH_3 synthesis process. For the conventional BtA system based on the GSF-WGS-AGR-fuel synthesis (FS) route with ASU, Xu *et al.*[316] reported the η_{ex} of 53.5%, and the energy consumption of NH_3 (EC_{NH_3}) of 36.33 GJ per ton_{NH_3}. Then, the BtA system was retrofitted to achieve the classified utilization of materials and simple and efficient capture of CO_2 in the aspects of removing the WGS, replacing the HRSG Rankine cycle with the Allam cycle, and replacing the AGR with the PSA. As a result, by sacrificing the NH_3 yield per

unit biomass (by about 55%) and η_{ex} (by about 4%), the EC_{NH_3} was reduced by 7.61%. Acikalin *et al.*[317] investigated the introduction of solar energy into a similar system for gasification agent heating, with the internal heat recovery for power and heat generation, reporting the η_{ex} and η_{en} of 36.70% and 44.6%, respectively. The results indicated that the integration of a multigeneration system with renewable energy can provide both satisfactory thermal and environmental performances. The application of CaL technology can streamline syngas conditioning and increase the cost-effectiveness. Dziva *et al.*[318] proposed a BtA system based on the SEG-PSA-FS route with ASU and RC as waste recovery subsystems, reporting that the η_{en,NH_3}, $\eta_{en,total}$, EC_{NH_3}, tier-III GWP, and LCOA were 44.52%, 52.14%, 38.11 GJ per ton_{NH_3}, 0.73 $kg_{CO_2,eq}$ $kg_{NH_3}^{-1}$, and 0.69 \$ per kg_{NH_3}, respectively. Compared to the conventional GSF technology and the direct introduction of air without N_2 separation, the proposed system has comprehensively favorable performances. If considering the carbon credit created by biogenic CO_2 capture, the proposed system had a negative tier-III GWP of −2.79 $kg_{CO_2,eq}$ $kg_{NH_3}^{-1}$. Moreover, its LCOA (0.42 \$ per kg_{NH_3}) showed remarkable advantages under a carbon tax of 96 \$ per ton_{CO_2} compared with that based on large-scale biomass gasification (about 0.6 \$ per kg_{NH_3}) and large-scale coal gasification or methane reforming (about 0.5 \$ per kg_{NH_3}).

The application of CL can produce H_2- and N_2-rich streams in the SR and AR without energy penalty, respectively, and consequently high-purity H_2 and N_2 can be acquired after simple gas–liquid separation for the synthesis of NH_3. Sun *et al.*[319] proposed a CLC-FS-RGU-based BtA system, reporting the η_{ex,NH_3} of 44.36% and $\eta_{ex,total}$ of 46.09%. The exergoeconomic results showed that the CLC subsystem contributed about 70% of the exergy destruction, and the production cost for NH_3 was 35.56 \$ per GJ, which was 1/4 of the cost for the electricity. Moreover, it was pointed out that the refrigerator in the AS subsystem and the compressors for the gaseous agent had great exergo-cost reduction potential. In the case of the main reactors (such as FR, SR, AR, and combustor) and heat exchangers with great temperature difference, reducing the exergy loss is inevitable. For a similar system, Miyahira *et al.*[320] reported that recirculating part of CO_2-rich flue gas into FR as a gas enhancer led to higher NH_3 yields but lower power production (38.09% of η_{en,NH_3} and $\eta_{en,power}$ of 0.65%) than introducing extra steam (37.35% of η_{en,NH_3} and $\eta_{en,\ power}$ of 2.91%), respectively. The results further showed that the BtA system based on the GSF-CLC-FS-RGU route had both lower η_{en,NH_3} and $\eta_{en,power}$, which were 37.25% and 0.49%, respectively. Tang *et al.*[321] proposed an autothermal BtA system based on the GSF-SECLC-FS route with waste heat recovery, reporting that under CCR of 96.4%, the NH_3 yield and LCOA were 0.28 kg_{NH_3} $kg_{biomass}^{-1}$ and 0.49 \$ per kg_{NH_3}, respectively. For the comparison of CL-based and GSF-based BtA systems, Wen *et al.*[322] pointed out that the η_{ex} and η_{en} of the CL-based system were 3% higher than that of GSF-based system, with an increase by about 4% in the NH_3 yield.

In the presence of OC, CL is applied as an oxidation process. Similarly, the concept of chemical looping ammonia generation (CLAG) was proposed, with the development of nitrogen carriers (NC). For the typical alumina-based NC, the endothermic N-sorption reaction can be described as $Al_2O_3 + 3C + N_2 \leftrightarrow 2AlN + 3CO$, and the exothermic N-desorption reaction is the hydrolysis process of AlN, which is $2AlN + 3H_2O \leftrightarrow Al_2O_3 + 2NH_3$. Yan *et al.*[323] proposed a solar-assisted GSF-based BtA system. The syngas was divided into two flows. The first flow was sent to SOFC for power and high-purity N_2 production, and the second flow was combusted to supply heat to CLAG. In the CLAG, biochar and the high-purity N_2 from SOFC were used as throughout, and the gaseous product of N-sorption reaction was sent to the waste heat recovery subsystem (consisted of ORC, ARS, and HE), together with the hot flue gas from syngas combustion for CCHP. The systematic η_{ex} of 41.31% and η_{en} of 61.53% were reported, while the production of NH_3 only contributed 2.90% and 8.35% of the output exergy and energy, respectively. Weng *et al.*[324] also proposed a GSF-based BtA system, in which a chemical looping air separation (CLAS) subsystem produced N_2 for CLAP and O_2 for syngas combustion. The produced CO in the CLAP was combusted for power production, and part of the generated power drove the water electrolysis cell (WEC) to produce O_2 (as the gasifying agent) and H_2 with external wind power. The heat supply of CLAG was satisfied by the syngas oxy-combustion and introduction of solar energy. With 3.6 t h^{-1} of biomass input, the system produced 93.2 kmol h^{-1} N_2, 34.1 kmol h^{-1} NH_3, and 90.6 kmol h^{-1} H_2, exhibiting the $\eta_{en,H_2\ \&\ NH_3}$ of 43.55%. Although the application of CLAG can avoid energy-intensive hydrogen production and realize unidirectional synthesis at ambient pressure, it should be noted that with only char as the ammonia synthesis feedstock, the NH_3 yield decreased, and the utilization of syngas plays a vital role in the thermal performance.

4.3.3 Synthetic natural gas (SNG) production. The methanation reaction of CO and CO_2 ($CO + 3H_2 \leftrightarrow CH_4 + H_2O$, $CO_2 + 4H_2 \leftrightarrow CH_4 + 2H_2O$) is the main source of methane production, and a theoretical stoichiometric ratio should be satisfied for the ideal methane production, which is $(y_{H_2} - y_{CO_2})/(y_{CO} + y_{CO_2}) = 3$. Thus, the key to methane production is the choice of stoichiometric ratio adjustment method. In summary, the adjustment method can be realized by the removal of CO_2 using CCS, and the addition of extra H_2.

The application of pre-combustion capture can optimize the reaction conditions, while post-combustion capture can promote the environmental performance. Akbari *et al.*[325] proposed a W/BtSNG system based on the GSF-AGR-FS route with a waste heat recovery subsystem. Among the feedstocks of corn stover, wheat straw, forest residues, whole forest, organic fraction of municipal solid waste (OFMSW), and cow manure with moisture content in the range of 6% to 80%, the SNG produced from OFMSW had the lowest LCOSNG of 6.28 \$ per GJ due to its lowest feedstock cost (zero) and highest SNG yield.

The LCOSNG using the other 5 biomass feedstocks ranged from 6.32 to 10.46 $ per GJ. Cui *et al.*[326] proposed a W/BtSNG system based on the GSF-MR-AGR route using O_2-enriched air as the gasifying agent and ORC as the waste heat recovery subsystem, reporting the η_{ex} of 60.38%, η_{en} of 65.69%, and LCOSNG of 15.17 $ per GJ. Subramanian *et al.*[327] investigated the performance of a WtSNG system with the application of pre-combustion capture, reporting the η_{en} of 43.40%, and tier-I GWP of 47.57 $kg_{CO_2,eq}$ per GJ. With the further integration of post-combustion capture, the tier-I GWP decreased to 2.38 $kg_{CO_2,eq}$ per GJ, at the cost of a decrease of 4.4% in η_{en}. They also discussed the effects of the variation in the regional electricity emissions (687.5 $kg_{CO_2,eq}$ MW^{-1} h^{-1} in US and 16.4 $kg_{CO_2,eq}$ MW^{-1} h^{-1} in Norway, 2017-based values), which caused an increase in the tier-III GWP from 48.65 to 92.64 $kg_{CO_2,eq}$ per GJ and 3.86 to 64.55 $kg_{CO_2,eq}$ per GJ in the pre-combustion capture case and pre- & post-combustion capture case, respectively. The Norway- and US-based LCOSNG in the pre-combustion capture case was 17.5 $ per GJ and 21.8 $ per GJ, respectively, and the further integration of post-combustion capture resulted in an increase of about 3 $ per GJ in LCOSNG. The above-mentioned studies all indicated that only with strict regulatory conditions and powerful finical incentives, the economic feasibility can be competitive with fossil-based SNG, such as high carbon tax/credit and feedstocks subsidy.

Normally, the addition of extra H_2 is provided by the WEC, and the byproducts can be further used as a combustion or gasification agent. Generally, the WEC can operate based on the O_2 demands of the primary thermochemical process or the H_2 demands for the full methanation of CO and CO_2. If the supplied H_2 is not adequate for full methanation, the CO_2 in the syngas/flue gas needs to be partially or completely removed. Schmid *et al.*[328] compared GSF-based BtSNG systems integrating pre-combustion capture and SOEC as syngas adjustment methods, and the results showed that the integration of SOEC could promote the SNG yield and system efficiency with an increase in energy consumption. Compared to the system with pre-combustion capture, the proposed system with SOEC promoted the η_{en} from ~51% to ~61% in the O_2-sustained case and ~64% in the H_2-sustained case. Also, with an increase in the energy consumption by about 5 times and 14 times in the O_2-sustained case and H_2-sustained case, the SNG yield was promoted by over 60% and 200%, respectively. Rispoli *et al.*[329] also investigated the performance of a COMB-based WtSNG system under undersupplied, sufficient, and excess O_2 production in a PEMEC. The system yielded the highest η_{ex} of 26.40% and η_{en} of 36.00% with excess O_2 production, and if the energy consumption was supplied by a fossil source except the renewable-energy-driven PEMEC, the tier-II GWP and LCOSNG were 1.74 $kg_{CO_2,eq}$ kg_{SNG}^{-1} and 5 $ per MW per h, respectively. The captured CO_2 can also be directly electrolyzed with H_2O to produce syngas. Zhang *et al.*[330] compared the performance of a GSF-based BtSNG system with pre-combustion capture, steam electrolysis, and co-electrolysis of steam and CO_2. In terms of η_{en}, the ranking was steam electrolysis (~68%) > co-electrolysis (~66%) > pre-combustion capture (~51%), while in the case of LCOSNG, the ranking changed to co-electrolysis (26–32 $ per GJ) > steam electrolysis (23–30 $ per GJ) > pre-combustion capture (10–28 $ per GJ). Wang *et al.*[331,332] proposed two GSF-based BtSNG systems. In both systems, the gasified syngas was completely oxidized in the SOFC and water gas shift membrane reactor (WGSMR) burner, and the produced CO_2 was stored and co-electrolyzed with steam in a solar-driven SOEC. Eventually, the electrolysis syngas was further sent to MR for SNG production. The variation in the two proposed systems was the choice of waste heat recovery subsystem, which was ARS-HE for CCHP and ORC for CHP. In the case of the BtSNG-CCHP system, the η_{ex} and η_{en} were 42.2% and 69.56%, respectively. Regarding the BtSNG-CHP system, similar η_{ex} of 44.70% and η_{en} of 59.00% were reported, with the cost of 0.05 $ per kW per h for power production and 29.5 $ per GJ for SNG production. The exergoeconomic results revealed that the focus of optimization of SOFC and SOEC should be on lowering their cost rate. The tier-I GWP for SNG-CCHP and SNG-CHP was about 0.2 $ton_{CO_2,eq}$ per GJ and 0.15 $ton_{CO_2,eq}$ per GJ, respectively. With the assumed selling price of 18 $ per GJ for SNG and 0.13 kW h for electricity, which was close to the market price, both proposed systems could achieve the DPP of around 10 years.

4.3.4 Methanol (MeOH) and dimethyl ether (DME) production. The production of MeOH has a similar route with that of SNG, given that they both require the adjustment of syngas to the designated stoichiometric ratio $((y_{H_2} - y_{CO_2})/(y_{CO} + y_{CO_2}) = 3$ for SNG production and $(y_{H_2} - y_{CO_2})/(y_{CO} + y_{CO_2}) = 2$ for MeOH production), and the synthesis is also based on the hydrogenation of CO and CO_2 ($CO + 2H_2 \leftrightarrow CH_3OH$, $CO_2 + 3H_2 \leftrightarrow CH_3OH + H_2O$). Thus, the pivotal issue of the W/BtMeOH system is also the syngas adjustment method.

Regarding MeOH production, the stoichiometric ratio of the syngas can be adjusted internally by the application of AGR in advance of MeOH synthesis. AlNouss *et al.*[333] reported that when applying the GSF-AGR(Rectisol)-FS-FSP route in a BtMeOH system, using steam instead of oxygen as the gasifying agent promoted the tier-II GWP and LPOMeOH from ~9.27 to ~2.32 $kg_{CO_2,eq}$ kg_{MeOH}^{-1} and ~0.11 to ~0.41 $ per kg_{MeOH}, respectively. Wang *et al.*[334] evaluated the performance of a BtMeOH system based on the same route, reporting that the life cycle EC_{BtMeOH} was 51.02×10^4 MJ per ton_{MeOH}, tier-III GWP was 667.53 $kg_{CO_2,eq}$ per ton_{MeOH} (considering carbon credit created by biomass growth), and LCOMeOH was 502.00 $ per ton_{MeOH}. Thus, it showed a great GWP reduction potential in the biomass collection process. Also, compared to the conventional coal-based MeOH, the BtMeOH system decreased the tier-III GWP by 59.39%, with the cost of LCOMeOH increasing by 24.46%. Regarding a WtMeOH system based on the same route, Shi *et al.*[335] investigated the use of MDEA as the AGR solvent, reporting η_{ex} of 37.92%, tier-III GWP of 3.21 $kg_{CO_2,eq}$ kg_{MeOH}^{-1}, and LCOMeOH of 579.62 $ per t_{MeOH}. The results further indicated that the exergy loss of the GSF and AGR subsystems contributed a relatively dominant pro-

portion, and a subsidy of 20 $ per ton_{waste} was inevitable for a positive NPV. Afzal *et al.*[24] noted that for WtMeOH systems, if the selling price of MPW was reduced to below 0.02 $ per kg_{waste}, the MPW-based MeOH achieved cost parity with fossil-based MeOH. Biochar can be combusted for heat self-supply or exported as a byproduct. Poluzzi *et al.*[296] found that if biochar was combusted with part of the biomass feedstock in the DFB, instead of being exported form BFB, the MeOH yield was promoted by ~1%, with an increase of ~5% in LCOMeOH. The introduction of solar energy as the heat source can substitute the combustion of biochar. Nwai *et al.*[336] reported that for a BtMeOH system based on the GSF-AGR(MEA)-FS-FSP-RGU route, the η_{en} and LCOMeOH were improved from ~48% to ~61% and ~632 $ per ton_{MeOH} to ~392 $ per ton_{MeOH}, respectively, due to the solar assistance. Sun *et al.*[337] compared the performance of BtMeOH systems based on the solar-assisted and autothermal CLG-FS-FSP routes. The results showed that the solar-assisted case provided power output, while the autothermal case needed an extra energy supply. Also, compared to the autothermal case, the MeOH yield increased by ~55% and the total CO_2 emission reduced by ~63%, which contributed to a low tier-I GWP of 345.83 $kg_{CO_2,eq}$ t_{MeOH}^{-1}.

SEG or SEWGS can also be a good option for internal syngas adjustment. Del Grosso *et al.*[338] reported that for a BtMeOH system based on the GSF/SEG-FS-FSP-RGU route, the integration of SEG promoted η_{en} from 55% to 60% but decreased the CCE from 100% to 96% due to the lower gasifier temperature. AlNouss *et al.*[339] also reported that the application of SEG led to a 3–4% increase in MeOH yield and 4–5% reduction in tier-I GWP, with LPOMeOH decreasing by 3–5%. Liu *et al.*[340] proposed a BtMeOH system based on the GSF-SEWGS-FS-FSP-RGU route, in which the char was further reacted with the CO_2 released from the calciner to produce tunable syngas for FS. They reported the η_{ex} of ~64%, tier-III GWP of 4.39 $kg_{CO_2,eq}$ kg_{MeOH}^{-1}, and MeOH yield of 702.50 kg_{MeOH} $t_{biomass}^{-1}$. The Ca-based sorbent calcination process was responsible for the largest energy consumption and GWP emission. The use of a multistage-PSA (mPSA) subsystem can also adjust the syngas ratio internally. Im-orb *et al.*[341] proposed a BtMeOH system based on the GSF-POX-mPSA-FS-FSP route, where the three-stage PSA subsystem produced H_2-rich, CO-rich, and CO_2-rich stream separately. They reported the highest η_{ex} and η_{en} of 25.44% and 38.57%, respectively, and the recirculation of PSA residual gas to the gasifier could not benefit the overall performance. Li *et al.*[118] also proposed a WtMeOH system based on a similar route, reporting the η_{ex}, η_{en}, and LCOMeOH of 50.93%, 54.08%, and 41.09 $ per GJ, respectively. The mPSA subsystem contributed 9.68% of the total exergy destruction.

The external syngas adjustment method in the W/BtMeOH system refers to the addition of extra H_2. Renewable energy plays a more aggressive role in the energy supply chain nowadays, and thus applying WEC driven by green energy can be a good choice. Given that WEC can produce sufficient H_2 independently, in the upstream the feedstock can be partially oxidized for syngas production or completely combusted for power generation. In the case of syngas production, Safder *et al.*[342] reported that the application of the GSF-AGR-FS-FSP-WEF route with waste heat recovery subsystem results in the η_{ex} of 71.63%, η_{en} of 78.13%, tier-II GWP of 0.61 $kg_{CO_2,eq}$ kg_{MeOH}^{-1}, and LCOMeOH of 103 $ per ton_{MeOH}. Zhang *et al.*[343] and Wang *et al.*[344] investigated the performance of W/BtMeOH systems based on the same route, reporting the η_{ex} of 64–69%, η_{en} of 67–68%, and DPP of 3–5.5 years. The major exergy destructor was the GSF (~38%), WEC (~30%) and FS (~20%) subsystems. Anetjärvi *et al.*[345] further recovered the waste exergy from the residual gas, reporting $\eta_{en,MeOH}$ of 59.5%, $\eta_{en,total}$ of 85.8%, CCE of 89.8%, and LCOMeOH of 511 € per ton_{MeOH}. In the power generation case, the reported economic indicators are not preferable. Sun *et al.*[346] proposed a WtMeOH system based on the COMB-sCO_2-FS-FSP route, reporting the η_{ex} of 74.83 and LCOMeOH of 728.40 $ per ton_{MeOH}. Only when the cost of WEC was reduced to 40 M$ per 250 MW and the carbon emission credit was higher than 70 $ per t, the MSW-based MeOH was more economically advantageous than fossil-based MeOH. Pratschner *et al.*[347] further discussed a BtMeOH system based on a similar route, with the maximized system availability under the maximized renewable energy share in the total energy consumption. They reported that the annual operating hours decreased to 3000 h a^{-1} under the local conditions, and with an increase in the system capacity from 50 to 1000 MW_{el}, the LCOMeOH improved from 785.4 to 569 € per ton_{MeOH}. A high carbon tax of 308 € per t_{CO_2} was the premise of competition with the fossil-based MeOH.

Besides steam, CO_2 or syngas can also be input to the WEC as feedstock. Rajaee *et al.*[348] compared the performance of GSF-based BtMeOH systems with a steam electrolyzer, syngas electrolyzer, and steam-CO_2 co-electrolyzer in the SOEC. All cases exhibited a similar η_{en} of 67–69% (77–81% with district heating) and CCE of 91–93%, and it can be observed that the steam electrolyzer and syngas electrolyzer cases had comparable LCOMeOH (529.02 $ per ton_{MeOH} and 526.49 $ per ton_{MeOH}, respectively). The steam-CO_2 co-electrolyzer yielded the highest LCOMeOH of 582.43 $ per ton_{MeOH} due to its high TCI and electricity consumption. Overall, the investment in WEC could account for approximately 20% to 50% of the total TCI.[343–346,348]

Conventionally, the reforming of methane can be a convenient choice, given that the reforming gas introduces extra C and H contents, promoting the methanol production capacity. Ostadi *et al.*[349] proposed a BtMeOH system based on GSF-AGR-FS, with an NG pyrolysis subsystem as the external H_2 source. They discussed 5 situations of possible heat supply to the NG pyrolyzer, including electric heating, internal heat recovery, and combustion of H_2, syngas or NG. The results showed that for all cases, CCE, η_{en}, and LCOMeOH were very close, ranging from 49–53%, 49%–56%, and 440–470 $ per ton_{MeOH}, respectively. If considering the carbon credit created by biogenic CO_2 and carbon byproducts, the case applying the internal heat recovery had the lowest tier-III GWP (−141 $kg_{CO_2,eq}$ per ton_{MeOH}), while the case combusting NG had the highest one (636 $kg_{CO_2,eq}$ per ton_{MeOH}). Regarding the choice

of external H_2 source, Liu *et al.*[340] compared a BtMeOH system based on the GSF-SEWGS-FS-FSP-RGU route when using NG dry reforming (DRM) or SOEC as the external H_2 source. They claimed that the SOEC case showed a higher η_{ex} (71.60–57.14%) and a lower tier-I GWP (117.08–168.71 $kg_{CO_2,eq}$ per ton_{MeOH}), while the DRM case had a lower MSP (~470–510 \$ per ton_{MeOH}) due to the increased MeOH production capacity. Ostadi *et al.*[350] further compared the W/BtMeOH system based on the GSF-AGR-FS-FSP route, with NG pyrolysis or SOEC. It claimed that the CCE improved from 44.3–94.3% after the addition of extra H_2, and based on the same MeOH production capacity, applying NG pyrolysis yielded an LCOMeOH of 433 \$ per ton_{MeOH}, which was almost half of that of applying SOEC (853 \$ per ton_{MeOH}). Also, they proposed that the SOEC could be applied when the electricity price is low, and during the high-electricity-price period, the NG pyrolyzer could be a substitution.

Landfill gas is usually a mixture of CH_4 and CO_2, and aiming at the *in situ* synergistic utilization of excavated waste and landfill gas, Tang *et al.*[351] proposed a WtMeOH system based on GSF-AGR-FS-FSU-RGU route, with SOEC and landfill gas autothermal DRM as the H_2 source. They reported the η_{ex} of 72–75%, tier-III GWP of 700–900 $kg_{CO_2,eq}$ per ton_{MeOH}, and LCC of 300–310 \$ per ton_{MeOH}. In terms of GWP, the fugitive emission during the excavation process reduced the advantages of the proposed system to the fossil-based system, and with the Chinese energy structure becoming greener, the tier-III GWP was predicted to be reduced to 530–700 $kg_{CO_2,eq}$ per ton_{MeOH} by 2035.

Numerous studies have conducted a comparison of the performance of W/BtMeOH systems with the internal and external syngas adjustment method. Butera *et al.*[352] also reported that the integration of SOEC boosted the methanol yield in a GSF-based BtMeOH system compared to applying WGS-AGR ($\eta_{en,MeOH}$ improved from 18–46% to 65–82%). Regarding the choice of gasifying agent, using an $O_2/CO_2/H_2O$ mixture could yield a higher η_{en} (54.4%–48.6%) and CCE (57.5%–47.2%) compared to the use of an O_2/H_2O mixture, but it also resulted in increase in the SOEC area (from 3610.30 m^2 to 2687.00 m^2) due to the higher H_2 requirement. Sun *et al.*[353] compared the performance when applying WGS-AGR as the internal and additional SOEC as the external adjustment method in a WtMeOH system. The results showed that the integration of SOEC had a higher η_{ex} (60.8% to 41.5%) but lower LCOMeOH (355.89 \$ per ton_{MeOH} to 406.09 \$ per ton_{MeOH}), and to ensure the advantage of economic performance compared to fossil-based MeOH, it required a carbon tax over 350 \$ per ton_{CO_2} and PV electricity cost below 0.055 \$ per kW per h. Poluzzi *et al.*[354] also discovered that the integration of SOEC improved the MeOH yield by 59.63% in a BtMeOH system based on the SEG-FS-FSP-RGU route. Also, they pointed out that the increase in WEC capacity factor and decrease in WEC cost were the key to the reduction in LCOMeOH, and an MeOH selling price higher than about 500 € per ton_{MeOH} was required for economic feasibility. Klüh *et al.*[355] further discussed the effect of electrification ratio on the performance of a BtMeOH system. The results showed that compared to the baseline condition (internal AGR with partial combustion syngas for heat supply), combing direct electrification (heat supply electrically) with indirect electrification (additional H_2 for syngas adjustment) was the best choice, which could improve the CCE and $\eta_{en,MeOH}$ from ~43.50% to 94.00% and 54.70% to 60.30%, respectively, with a decrease in LCMeOH from 730 € per ton_{MeOH} to 706 € per ton_{MeOH}. If the electricity emission factor decreased to 0–200 g_{CO_2wq} kW^{-1} h^{-1}, the tier-II GWP of the biomass-based MeOH could be less than 50% of that of the fossil-based MeOH. Zhang *et al.*[356] also compared the performance of a BtMeOH system with adjustment methods of internal WGS-AGR (baseline), external H_2 supply by SOEC, NG pyrolysis, or NG chemical looping reforming. The baseline case showed a CCE of 63.11%, η_{ex} of 38.50%, tier-II GWP of 2.88 $kg_{CO_2,eq}$ kg_{MeOH}^{-1}, and LCOMeOH of 2019.29 \$ per ton_{MeOH}. The optimal case in the aspects of exergy effectiveness, environmental sustainability, and economical attractiveness was NG (CCE of 91.42%, η_{ex} of 63.95%, tier-II GWP of 1.41 $kg_{CO_2,eq}$ kg_{MeOH}^{-1}, and LCOMeOH of 1610.00 \$ per ton_{MeOH}), SOEC (CCE of 85.69%, η_{ex} of 53.58%, tier-II GWP of 1.07 $kg_{CO_2,eq}$ kg_{MeOH}^{-1}, and LCOMeOH of 2334.77 \$ per ton_{MeOH}), and NG chemical looping reforming (CCE of 89.93%, η_{ex} of 55.35%, tier-II GWP of 1.13 $kg_{CO_2,eq}$ kg_{MeOH}^{-1}, and LCOMeOH of 1402.58 \$ per ton_{MeOH}), respectively. With an increase in the plant scale from 0.1×10^6 $ton_{biomass}$ per a to 1.7×10^6 $ton_{biomass}$ per a, the LCOMeOH of all cases had a reduction of ~57%.

Given that MeOH is a vital precursor of DME, the production of DME can be seen as an extension of the production of MeOH. Besides the choice of syngas adjustment methods, synthesizing DME from syngas can be divided into a one-stage and two-stage process. In the two-stage synthesis process, the WGS reaction and hydrogenation of CO and CO_2 firstly occur in the MeOH synthesizer, and the produced MeOH undergoes a shrinkage process to produce DME in the DME synthesizer. Alternatively, in the two-stage process, all the above-mentioned reactions occur together in the standalone DME synthesizer.

Regarding the two-stage synthesis process, Xu *et al.*[357] reported that with the application of internal WGS-AGR adjustment and a sCO_2 subsystem to recover the waste heat, the proposed BtDME system yielded the η_{ex} of 41.12%, η_{en} of 49.54%, and LCODME of 286–686 \$ per ton_{DME}. The exergy loss shares in the FS and GSF subsystem were 58% and 31%, respectively. Zhang *et al.*[358] proposed a BtDME system based on the GSF-CLC-FS-FSP route, with sCO_2 subsystem to recover internal heat, and part of the H_2 was split for NH_3 by-production. They reported the η_{ex} of 46.70% and η_{en} of 60.15%. GSF, FS&FSP, and AR exhibited the largest exergy losses, accounting for 43.02%, 33.24%, and 4.50% of the total exergy loss, respectively. With DME being sold at 686 \$ per ton_{DME}, the BtDME system yielded a DPP of 8 years. Sun and Tang[85] reported that the η_{ex}, tier-II GWP, and MSP of the WtDME system with SOEC were 57.37%, 4.38 $kg_{CO_2,eq}$ kg_{DME}^{-1}, and 653.9 \$ per ton_{DME}, respectively. Regarding the one-stage synthesis process, Im-orb *et al.*[359,360] also investigated the performance of a BtDME

system applying internal WGS-AGR adjustment, reporting the η_{en} of 59.5% and tier-II GWP of 1.45 $kg_{CO_2,eq}$ kg_{DME}^{-1}. The GWP was dominated by the energy consumption (mainly in the AGR subsystem), and regarding the endpoint LCA indicators, the ecosystem was more significantly influenced than human health. The results were also favorable for economic performance, given that a negative NPV was reported with DME sold at 840 $ per ton_{DME}. For the comparison between the one-stage and two-stage process, Kofler *et al.*[361,362] compared the performance of a BtDME system with WEC as the external H_2 source when applying the one-stage or two-stage process, and the results showed that the two-stage process promoted both the η_{en} and CCE by 3–13% and 10–40%, respectively, due to its higher DME yield. Economically, the one-stage process benefited more from low biomass prices and high process heat revenues, while the two-stage process benefited more from low WEC prices and electric prices due to its large hydrogen consumption. Moreover, in both processes, the introduction of POX led to an increase in carbon efficiency, while that of hydrogen quenching only had a positive impact on the CCE of the two-stage process.

4.4 Comparison of W/BtE systems with various production purposes

The fundamental factor in the performance of W/BtE systems is the variation in the feedstock. Qi *et al.*[10] comprehensively compared the basic characteristics of MSW and biomass through statistical analysis, reporting that the ultimate and proximate results of the MSW had a wider distribution range than the biomass due to the diversity of MSW compositions. Furthermore, on average, MSW had a higher value of C, H, and volatile content, but lower value of O and fixed carbon content, which resulted in the promotion of light combustible gas production, with the suppression of generation of oxygen-containing substances, and *vice versa* for biomass. In the case of the typical MSW compositions, a high carbon content is often related to high molecular weight polymers (such as plastics, waste tires and chemical fiber), but it also brings an unexpected Cl content.[363] The main contributor of S content is food waste and rubber, and waste paper also has a modest S (also Cl) content.[364] The use of biomass as the feedstock results in a lower environmental burden not only due to its lower S and Cl contents, but also its complete biogenic carbon content. The biogenic carbon content refers to the carbon sequestered during biomass cultivation,[334] the emission of which is considered carbon-neutral, and consequently the capture of biogenic carbon creates a negative value of GWP as carbon credit.[194,365] Some studies also considered the production of biochar and the oriented activated carbon as a type of carbon credit.[366] Meanwhile, the emission of fossil carbon is seen as a positive value of GWP. Given that the reported biogenic CO_2 fraction in MSW is in the range of 40% to 80%, WtE systems often have a positive GWP, only when considering the avoided carbon emission from landfill.[367] Also, the differences in policies and regulations in the field of waste or biomass treatment matter, and firstly located in the cost of acquiring feedstock. In the case of biomass, its acquisition is often seen as a purchase process, which occupies a large share of variable cost. Alternatively, regarding waste, its disposal brings extra income in the forms of a subsidy or gate fee, which plays a decisive role in some cases, especially when using sludge with a high moisture and ash content as the feedstock. Besides, with the differences in biogenic content, more carbon tax can be levied for WtE systems, and if there are incentives for low-carbon products, the carbon-related economic performance will become more significant.[368]

Another influential factor for various W/BtE systems is the determination of their final product.

As mentioned in chapter 3, when the final product varies, the results of energy, exergy, and advanced exergy do not seem to be comparable, given that the difference in the product energy/exergy level and the assumed assessment boundary causes an ununiformed benchmark and end point of calculation. Typically, the thorough W/BtP conversion is reported to be less exergy effective than the that of W/BtF because the conversion of fuel to power or heat is not discussed inside the boundary. Alternatively, environmental and economic indicators from the perspectives of the feedstock and the whole system can be applicable. The systematic indicators include total periodical emission, NPV, DPP, and IRR. Also, it is recommended that the environmental impact and levelized cost or profit of per unit feedstock treatment be determined. Sun *et al.*[87] compared the comprehensive performance of WtH, WtNG, and WtP systems, pointing out that WtH and WtNG reduced the tier-I GWP by 90–95% to that of the WtP system without CCS, with an increase in LPOMSW from 40–60 ¥ per ton_{MSW} to 238.35 and 96.42 ¥ per ton_{MSW}, respectively. Also, the WtP system is more sensible to the fluctuation of electricity sales tariff and MSW subsidy price, given that these two aspects are the main income source. If the carbon tax is only to the levied direct emission, both WtH and WtNG show strong economic resistibility to the boosting of carbon tax due to the low tier-I GWP and the high added-value of the product. Regarding the choice of NG, MeOH and DME, Sun *et al.*[85] further reported that the IRR of the WtNG, WtMeOH and WtDME systems with WEC was 11.37%, 9.42% and 15.60%, respectively. All three systems had a close TPC, and the differences in IRR were mainly attributed to the higher revenue from selling fuel in the WtDME system, and the excess oxygen selling in the WtNG system. Besides, the tier-II GWP of WtDME and WtNG was about 8% and 3% higher than that of WtMeOH system, respectively. The breakeven renewable energy on-grid tariff for WtNG and WtMeOH system was 0.04–0.05 $ per kW per h, and for WtDME system was 0.05–0.06 $ per kW per h. Eisavi *et al.*[369,370] also revealed that BtNG system had better environmental and economic performance than BtMeOH system. Urea production can be seen as an extension of NH_3 production, given that it can be synthesized using NH_3 with the captured CO_2 from the WGS subsystem. AlNouss *et al.*[333] pointed out that for the BtNG, BtMeOH and BtA&urea systems, using steam as the gasifying agent was the best option to obtain value-added products with higher profits and

lower emissions. With the goal of the optimal syngas utilization, they reported the tier-II GWP of 0.72 $kg_{CO_2,eq}$ $kg_{biomass}^{-1}$, 0.97 $kg_{CO_2,eq}$ $kg_{biomass}^{-1}$, and 1.25 $kg_{CO_2,eq}$ $kg_{biomass}^{-1}$ for the BtMeOH, BtP and BtA&urea systems, respectively. Alternatively, in terms of economic performance, the ranking was BtMeOH > BtA&urea > BtP, with the LPOB of 0.114 $ per $kg_{biomass}$, 0.105 $ per $kg_{biomass}$, and 0.098 $ per $kg_{biomass}$, respectively. Overall, compared to the conventional W/BtP system, the production of value-added fuel proved its potential in reducing the environmental impact with enhanced economic feasibility under the premise of foreseeable restricted policies and regulations.

Regarding W/BtE systems with various production purposes, the treatment of tar is an unavoidable issue. The formation of tar in W/BtE systems leads to the potential risk of catalyst deactivation and the issues of blockage and corrosion in the downstream equipment. The tar removal strategies can be divided into *in situ* and *ex situ* methods.[371] The *in situ* method strategy aims to reduce the tar content in the gasifier or pyrolizer outlet by reactor design refinement (*e.g.*, Fig. S7(2.d) and S8(4.c)†), optimization of the operation conditions (see Table 4), and the application of an *in situ* catalyst (*e.g.*, application of SEG). The common *ex situ* tar removal strategy works independently as a downstream section of the gasifier or pyrolizer, including physical removal, thermal cracking, and catalytic cracking.[372] Physical removal of tar depends on inertial separation in the cyclone, adsorption of porous solid solvents in the tube, or adsorption of liquid solvents (water or oil) in the scrubber. Regarding these methods, tar is just separated from the main product flow, and if the tar is not further utilized, it would cause considerable loss in energy efficiency and extra consumption of power and chemicals for the auxiliary device operation.[373] The thermal cracking method refers to the cracking of tar within the reaction temperature above 1000 °C,[374] and this method is seldom used in W/BtF systems given that the initial temperature for PY and GSF is usually under the required temperature window. The catalytic cracking method refers to the reforming of tar in the presence of a catalyst and a reforming agent (such as steam, CO_2, and O_2) in the temperature range of 500–900 °C.[295] Several studies have reported the application of the catalytic cracking method,[295,297,375] and they reported the promotion of H_2 yield after the catalytic cracking of tar. Generally, previous studies tended to report the specific results of systematic TEE performance when considering the effect of the formation and the removal of tar, but few quantitatively compared the TEE performance with and without tar removal. Thus, future studies are encouraged to report and compare the TEE performance for the same W/BtE system with different tar removal strategies.

5 Prospects and shortcomings

5.1 Enhancement in data source quality

The quality of data sources directly determines the accuracy and credibility of the assessment results. The quality of the data sources can be enhanced in the aspects of scale-up validation and design data, and regionalized background data databases. Regarding the design and validation of the proposed W/BtE systems, recent studies mostly use existing results of laboratory-scale experiments as references of the thermochemical processes, and given that the scale of the proposed systems is usually far beyond the laboratory scale, the participation of results from pilot plants or even real operating facilities is necessary. Besides, plenty of studies have investigated the effect of catalysts or additives applied in the W/BtE process, and the ones with good performance were screened. Although the experiment results are well-presented and discussed in-depth, the quantified and detailed descriptions of the reactions parameters are rarely reported (such as kinetic model parameters). Thus, revealing the operation data from plants beyond the pilot scale and the application of fine-scale reaction models can significantly improve the data fidelity during the scale-up simulation.

The establishment of a regionalized background database can help refine the environmental assessment results, given that W/BtE systems can be influenced by many local factors. The first factor is the feedstock characteristics. Most W/BtE systems tend to choose feedstocks with low cost, easy and nearby collection accessibility, and sufficient supply capability. The composition can have strong regional patterns, given that both the category and the cultivation process are deeply influenced by the local additions.[376–378] The MSW composition is even more sensible, given that it is directly related to the local sociocultural, environmental and economic variables.[379,380] Then, the W/BtE process is always accompanied with the large consumption of energy and auxiliary chemicals. The value of electricity emission factors is determined by the development of the regional energy supply structure, and it can differ greatly at the national level or even provincial level.[381–383] For the acquisition of chemicals, advanced manufacturing technologies can reduce the environmental impact of chemical production.[384] This means that more developed regions can consume energy and chemicals with lower cost and impact, and if the background data cannot reflect the actual level in these regions, the environmental impacts can be exaggerated. Similarly, these reasons can be also applicable to the feedstock collection and the waste disposal processes. To date, several LCA databases have been fully developed and under comprehensive application, including ecoinvent, ELCD, GaBi, and U.S.LCI.[385,386] Notably, the establishment of the above-mentioned databases is mainly based on the data from developed countries. In the case of developing countries, especially in China, more effort should be devoted to establishing and improving the databases, among which the CLCD and Tiangong databases are the most recognized ones.

5.2 In-depth consideration of realistic conditions – from geographical to technical

Given that recent studies conducting a system-level TEE assessment tended to focus more on the mid-term and long-term performances, the basic assumptions of W/BtE systems needs

to be based on the realistic geographical and technical conditions, and the sensitivity analysis should be conducted to show the performance fluctuations due to the changed conditions. Geographical conditions are always related to the supply of the feedstock and the generation of renewable energy. The feedstock supply chain has uncertainties in terms of availability, characteristics, and acquisition cost. Biomass harvesting is seasonal, and the quality of the biomass can be affected by a change in the climate. If the biomass is in short supply and the quality of the feedstock decreases, the price of biomass will also increase, and potentially extra cost is due to the additional purchasing of biomass or longer transportation distance. Also, the same phenomena occur in the supply chain of waste, especially with the implication of waste classification policy, where the quality of waste is expected to improve (see Fig. 11(a)),[387] and the subsidy for waste treatment will fluctuate relatively.[388] Then, for the generation of renewable energy, it strong relies on the location conditions, which decides the proportion of renewable energy in the total energy supply.[389] If the energy consumption is satisfied by renewable energy, the compatibility between the designed energy consumption and the theoretical renewable energy generation capacity should be carefully considered. It is meaningless to discuss the participation of renewable energy when the local conditions can not satisfy the assumed requirements, and even if the system performance is outstanding, the result cannot provide any references for realistic operation.

Technical condition is the in-depth reflection of the geographical conditions. The geographic information system (GIS) tool can be applied for waste[391,393–395] or biomass[396–398] supply chain optimization, given that spatial variability has a significant impact (see Fig. 11(c)). The results show that transportation costs will increase due to insufficient biomass availability, long transportation distances, and even backward transportation network for W/BtE systems with a large production capacity. In terms of the possible dynamic variation of the feedstock characteristics, the operation adjustment in the original system with new parameters should be investigated,

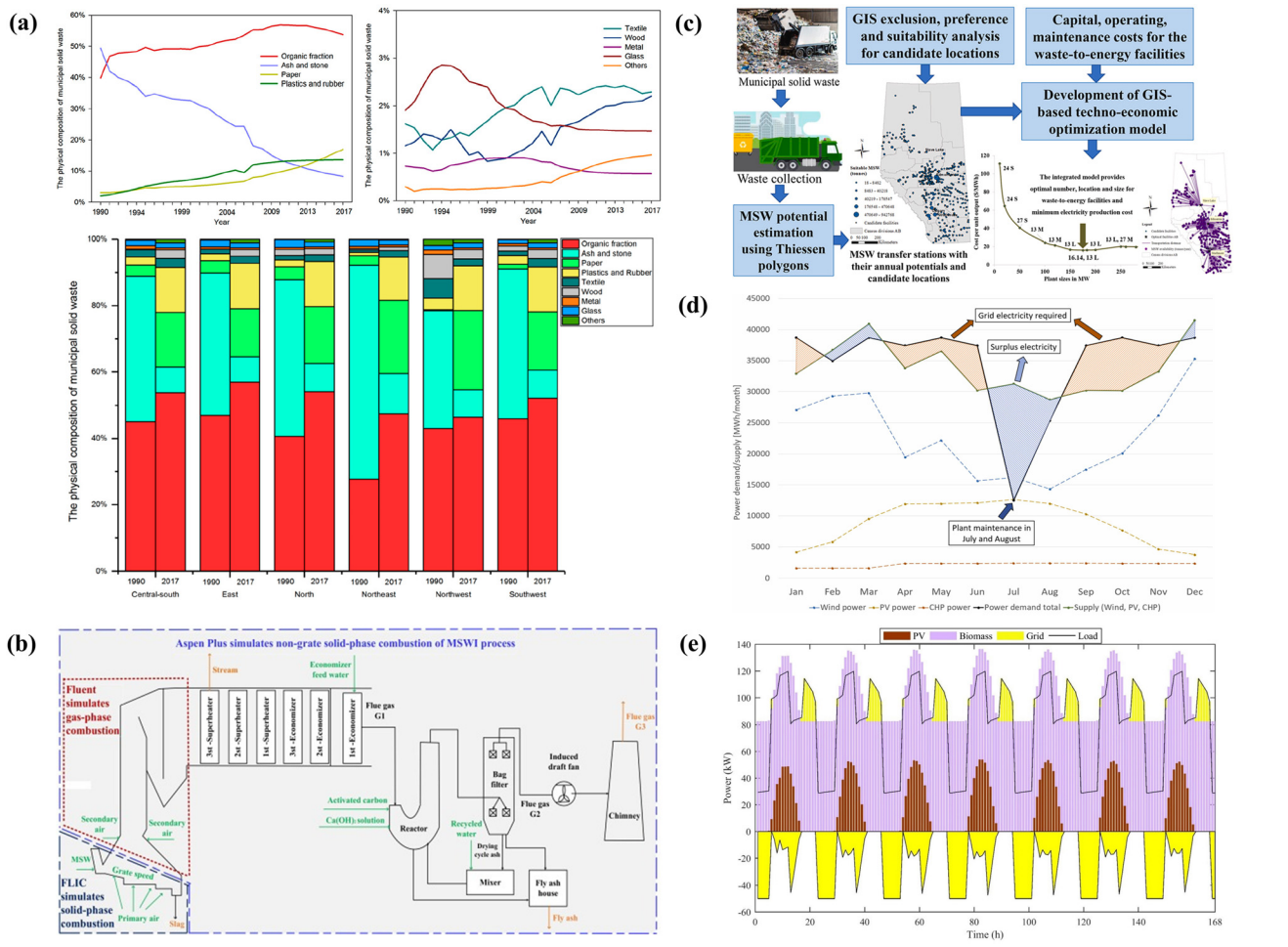

Fig. 11 Technical considerations for realistic conditions. (a) Fluctuation in characteristics of MSW. Reprinted with the permission.[390] Copyright 2020, the American Chemical Society. (b) Integration of different models in simulating the MSW incineration system. Reprinted with permission.[160] Copyright 2023, Elsevier, Ltd. (c) Role of feedstock supply chain in W/BtE systems. Reprinted with permission.[391] Copyright 2023, Elsevier, Ltd. (d) Power demand-supply curve for W/BtE systems. Reprinted with permission.[347] Copyright 2023, Elsevier, Ltd. (e) Grid balance of multi-source energy. Reprinted with permission.[392] Copyright 2024, Elsevier, Ltd.

instead of using new parameters as the initial conditions for a newly proposed system, which is also applicable for the sensitivity analysis of other parameters. Similar to the reactor level, the operation adjustment can not only influence the eventual product generation, but also destabilize the distribution of various field parameters. To solve this issue, it is recommended to investigate the dynamic performance by applying multiple simulation models. Tang *et al.*[160] provided a potential combination, by simulating the solid-phase combustion on a grate, the gas-phase combustion in a furnace, and non-grate solid-phase combustion in a WtP system by FILC, Fluent, and Aspen Plus, respectively (see Fig. 11(b)). The simulation results provided references for both the adjustment range of the manipulated variables and the visualized and optimized control operation, given that it can optimize the comprehensive systematic performance when avoiding process safety risks in the furnace. The process in the W/BtF system is always energy consuming, and maximizing the proportion of renewable energy in the total consumption of the W/BtE system is the main technical challenge. For the direct utilization of solar energy as the heat source, the relationship among solar heat input, other additional heat sources, and temporary heat storage can be clarified in the scale of hours, months, and seasons with a change in the direct normal irradiance.[309,399,400] For the utilization of renewable electricity, locating the supply-demand gap and covering it with grid electricity is an inescapable issue in the continuous system operation.[322,401,402] Pratschner *et al.*[347] pointed out that with the balance of maximizing the plant availability and the renewable electricity share in the total energy supply, the annual operating hours can decrease due to the daily and seasonal intermittency (see Fig. 11(d)). In terms of the energy-export W/BtP system, with the foreseeable future of increasing penetration of intermittent renewable electricity, the effect of grid balancing can be significant (see Fig. 11(e)),[392,403] given that thermal W/BtP systems would not be dispatched frequently, and the application of the power storage system can increase the annual operating hours to promoting the economic system.[404] The integration of the CCS subsystem also faces the challenge of balancing the internal heat requirement and the local heating supply.[405]

6 Conclusion

W/BtE technology plays an increasingly vital role in the future energy structure and environmental management, where combustion, gasification and pyrolysis are the three classical primary thermochemical W/BtE processes. This study highlighted the importance of the ex ante TEE assessment based on process simulation, and comprehensively reviewed the basic structure, principles and calculation method. The key findings can be concluded as follows:

• The model establishment for process simulation at the reactor level is mainly based on the choice of modelling approaches according to the assumed operational conditions. With the input of simple initial conditions, the thermodynamic equilibrium model can give rapid equilibrium-state results at low computing cost and shows great accuracy at high reaction temperatures. When considering the non-equilibrium predictions with finite time and volume and the needs of geographical field parameter distribution, the kinetic model is preferable, given that it simulates the overall reaction rate with parameters. If further integrating hydrodynamic and thermodynamic governing functions groups, the kinetic model is improved to become the CFD model, which can predict detailed field parameters in both the steady and non-steady state, but the difficulties are the model complexity and considerable computing power. The ML model can be applied for almost all conditions with excellent solution capacity for complex non-linear relationships, but its non-interpretability and high data-dependency are its main weaknesses.

• The common techno-environmental-economic assessment method mainly includes the 7Es of energy, exergy, advanced exergy, environmental, economic, exergoenvironmental, and exergoeconomic analysis. The energy, exergy, and advanced exergy analyses all facilitate the understanding of the principle of energy conversion inside W/BtE systems, and the comparison of the results should be based on same production purposes and calculation benchmark. The environmental analysis at different tiers can evaluate the environmental impacts of daily operations and technological improvement in W/BtE systems at various levels, and it is suggested to compare the results based on the same choice of assessment methods. The economic analysis is always based on several simplified assumptions, and thus modification of the result by engineering data and the comprehensive sensitivity analysis is necessary. The exergoenvironmental and exergoeconomic assessments identify the environmental impact mitigation priority and the cost-effectiveness of the components inside W/BtE systems, and the selection of LCIA method and economic assumptions are the foundation for the result comparability.

• The primary thermochemical process is the core of the W/BtE system, and the process simulation should provide specific parametric guidance aimed at targeted performance indicators. According to the production purposes, W/BtE systems can be classified into W/BtP and W/BtF systems. Regarding the W/BtP system, the integration of a CCS subsystem can promote the GWP with extra energy penalty and economic cost, and if the carbon tax or credit improves to a certain high level, the W/BtP system can be more beneficial that the fossil-based system. Regarding the choice of CCS, post-combustion capture has the vastest adaptability with great energy penalty and capture cost. Pre-combustion capture has comprehensive techno and economic advantages, but its application scenarios and carbon capture efficiency need to be further improved. Oxy-fuel combustion capture is attractive owing to its high carbon capture efficiency and convenient carbon capture subsystem design, but it lacks industrial experience in the issues of construction cost and operation safety. The expansion from the W/BtP system to W/BtCHP and W/BtCCHP systems is based on the construction of multi-stage heat utiliz-

ation subsystems. Given that the limited exergy recovery rate is always covered by a large energy recovery rate, and the economic cost and tier-III systematic GWP will fluctuate with the complexity of the utilized subsystems, the coproduction process should balance the comprehensive balance carefully. Regarding solar assistance in W/BtP systems, it includes photovoltaic and photothermal ways, where the latter remains a more pragmatic choice for heating the feedstock, gasifying agent, and working mediums in the power cycles. CAES, TCES and WES can be good choices as energy storage systems.

• W/BtF systems include W/BtH, W/BtA, W/BtSNG, W/BtMeOH, and W/BtDME systems. In the case of the W/BtH system, it includes GSF-based, PY-based, CLC-based, and CLG-based routes from initial thermochemical process perspectives, and WGS-based, SEWGS-based, and SEG-based routes from intermediate reaction perspectives. The GSF-based route can maximize the syngas yield, which benefits the promotion of the H_2 yield, while the PY-based route lowers the H_2 yield due to the coproduction of bio-oil and bio-char, and the CLC-based and CLG-based routes can directly obtain a high-purity H_2 stream from the SR. The WGS-based route is the most conventional way, which is always integrated with pre-combustion capture, and the application of SEWGS and SEG realizes higher H_2 yields and CO_2 capture rates due to the fact that *in situ* CO_2 capture pushes the reaction equilibrium of GSF and WGS forward to the generation of H_2. However, it also brings the potential consumption of energy to a higher level. The W/BtA system is an extension of the W/BtH system, given that the H_2 product of the W/BtH system is further utilized for NH_3 synthesis, most commonly with N_2 from the internal source, such as ASU, AR in the CL, and cathode of the FC. The application of CL is more advanced, given that it can produce hydrogen- and nitrogen-rich streams in the SR and AR without energy penalty, and consequently high-purity hydrogen and nitrogen can be acquired after simple gas–liquid separation for the synthesis of NH_3, respectively. The newly discovered concept of NC can also be applied in W/BtA systems with biochar as the feedstock. The choice of adjustment method is the key point in the W/BtSNG, W/BtMeOH, and W/BtDME systems, which concentrates on steam reforming and CO_2 removal as the internal method, and H_2 addition as the external method. It was reported that with the extra consumption of renewable energy, applying WEC as an external H_2 source can promote the product yields and levelized product cost. Compared to the W/BtP system, the W/BtF system has proven its potential in reducing the environmental impact with enhanced economic feasibility under the premise of foreseeable restricted policies and regulations.

• The prospects of the process simulation-based ex ante TEE assessment of thermochemical W/BtE systems are focused on the enhancement in data source quality and in-depth consideration of realistic conditions. More results from pilot- or commercial-scale systems and refined reaction models should participate in the validation and establishment of the simulation model. The application of regionalized background databases can remarkably increase the accuracy of the results with the consideration of local factors. Besides, realistic geographical and technical conditions should be considered more in-depth in the assessment, such as the local feedstock supply chain, intermittent renewable energy supply, and the balance of grid and heat supply network. It is strongly recommended to investigate the operation adjustment in the original system with new parameters, instead of using new parameters as the initial conditions for a newly proposed system, with the application of multiple simulation models.

Overall, the ex ante TEE assessment based on process simulation can realize the risk avoidance and advantage positioning before the application of low-carbon W/BtE technologies. With the development of advanced W/BtE technologies, the importance of assessment would also become more outstanding, given that it bridges the gap from laboratory to potential application scenes.

Abbreviations

AEC	Alkaline electrolysis cell
AGR	Acid gas removal
APC	Air pollution control
API	Annual production income
AR	Absorption refrigeration
ASU	Air separation unit
ATP	After tax profit
BEC	Bare erected cost
BFB	Bubbling fluidized bed
CAC	Carbon avoided cost
CAES	Compressed air energy storage
CaL	Calcium looping
CBR	CO_2 to biomass ratio
CCC	Carbon captured cost
CCE	Carbon conversion efficiency
CCR	CO_2 capture rate
CCS	Carbon capture and storage
CCHP	Combine cooling, heat, and power production
CEPCI	Chemical engineering plant cost index
CFD	Computational fluid dynamics
CHP	Combined heat and power production
CHU	Cascade heat utilization
CKPW	Computer keyboard plastic waste
CL	Chemical looping
CLAG	Chemical looping ammonia generation
CLC	Chemical looping combustion
CLG	Chemical looping gasification
COMB	Combustion
DDBM	Double declining balance method
DEM	Discrete element method
DFB	Dual fluidized bed
DME	Dimethyl ether
DO	Discrete ordinates
DPP	Dynamic payback period
DRM	Dry reforming of methane
EPCC	Engineering procurement and construction cost

ER	Equivalence ratio
ESW	Electrical switch waste
FC	Fuel cell
FCI	Fixed capital investment
FS	Fuel synthesis
FSP	Fuel separation & purification
SGSF	Steam gasification
SLM	Straight line method
SNCR	Selective non-catalytic reduction
SNG	Synthetic natural gas
SOFC	Solid oxide fuel cell
SR	Steam ratio or steam reactor
SYDM	Sum of the years digits method
TASC	Total as-spent cost
TCC	Total capital cost
TCES	Thermochemical energy storage
GSF	Gasification
HE	Heat exchanger
ICE	Internal combustion engine
IRR	Internal rate of return
LC	Levelized cost
LCA	Life cycle assessment
LCC	Life cycle cost
LCI	Life cycle inventory analysis
LCIA	Life cycle impact analysis
LHV	Lower heating value
LP	Levelized profit
MACRS	Modified accelerated cost recovery system
MED	Multi-effect distillation
MeOH	Methanol
M&S	Marshall and Swift index
MSP	Minimum selling price
MSW	Municipal solid waste
MPW	Mixed plastic waste
NC	Nitrogen carrier
NETL	National energy technology laboratory
NGR	Natural gas regasification
NPV	Net present value
OC	Oxygen carrier
OCOMB	Oxy-combustion
OFA	Over-fired air
OGSF	Oxy-gasification
ORC	Organic Rankine cycle
PA	Primary air
PCB	Printed circuit board
PEMEC	Proton exchange membrane electrolysis cell
POX	Partial oxidation
PP	Polypropylene
PSA	Pressure swing adsorption
PY	Pyrolysis
RANS	Reynolds averaged Navier–Stokes
RC	Rankine cycle
RGU	Residual gas utilization
SA	Secondary air
sCO_2	Supercritical CO_2 cycle
SECLG	Sorption-enhanced chemical looping gasification
SEG	Sorption-enhanced gasification
SEWGS	Sorption-enhanced water gas shift
SER	Steam ejector refrigerator
TE	Thermodynamic equilibrium
TEE	Techno-environmental-economic
TOC	Total overnight cost
TPC	Total plant cost
W/BtE	Waste or biomass to energy
WC	Working capital
WEC	Water electrolysis cell
WGS	Water gas shift
WtE	Waste to energy
W/BtF	Waste or biomass to fuel

Author contributions

Jiehong Tang: conceptualization, methodology, software, data curation, writing – original draft, writing – review & editing. Yuting Tang: supervision, writing – review & editing. Hongyu Liu: methodology, software, data curation. Xinfei Chen: methodology, software, data curation. Ziwei Sun: software, data curation. Xikui Zhang: methodology, software, data curation. Yin Chen: software, data curation. Shuang Liang: software, data curation. Junxuan Huang: software, data curation. Wen Teng: software, data curation. Ziwei Sun: software, data curation. Xiaoqian Ma: supervision.

Data availability

No original research findings, software, or code were included, and no new data were generated or analyzed in this review. Existing data from publications that support this article have been compiled.

Conflicts of interest

The authors declared no potential conflicts of interest with respect to the research, authorship, and/or publication of this article.

Acknowledgements

This study was financially supported by the National Key R&D Program of China (2024YFC3909002, 2020YFC1908901), Guangdong Basic and Applied Basic Research Foundation (2023A1515030016, 2024A1515011744), National Natural Science Foundation of China (52306289).

References

1 U. N. E. Programme and I. S. W. Association, *Global Waste Management Outlook 2024*, 2024.

2 G. Liu, Q. Huang, K. Song, Y. Pan and H. Zhang, *Waste Manage.*, 2024, **174**, 164–173, DOI: 10.1016/j.wasman.2023.12.001.
3 S. Ma, N. Deng, C. Zhao, P. Wang, C. Zhou, C. Sun, D. Guan, Z. Wang and J. Meng, *Environ. Sci. Technol.*, 2024, **58**, 11342–11351, DOI: 10.1021/acs.est.4c00408.
4 H. D. Beyene, A. A. Werkneh and T. G. Ambaye, *Renewable Energy Focus*, 2018, **24**, 1–11, DOI: 10.1016/j.ref.2017.11.001.
5 M. A. Alao, O. M. Popoola and T. R. Ayodele, *Clean. Energy Syst.*, 2022, **3**, 100034, DOI: 10.1016/j.cles.2022.100034.
6 K. Zhou, Y. Li, Y. Tang, Y. Yang, G. Tian, Bo Liu, B. Bian and C. He, *npj Sustainable Agric.*, 2024, **2**, 9, DOI: 10.1038/s44264-024-00019-z.
7 J. Hao, M. Ren, J. Xu, Z. Liu, X. Zhou and T. Zhang, *Strateg. Study CAE*, 2024, **26**, 80–88, DOI: 10.15302/j-sscae-2024.01.004.
8 K. Cen, M. Ni, J. Yan, X. Li and Y. Chi, *Technologies of Combustible Solid Waste to Energy*, Chemical Industry Press, Co, Ltd, Beijing, 2016.
9 G. Chen, B. Yan and Z. Cheng, *Pyrolysis-Gasification of the Organic Wastes*, Chemical Industry Press Co., Ltd, Beijing, 2022.
10 J. Qi, Y. Wang, P. Xu, M. Hu, T. Huhe, X. Ling, H. Yuan and Y. Chen, *Energy*, 2024, **290**, 130178, DOI: 10.1016/j.energy.2023.130178.
11 I. Khan and Z. Kabir, *Rewnewable Energy*, 2020, **150**, 320–333, DOI: 10.1016/j.renene.2019.12.132.
12 M. A. Rajaeifar, H. Ghanavati, B. B. Dashti, R. Heijungs, M. Aghbashlo and M. Tabatabaei, *Renewable Sustainable Energy Rev.*, 2017, **79**, 413–439, DOI: 10.1016/j.rser.2017.04.109.
13 U. Arena, *Waste Manage.*, 2012, **32**, 625–639, DOI: 10.1016/j.wasman.2011.09.025.
14 A. Batuer, J. S. Long, H. L. Du and D. Z. Chen, *J. Anal. Appl. Pyrolysis*, 2022, **163**, 105478, DOI: 10.1016/j.jaap.2022.105478.
15 D.-J. Lee, J.-S. Lu and J.-S. Chang, *Bioresour. Technol.*, 2020, **318**, 123912, DOI: 10.1016/j.biortech.2020.123912.
16 M. Zhang, Y. Qi, W. Zhang, M. Wang, J. Li, Y. Lu, S. Zhang, J. He, H. Cao, X. Tao, H. Xu and S. Zhang, *Renewable Sustainable Energy Rev.*, 2024, **199**, 114531, DOI: 10.1016/j.rser.2024.114531.
17 M. Afraz, F. Muhammad, J. Nisar, A. Shah, S. Munir, G. Ali and A. Ahmad, *Waste Manag. Bull.*, 2024, **1**, 30–40, DOI: 10.1016/j.wmb.2023.08.004.
18 Y. Zang, S. Ge, Y. Lin, L. Yin and D. Chen, *Waste Manage.*, 2024, **176**, 159–168, DOI: 10.1016/j.wasman.2024.01.026.
19 B. Wang, R. Gupta, L. Bei, Q. Wan and L. Sun, *Int. J. Hydrogen Energy*, 2023, **48**, 26676–26706, DOI: 10.1016/j.ijhydene.2023.03.086.
20 D. T. Pio, L. A. C. Tarelho and M. A. A. Matos, *Energy*, 2017, **120**, 915–925, DOI: 10.1016/j.energy.2016.11.145.
21 D. T. Pio, H. G. M. F. Gomes, L. A. C. Tarelho, A. C. M. Vilas-Boas, M. A. A. Matos and F. M. S. Lemos, *Renewable Energy*, 2022, **181**, 1223–1236, DOI: 10.1016/j.renene.2021.09.083.
22 S. Cheng, X. Ding, X. Dong, M. Zhang, X. Tian, Y. Liu, Y. Huang and B. Jin, *Carbon Resour. Convers.*, 2023, **6**, 184–204, DOI: 10.1016/j.crcon.2023.03.003.
23 A. Veksha, A. Giannis, G. Yuan, J. Tng, W. P. Chan, V. W.-C. Chang, G. Lisak and T.-T. Lim, *Renewable Energy*, 2019, **136**, 1294–1303, DOI: 10.1016/j.renene.2018.09.104.
24 S. Afzal, A. Singh, S. R. Nicholson, T. Uekert, J. S. DesVeaux, E. C. D. Tan, A. Dutta, A. C. Carpenter, R. M. Baldwin and G. T. Beckham, *Green Chem.*, 2023, **25**, 5068–5085, DOI: 10.1039/d3gc00679d.
25 G. Su, N. W. M. Zulkifli, L. Liu, H. C. Ong, S. Ibrahim, K. L. Yu, Y. Wei and F. Bin, *Energy Convers. Manage.*, 2023, **293**, 117481, DOI: 10.1016/j.enconman.2023.117481.
26 L. Makarichi, W. Jutidamrongphan and K.-a. Techato, *Renewable Sustainable Energy Rev.*, 2018, **91**, 812–821, DOI: 10.1016/j.rser.2018.04.088.
27 A. D. Pozzo, G. Antonioni, D. Guglielmi, C. Stramigioli and V. Cozzani, *Waste Manage.*, 2016, **51**, 81–90, DOI: 10.1016/j.wasman.2016.02.029.
28 H. Zhang, S. Yu, L. Shao and P. He, *J. Environ. Sci.*, 2019, **75**, 370–377, DOI: 10.1016/j.jes.2018.05.019.
29 N. AlQattan, M. Acheampong, F. M. Jaward, F. C. Ertem, N. Vijayakumar and T. Bello, *Renewable Energy Focus*, 2018, **27**, 97–110, DOI: 10.1016/j.ref.2018.09.005.
30 J. Liang, G. Lu, R. Wang, T. Tang, K. Huang, F. Jiang, W. Yu, X. Tao, H. Yin and Z. Dang, *J. Hazard. Mater.*, 2020, **399**, 123004, DOI: 10.1016/j.jhazmat.2020.123004.
31 Y. Tang, D. Tao, G. Li, C. Ye, Z. Bu, R. Shen, Y. Lin and W. Lv, *Environ. Pollut.*, 2024, **350**, 124011, DOI: 10.1016/j.envpol.2024.124011.
32 H. Kargbo, J. S. Harris and A. N. Phan, *Renewable Sustainable Energy Rev.*, 2021, **135**, 110168, DOI: 10.1016/j.rser.2020.110168.
33 F. Fei, Z. Wen, J. Zhang, Y. Xing, H. Zhang and Y. Li, *J. Environ. Manage.*, 2024, **355**, 120514, DOI: 10.1016/j.jenvman.2024.120514.
34 K. Li and B. Lin, *Energy*, 2018, **143**, 812–821, DOI: 10.1016/j.energy.2017.11.047.
35 H. Tang, S. Zhang and W. Chen, *Environ. Sci. Technol.*, 2021, **55**, 11225–11235, DOI: 10.1021/acs.est.1c03401.
36 G. Thomassen, M. V. Dael, S. V. Passel and F. You, *Green Chem.*, 2019, **21**, 4868–4886, DOI: 10.1039/C9GC02223F.
37 J. Lu, W. Liao, N. Zhang, D. Gu, P. Rao and G. Li, *Clean Coal Technol.*, 2023, **29**, 11–18, DOI: 10.13226/i.issn.1006-6772.CN22082501.
38 N. Tsoy, B. Steubing, C. v. d. Giesen and J. Guinée, *Int. J. Life Cycle Assess.*, 2020, **25**, 1680–1692, DOI: 10.1007/s11367-020-01796-8.
39 H. Ali, N. H. Eldrup, F. Normann, R. Skagestad and L. E. Øi, Cost Estimation of CO_2 Absorption Plants for CO_2 Mitigation – Method and Assumptions, *Int. J. Greenh. Gas Con.*, 2019, **88**, 10–23, DOI: 10.1016/j.ijggc.2019.05.028.
40 S. Vikram, P. Rosha and S. Kumar, *Energy Fuels*, 2021, **35**, 7406–7433, DOI: 10.1021/acs.energyfuels.1c00251.

41 S. Hameed, A. Sharma, V. Pareek, H. Wu and Y. Yu, *Biomass Bioenergy*, 2019, **123**, 104–122, DOI: 10.1016/j.biombioe.2019.02.008.
42 I. P. Silva, R. M. A. Lima, G. F. Silva, D. S. Ruzene and D. P. Silva, *Renewable Sustainable Energy Rev.*, 2019, **114**, 109305, DOI: 10.1016/j.rser.2019.109305.
43 A. Ramos, E. Monteiro and A. Rouboa, *Renewable Sustainable Energy Rev.*, 2019, **110**, 188–206, DOI: 10.1016/j.rser.2019.04.048.
44 J. Zhuang, J. Tang and L. Aljerf, *Fuel*, 2022, **320**, 123826, DOI: 10.1016/j.fuel.2022.123826.
45 X.-Y. Zhao, W. Jiang, Y.-F. Shan and J.-P. Cao, *Energy Fuels*, 2021, **36**, 502–513, DOI: 10.1021/acs.energyfuels.1c03818.
46 H. Siddiqi, U. Kumari, S. Biswas, A. Mishra and B. C. Meikap, *Energy*, 2020, **204**, 117933, DOI: 10.1016/j.energy.2020.117933.
47 A. A. Erdogan and M. Z. Yilmazoglu, *Appl. Energy*, 2024, **353**, 122014, DOI: 10.1016/j.apenergy.2023.122014.
48 C. Ma, R. Zhu, Y. Ma, Y. Yu, C. Tan, S. Yang, H. Liu, J. Hu and H. Wang, *Biomass Bioenergy*, 2025, **193**, 107568, DOI: 10.1016/j.biombioe.2024.107568.
49 Y. Zhang, Y. Ji and H. Qian, *Green Chem. Eng.*, 2021, **2**, 266–283, DOI: 10.1016/j.gce.2021.06.003.
50 X. Gao, J. Yu, L. Lu and W. A. Rogers, *Part. Technol. Fluid.*, 2021, **67**, e17139, DOI: 10.1002/aic.17139.
51 J. Qi, K. Zhang, M. Hu, P. Xu, T. Huhe, X. Ling, H. Yuan, Y. Wang and Y. Chen, *J. Environ. Chem. Eng.*, 2023, **11**, 111314, DOI: 10.1016/j.jece.2023.111314.
52 P. Parmar, S. Mukherjee and B. C. Meikap, *Process Saf. Environ. Prot.*, 2024, **188**, 350–362, DOI: 10.1016/j.psep.2024.05.083.
53 M. E. Mostafa, R. A. Alsulami and Y. M. Khedr, *J. Anal. Appl. Pyrolysis*, 2024, **179**, 106431, DOI: 10.1016/j.jaap.2024.106431.
54 K. W. Kuttin, H. Yu, M. Yang, L. Ding, X. Chen, G. Yu and F. Wang, *Green Carbon*, 2024, **2**, 176–196, DOI: 10.1016/j.greenca.2024.04.003.
55 R. Palange, C. De Blasio and M. Krishnan, *Energy*, 2023, **285**, 129487, DOI: 10.1016/j.energy.2023.129487.
56 A. M. Salem, I. N. Zaini, M. C. Paul and W. Yang, *Biomass Bioenergy*, 2019, **130**, 105377, DOI: 10.1016/j.biombioe.2019.105377.
57 S. Safarian, R. Unnþórsson and C. Richter, *Renewable Sustainable Energy Rev.*, 2019, **110**, 378–391, DOI: 10.1016/j.rser.2019.05.003.
58 M. HajiHashemi, S. Mazhkoo, H. Dadfar, E. Livani, A. Naseri Varnosefaderani, O. Pourali, S. Najafi Nobar and A. Dutta, *Energy*, 2023, **276**, 127506, DOI: 10.1016/j.energy.2023.127506.
59 S. Ferreira, E. Monteiro, P. Brito and C. Vilarinho, *Energies*, 2019, **12**, 160, DOI: 10.3390/en12010160.
60 H. M. U. Ayub, M. A. Qyyum, K. Qadeer, M. Binns, A. Tawfik and M. Lee, *J. Cleaner Prod.*, 2021, **321**, 128954, DOI: 10.1016/j.jclepro.2021.128954.
61 I. P. Silva, R. M. A. Lima, H. E. P. Santana, G. F. Silva, D. S. Ruzene and D. P. Silva, *Energy*, 2022, **241**, 122894, DOI: 10.1016/j.energy.2021.122894.
62 K. Rabea, S. Michailos, K. J. Hughes, D. Ingham and M. Pourkashanian, *Energy Convers. Manage.*, 2023, **298**, 117812, DOI: 10.1016/j.enconman.2023.117812.
63 V. Marcantonio, E. Bocci, J. P. Ouweltjes, L. D. Zotto and D. Monarca, *Int. J. Hydrogen Energy*, 2020, **45**, 6651–6662, DOI: 10.1016/j.ijhydene.2019.12.142.
64 A. Raje, A. A. Bhise, D. V. Surya and A. Kulkarni, *J. Anal. Appl. Pyrolysis*, 2024, **179**, 106477, DOI: 10.1016/j.jaap.2024.106477.
65 F. Alobaid, N. Almohammed, M. M. Farid, J. May, P. Rossger, A. Richter and B. Epple, *Prog. Energy Combust. Sci.*, 2022, **91**, 100930, DOI: 10.1016/j.pecs.2021.100930.
66 G. Lian and W. Zhong, *Fuel*, 2023, **350**, 128858, DOI: 10.1016/j.fuel.2023.128858.
67 L. Lu, X. Gao, J.-F. Dietiker, M. Shahnam and W. A. Rogers, *Chem. Eng. Sci.*, 2022, **248**, 117137, DOI: 10.1016/j.ces.2021.117131.
68 R. Deng, L. Wang, R. Zhang and Y. Luo, *Fuel*, 2021, **305**, 121442, DOI: 10.1016/j.fuel.2021.121442.
69 L. Wang, R. Zhang, R. Deng, Z. Liu and Y. Luo, *Appl. Energy*, 2023, **348**, 121525, DOI: 10.1016/j.apenergy.2023.121525.
70 C. B. Nguyen, M. Massoudi Farid, J. Scherer, Q. Guo, M. Gräbner and A. Richter, *Combust. Flame*, 2022, **240**, 112040, DOI: 10.1016/j.combustflame.2022.112040.
71 I. H. Mafat, D. V. Surya, S. K. Sharma and C. S. Rao, *J. Anal. Appl. Pyrolysis*, 2024, **180**, 106512, DOI: 10.1016/j.jaap.2024.106512.
72 H. Lee, I.-H. Choi and K.-R. Hwang, *J. Anal. Appl. Pyrolysis*, 2024, **179**, 106486, DOI: 10.1016/j.jaap.2024.106486.
73 R. Wang, Z. He, H. Chen, S. Guo, S. Zhang, K. Wang, M. Wang and S.-H. Ho, *Sci. Total Environ.*, 2024, **927**, 172310, DOI: 10.1016/j.scitotenv.2024.172310.
74 M. Ajorloo, M. Ghodrat, J. Scott and V. Strezov, *J. Energy Inst.*, 2022, **102**, 395–419, DOI: 10.1016/j.joei.2022.05.003.
75 A. Kushwah, T. R. Reina and M. Short, *Sci. Total Environ.*, 2022, **834**, 155243, DOI: 10.1016/j.scitotenv.2022.155243.
76 Y. Hu, X. Yu, J. Ren, Z. Zeng and Q. Qian, *Sci. Total Environ.*, 2024, **942**, 173561, DOI: 10.1016/j.scitotenv.2024.173561.
77 R. Garma, D. Sioud, H. Binous and A. Bellagi, *Comput. Appl. Eng. Educ.*, 2024, **32**, e22714, DOI: 10.1002/cae.22714.
78 M. Hussain, O. Ali, N. Raza, H. Zabiri, A. Ahmed and I. Ali, *RSC Adv.*, 2023, **13**, 23796–23811, DOI: 10.1039/d3ra01219k.
79 W. George Davies, S. Babamohammadi, Y. Yang and S. Masoudi Soltani, *Gas Sci. Eng.*, 2023, **118**, 205104, DOI: 10.1016/j.jgsce.2023.205104.
80 R. Molina, G. Orcajo, Y. Segura, J. Moreno and F. Martínez, *Educ. Chem. Eng.*, 2021, **34**, 127–137, DOI: 10.1016/j.ece.2020.09.003.
81 Y. Zhang, B. Li, H. Li and H. Liu, *Thermochim. Acta*, 2011, **519**, 65–71, DOI: 10.1016/j.tca.2011.03.005.
82 Y. Kalinci, A. Hepbasli and I. Dincer, *Int. J. Hydrogen Energy*, 2010, **35**, 4991–5000, DOI: 10.1016/j.ijhydene.2009.08.079.

83 L. Jiao, J. Li, B. Yan, G. Chen and S. Ahmed, *Appl. Energy*, 2022, **319**, 119255, DOI: 10.1016/j.apenergy.2022.119255.
84 R. K. Singh, K. Jena, J. P. Chakraborty and A. Sarkar, *Int. J. Hydrogen Energy*, 2020, **45**, 18922–18936, DOI: 10.1016/j.ijhydene.2020.05.045.
85 Y. Sun and Y. Tang, *Chem. Eng. Res. Des.*, 2023, **191**, 14–26, DOI: 10.1016/j.cherd.2023.01.023.
86 P. Mongkolsiri, S. Jitkeaw, Y. Patcharavorachot, A. Arpornwichanop, S. Assabumrungrat and S. Authayanun, *Int. J. Hydrogen Energy*, 2019, **44**, 2216–2229, DOI: 10.1016/j.ijhydene.2018.07.176.
87 Y. Sun, Z. Qin, Y. Tang, T. Huang, S. Ding and X. Ma, *J. Environ. Chem. Eng.*, 2021, **9**, 106108, DOI: 10.1016/j.jece.2021.106108.
88 D. R. Morris and J. Szargut, *Energy*, 1986, **11**, 733–755, DOI: 10.1016/0360-5442(86)90013-7.
89 H. Shahbeig, A. Shafizadeh, M. A. Rosen and B. F. Sels, *Biofuel Res. J.*, 2022, **9**, 1592–1607, DOI: 10.18331/brj2022.9.1.5.
90 M. H. Khoshgoftar Manesh and E. Jadidi, *Energy Sources, Part A*, 2020, 1–22, DOI: 10.1080/15567036.2020.1752856.
91 Y. Ayub, J. Ren, C. He and C. Azzaro-Pantel, *Chem. Eng. J.*, 2024, **480**, 148080, DOI: 10.1016/j.cej.2023.148080.
92 S. Kelly, G. Tsatsaronis and T. Morosuk, *Energy*, 2009, **34**, 384–391, DOI: 10.1016/J.ENERGY.2008.12.007.
93 S. Kelly, G. Tsatsaronis and T. Morosuk, *Energy*, 2009, **34**, 384–391, DOI: 10.1016/j.energy.2008.12.007.
94 S. Kelly, PhD, Technische Universität Berlin, 2008.
95 F. Petrakopoulou, G. Tsatsaronis, T. Morosuk and A. Carassai, *Energy*, 2012, **41**, 146–152, DOI: 10.1016/j.energy.2011.05.028.
96 J. Zhou, J. Ren and C. He, *Process Saf. Environ. Prot.*, 2023, **178**, 342–359, DOI: 10.1016/j.psep.2023.08.040.
97 J. Ferdous, F. Bensebaa, K. Hewage, P. Bhowmik and N. Pelletier, *Clean. Environ. Syst.*, 2024, 100215, DOI: 10.1016/j.cesys.2024.100215.
98 X. Chen, H. S. Matthews and W. M. Griffin, *Resour., Conserv. Recycl.*, 2021, **172**, 105678, DOI: 10.1016/j.resconrec.2021.105678.
99 Z. Liang, X. Ma, H. Lin and Y. Tang, *Appl. Energy*, 2011, **88**, 1120–1129, DOI: 10.1016/j.apenergy.2010.10.010.
100 Z. Chen, Y. Wang, B. Huang, S. Li, J. Song, X. Xu, M. Xie, X. Wang and Y. Long, *Environ. Impact Assess. Rev.*, 2024, **105**, 107394, DOI: 10.1016/j.eiar.2023.107394.
101 J. Miao, X. Wang, S. Bai, Y. Xiang and L. Li, *J. Cleaner Prod.*, 2021, **314**, 128010, DOI: 10.1016/j.jclepro.2021.128010.
102 R. Turton, J. A. Shaeiwitz, D. Bhattachartta and W. B. Whiting, *Analysis Synthesis and Design of Chemical Processes*, Pearson Education, Inc., 5th edn, 2018.
103 M. S. Peters, K. Timmerhaus and R. E. West, *Plant Design and Economics for Chemical Engineers*, McGraw Hill, 5th edn, 2003.
104 G. E. Dieter and L. C. Schmidt, *Plant Design and Economics for Chemical Engineers*, McGraw-Hill, 6th edn, 2020.
105 R. Turton, J. A. Shaeiwitz, D. Bhattachartta and W. B. Whiting, *Analysis Synthesis and Design of Chemical Processes*, Pearson Education, Inc., 5th edn, 2018.
106 NETL, *Fossil Energy Baseline Revision* 4a, 2022.
107 H. Ali, N. H. Eldrup, F. Normann, R. Skagestad and L. E. Øi, *Int. J. Greenh. Gas Control.*, 2019, **88**, 10–23, DOI: 10.1016/j.ijggc.2019.05.028.
108 D. C. Makepa, C. H. Chihobo, W. R. Ruziwa and D. Musademba, *Fuel Commun.*, 2023, **14**, 100086, DOI: 10.1016/j.jfueco.2023.100086.
109 H. J. Lang, *Chem. Eng.*, 1948, **55**, 112–113.
110 W. Hand, *Pet. Refin.*, 1958, **37**, 331.
111 E. S. Rubin, C. Short, G. Booras, J. Davison, C. Ekstrom, M. Matuszewski and S. McCoy, *Int. J. Greenh. Gas Control.*, 2013, **17**, 488–503, DOI: 10.1016/j.ijggc.2013.06.004.
112 NETL, *Cost and Performance Baseline for Fossil Energy Plants Supplement: Sensitivity to CO2 Capture Rate in Coal-Fired Power Plants*, 2020.
113 M. Ishaq and H. Ishaq, *J. Cleaner Prod.*, 2023, **425**, 138657, DOI: 10.1016/j.jclepro.2023.138657.
114 D. Yancy-Caballero, R. Hughes, M. A. Zamarripa, B. Omell, M. Matuszewski and D. Bhattacharyya, *Int. J. Greenh. Gas Control.*, 2023, **128**, 103957, DOI: 10.1016/j.ijggc.2023.103957.
115 D. Thanganadar, F. Asfand, K. Patchigolla and P. Turner, *Energy Convers. Manage.*, 2021, **242**, 114294, DOI: 10.1016/j.enconman.2021.114294.
116 V. Spallina, G. Motamedi, F. Gallucci and M. v. S. Annaland, *Int. J. Greenh. Gas Control.*, 2019, **88**, 71–84, DOI: 10.1016/j.ijggc.2019.05.026.
117 M. Moosazadeh, A. S. T. Charmchi, P. Ifaei, V. Taghikhani, R. G. Moghanloo and C. Yoo, *Energy Convers. Manage.*, 2024, **300**, 117926, DOI: 10.1016/j.enconman.2023.117926.
118 J. Li, H. Wang, H. Chen, H. Wu, G. Xu, Y. Dong, Q. Zhao and T. Liu, *Appl. Therm. Eng.*, 2023, **221**, 119762, DOI: 10.1016/j.applthermaleng.2022.119762.
119 Y. Gu, D. Wang, Q. Chen and Z. Tang, *Int. J. Hydrogen Energy*, 2022, **47**, 5085–5100, DOI: 10.1016/j.ijhydene.2021.11.148.
120 X. Qiu, J. Zhao, Y. Yu and T. Ma, *Front. Eng. Manag.*, 2022, **9**, 392–408, DOI: 10.1007/s42524-022-0212-6.
121 A. Lazzaretto and G. Tsatsaronis, *Energy*, 2006, **31**, 1257–1289, DOI: 10.1016/j.energy.2005.03.011.
122 A. Ghasemi, H. Nikafshan Rad, M. Akrami and M. Marefati, *Therm. Sci. Eng. Prog.*, 2024, **48**, 102407, DOI: 10.1016/j.tsep.2024.102407.
123 Y. Huang, L. Zhu, Y. He, X. Zeng, Y. Wang, Q. Hao, C. Zhang and Y. Zhu, *Energy*, 2024, **306**, 132379, DOI: 10.1016/j.energy.2024.132379.
124 L. Meyer, G. Tsatsaronis, J. Buchgeister and L. Schebek, *Energy*, 2009, **34**, 75–89, DOI: 10.1016/j.energy.2008.07.018.
125 C. Zhang, L. Zhu, Q. Hao, Y. Huang, X. Zeng, Y. Wang, J. Fan and Y. He, *Energy Convers. Manage.*, 2024, **300**, 117951, DOI: 10.1016/j.enconman.2023.117951.

126 S. A. Zaman, D. Roy and S. Ghosh, *Biomass Bioenergy*, 2020, **143**, 105847, DOI: 10.1016/j.biombioe.2020.105847.
127 S. Vikram, P. Rosha, S. Kumar and S. Mahajani, *Energy*, 2022, **241**, 122854, DOI: 10.1016/j.energy.2021.122854.
128 Z. Yu, H. Xie, L. Wang, Z. Shao, C. Huang and S. Yang, *J. Therm. Anal. Calorim.*, 2024, **149**, 3497–3512, DOI: 10.1007/s10973-024-12905-2.
129 P. Mondal, *Int. J. Hydrogen Energy*, 2022, **47**, 20064–20075, DOI: 10.1016/j.ijhydene.2022.04.150.
130 I. A. Jamro, A. Raheem, S. Khoso, H. A. Baloch, A. Kumar, G. Chen, W. A. Bhagat, T. Wenga and W. Ma, *J. Environ. Manage.*, 2023, **328**, 117014, DOI: 10.1016/j.jenvman.2022.117014.
131 A. Nemmour, A. Inayat, I. Janajreh and C. Ghenai, *Fuel*, 2023, **349**, 128698, DOI: 10.1016/j.fuel.2023.128698.
132 K. Viswanathan, S. Abbas and W. Wu, *Waste Manag.*, 2022, **144**, 132–143, DOI: 10.1016/j.wasman.2022.03.018.
133 L. Qian, S. Wang, S. Wang, S. Zhao and B. Zhang, *Int. J. Hydrogen Energy*, 2021, **46**, 89–99, DOI: 10.1016/j.ijhydene.2020.09.200.
134 D. Cvetinović, A. Erić, M. Mladenović, J. Buha-Marković and B. Janković, *Energy Convers. Manage.*, 2024, **313**, 118639, DOI: 10.1016/j.enconman.2024.118639.
135 Y. Ayub, J. Zhou, J. Ren, T. Shi, W. Shen, C. He and K. Srinivasan, *Int. J. Energy Res.*, 2023, **2023**, 1–14, DOI: 10.1155/2023/7787947.
136 D. K. Singh and J. V. Tirkey, *Biomass Bioenergy*, 2022, **158**, 106370, DOI: 10.1016/j.biombioe.2022.106370.
137 Y. Xu, M. Zhai, D. Yang, Z. Ma, G. Kumar, P. Dong and J. Zhu, *Environ. Technol.*, 2023, **44**, 480–491, DOI: 10.1080/09593330.2021.1976281.
138 I. A. Jamro, A. Kumar, S. Khoso, M. Ahmad, H. A. Baloch, S. A. Raheel Shah, L. Kumari, T. Wenga, M. Nadeem, A. A. Laghari, G. Chen and W. Ma, *Int. J. Hydrogen Energy*, 2023, **48**, 21636–21653, DOI: 10.1016/j.ijhydene.2023.03.053.
139 D. K. Singh and J. V. Tirkey, *Environ. Technol.*, 2022, **43**, 4291–4305, DOI: 10.1080/09593330.2021.1946599.
140 D. Gündüz Han, K. Erdem and A. Midilli, *Int. J. Hydrogen Energy*, 2023, **48**, 39315–39329, DOI: 10.1016/j.ijhydene.2023.07.038.
141 Y. Cao, Y. Bai and J. Du, *Int. J. Hydrogen Energy*, 2024, **73**, 265–273, DOI: 10.1016/j.ijhydene.2024.06.037.
142 Y. Zhou, W. Li and Y. Song, *Process Saf. Environ. Prot.*, 2024, **190**, 1450–1460, DOI: 10.1016/j.psep.2024.08.028.
143 T. Aentung, W. Wu and Y. Patcharavorachot, *J. Taiwan Inst. Chem. Eng.*, 2024, **164**, 105688, DOI: 10.1016/j.jtice.2024.105688.
144 W. Jiang, J. Tao, X. Zhong, Y. Ye, J. Kang, Q. Tang, D. Liu, Y. Ren, D. Li, H. Cai and D. Li, *Environ. Res.*, 2023, **235**, 116684, DOI: 10.1016/j.envres.2023.116684.
145 M. Ajorloo, M. Ghodrat, J. Scott and V. Strezov, *Energy*, 2022, **256**, 124638, DOI: 10.1016/j.energy.2022.124638.
146 F.-H. Wu and Y.-T. Hsu, *Int. J. Hydrogen Energy*, 2024, **83**, 29–38, DOI: 10.1016/j.ijhydene.2024.08.089.
147 N. Ranjan, S. Kumar and S. M. Mahajani, *Int. J. Hydrogen Energy*, 2024, **81**, 1045–1061, DOI: 10.1016/j.ijhydene.2024.07.218.
148 N. Ranjan, N. Yadav, H. Singh, S. Kumar and S. M. Mahajani, *Energy Convers. Manage.*, 2023, **297**, 117714, DOI: 10.1016/j.enconman.2023.117714.
149 J. Cai, W. Zheng, M. Luo and X. Tang, *Process Saf. Environ. Prot.*, 2021, **147**, 985–992, DOI: 10.1016/j.psep.2021.01.022.
150 R. Bakari, T. Kivevele, X. Huang and Y. A. C. Jande, *J. Anal. Appl. Pyrolysis*, 2020, 104891, DOI: 10.1016/j.jaap.2020.104891.
151 D. C. Makepa, C. H. Chihobo, W. R. Ruziwa and D. Musademba, *Heliyon*, 2023, **9**, e14688, DOI: 10.1016/j.heliyon.2023.e14688.
152 K. Benamara, S. Amara and F. Tabet, *Biofuels*, 2024, **15**, 349–361, DOI: 10.1080/17597269.2023.2250636.
153 K. Thu, T. Reungpeerakul, R. Yamsaengsung and C. Sangwichien, *Environ. Prog. Sustain. Energy*, 2021, **41**, e13717, DOI: 10.1002/ep.13717.
154 Y. Elhenawy, K. Fouad, A. Mansi, M. Bassyouni, M. Gadalla, F. Ashour and T. Majozi, *J. Therm. Anal. Calorim.*, 2024, **149**, 10369–10383, DOI: 10.1007/s10973-024-12987-y.
155 S. Gupta, P. Patel and P. Mondal, *Fuel*, 2022, **310**, 122230, DOI: 10.1016/j.fuel.2021.122230.
156 P. Rosha, S. Kumar and H. Ibrahim, *Energy*, 2022, **247**, 123545, DOI: 10.1016/j.energy.2022.123545.
157 S. El Kourdi, S. Abderafi, A. Cheddadi, J. Mabrouki and M. A. Abbassi, *Energy Convers. Manage.*, 2024, **304**, 118206, DOI: 10.1016/j.enconman.2024.118206.
158 A. Temireyeva, Y. Sarbassov and D. Shah, *Fuel*, 2024, **367**, 131494, DOI: 10.1016/j.fuel.2024.131494.
159 Q. N. Hoang, J. Van Caneghem, T. Croymans, R. Pittoors and M. Vanierschot, *Fuel*, 2022, **326**, 124963, DOI: 10.1016/j.fuel.2022.124963.
160 J. Tang, J. B. Zhuang, L. Aljerf, H. Xia, T. Z. Wang and B. Y. Gao, *Process Saf. Environ. Prot.*, 2023, **176**, 506–527, DOI: 10.1016/j.psep.2023.05.101.
161 X. Su, L. Ma, Q. Fang, C. Yin, H. Zhuang, Y. Qiao, C. Zhang and G. Chen, *Appl. Therm. Eng.*, 2024, **238**, 122043, DOI: 10.1016/j.applthermaleng.2023.122043.
162 M. Yan, Antoni, J. Y. Wang, D. Hantoko and E. Kanchanatip, *Fuel*, 2021, **285**, 119193, DOI: 10.1016/j.fuel.2020.119193.
163 M. Zheng, J. Sun, L. Gong, Y. Fan, J. Tu and J. Dong, *Appl. Therm. Eng.*, 2024, **236**, 121763, DOI: 10.1016/j.applthermaleng.2023.121763.
164 W. Zeng, Y. Wang, Q. Bu, S. Ma, H. Hu, D. Ma and H. Ma, *Process Saf. Environ. Prot.*, 2024, **185**, 325–339, DOI: 10.1016/j.psep.2024.03.017.
165 X. Yang, Y. Liao, X. Ma and J. Zhou, *Appl. Therm. Eng.*, 2022, **201**, 117706, DOI: 10.1016/j.applthermaleng.2021.117706.
166 X. Yang, Y. Liao, Y. Wang, X. Chen and X. Ma, *Fuel*, 2022, **314**, 122769, DOI: 10.1016/j.fuel.2021.122769.

167 A. Zhou, H. Xu, X. Meng, W. Yang and R. Sun, *Chem. Eng. J.*, 2021, **405**, 126604, DOI: 10.1016/j.cej.2020.126604.
168 X. Qi, X. Q. Ma, Z. S. Yu, Z. G. Huang and W. Teng, *Fuel*, 2023, **345**, 128115, DOI: 10.1016/j.fuel.2023.128115.
169 T. Lin, Y. F. Liao, T. H. Dai and X. Q. Ma, *Fuel*, 2023, **343**, 127882, DOI: 10.1016/j.fuel.2023.127882.
170 X. Yang, Y. Liao, T. Lin and X. Ma, *Proc. CSEE*, 2020, **40**, 6964–6973, DOI: 10.13334/j.0258-8013.pcsee.200820.
171 X. Huang, X. Jin, L. Dong, R. Li, K. Yang, Y. Li, L. Deng and D. Che, *J. Energy Inst.*, 2024, **113**, 101550, DOI: 10.1016/j.joei.2024.101550.
172 Y. Liu, S. Liu, Y. Li, Y. Li and J. He, *ACS Omega*, 2021, **6**, 12530–12540, DOI: 10.1021/acsomega.1c00270.
173 O. Karlström, E. Vainio, M. Engblom, A. Brink and M. Hupa, *Fuel*, 2022, **330**, 125565, DOI: 10.1016/j.fuel.2022.125565.
174 Z. H. Wan, J. H. Hu and X. J. Qi, *Energy*, 2021, **225**, 120254, DOI: 10.1016/j.energy.2021.120254.
175 Z. Yang, Q. Hu, Q. Chen, Y. Q. Chen, H. Li, H. P. Yang and H. P. Chen, *Energy Fuels*, 2024, **38**, 4273–4289, DOI: 10.1021/acs.energyfuels.3c04754.
176 L. Wang, X. Du, L. Xu and J. Sun, *Renewable Energy*, 2020, **162**, 1065–1075, DOI: 10.1016/j.renene.2020.08.093.
177 S. Du, S. Yuan and Q. Zhou, *Renewable Energy*, 2021, **172**, 424–439, DOI: 10.1016/j.renene.2021.03.035.
178 J. Manu and V. Madav, *Case Stud. Therm. Eng.*, 2022, **39**, 102429, DOI: 10.1016/j.csite.2022.102429.
179 L. Lu, X. Gao, A. Gel, G. M. Wiggins, M. Crowley, B. Pecha, M. Shahnam, W. A. Rogers, J. Parks and P. N. Ciesielski, *Chem. Eng. J.*, 2021, **421**, 127789, DOI: 10.1016/j.cej.2020.127789.
180 M. Pourhoseinian, N. Asasian-Kolur and S. Sharifian, *Biomass Bioenergy*, 2024, **180**, 107026, DOI: 10.1016/j.biombioe.2023.107026.
181 X. Liu, G. Zhu, T. Asim and R. Mishra, *Energy*, 2022, **248**, 123647, DOI: 10.1016/j.energy.2022.123647.
182 C. Pieper, S. Wirtz, S. Schaefer and V. Scherer, *Fuel*, 2021, **283**, 118951, DOI: 10.1016/j.fuel.2020.118951.
183 H. Khodaei, C. Álvarez-Bermúdez, S. Chapela, C. Olson, M. D. MacKenzie, M. A. Gómez and J. Porteiro, *Energy*, 2024, **288**, 129895, DOI: 10.1016/j.energy.2023.129895.
184 K. W. Kuttin and L. Ding, *Biomass Bioenergy*, 2024, **186**, 107270, DOI: 10.1016/j.biombioe.2024.107270.
185 H. R. Sun, S. L. Yang, G. R. Bao, J. H. Hu and H. Wang, *Energy*, 2023, **283**, 128496, DOI: 10.1016/j.energy.2023.128496.
186 H. Yu, H. Sun, S. Yang, G. Bao and H. Wang, *Renewable Energy*, 2024, **223**, 120068, DOI: 10.1016/j.renene.2024.120068.
187 Y. H. Bello, M. A. Ahmed, S. Ookawara and A. E. Elwardany, *Energy*, 2022, **239**, 122179, DOI: 10.1016/j.energy.2021.122179.
188 N. Raza, M. Ahsan, M. T. Mehran, S. R. Naqvi and I. Ahmad, *Powder Technol.*, 2022, **405**, 117500, DOI: 10.1016/j.powtec.2022.117500.
189 L. Mu, L. Zhao, T. Hu, B. Zhang, Z. Zhai, Y. Shang and H. Yin, *Ind. Eng. Chem. Res.*, 2021, **60**, 15618–15634, DOI: 10.1021/acs.iecr.1c02010.
190 Y. Cao, J. Wang, Y. Li, W. Fu and B. Liu, *Energy Convers. Manage.*, 2023, **283**, 116925, DOI: 10.1016/j.enconman.2023.116925.
191 T. Yasui, M. Aoki, T. Uchino and C. Fushimi, *ACS Eng. Au*, 2023, **3**, 498–511, DOI: 10.1021/acsengineeringau.3c00029.
192 A. Bore, G. Dziva, C. Chu, Z. Huang, X. Liu, S. Qin and W. Ma, *J. Environ. Manage.*, 2024, **349**, 119280, DOI: 10.1016/j.jenvman.2023.119280.
193 Y. Zhang, S. Wu, D. Cui, S.-J. Yoon, Y.-S. Bae, B. Park, Y. Wu, F. Zhou, C. Pan and R. Xiao, *Fuel Process. Technol.*, 2022, **238**, 107476, DOI: 10.1016/j.fuproc.2022.107476.
194 D. M. Saharudin, H. K. Jeswani and A. Azapagic, *Appl. Energy*, 2023, **349**, 121506, DOI: 10.1016/j.apenergy.2023.121506.
195 C. Ortiz, S. García-Luna, R. Chacartegui, J. M. Valverde and L. Pérez-Maqueda, *J. Cleaner Prod.*, 2023, **403**, 136776, DOI: 10.1016/j.jclepro.2023.136776.
196 G. Y. Zang, J. N. Zhang, J. X. Jia, E. S. Lora and A. Ratner, *Renewable Energy*, 2020, **149**, 336–346, DOI: 10.1016/j.renene.2019.12.013.
197 M. Gazzani, E. Macchi and G. Manzolini, *Fuel*, 2013, **105**, 206–219, DOI: 10.1016/j.fuel.2012.07.048.
198 L. Han, J. Zhao, N. Rong, Z. Wang, Z. Qi, Z. Shen, H. Ding and H. Yu, *Biomass Convers. Biorefin.*, 2023, **14**, 23649–23666, DOI: 10.1007/s13399-023-04357-9.
199 J. L. J. Ling, S. S. Oh, H. J. Park and S. H. Lee, *Renewable Sustainable Energy Rev.*, 2023, **182**, 113380, DOI: 10.1016/j.rser.2023.113380.
200 Y. L. Xiang, L. Cai, Y. W. Guan, W. B. Liu, T. Z. He and J. Li, *Energy*, 2019, **179**, 571–580, DOI: 10.1016/j.energy.2019.05.011.
201 M. J. Greencorn, S. D. Jackson, J. S. J. Hargreaves, S. Datta and M. C. Paul, *Energy Convers. Manage.*, 2023, **277**, 116601, DOI: 10.1016/j.enconman.2022.116601.
202 S. Saqline, Z. Y. Chua and W. Liu, *Energy Convers. Manage.*, 2021, **244**, 114455, DOI: 10.1016/j.enconman.2021.114455.
203 O. Emenike, S. Michailos, K. N. Finney, K. J. Hughes, D. Ingham and M. Pourkashanian, *Sustain. Energy Technol. Assess.*, 2020, **40**, 100743, DOI: 10.1016/j.seta.2020.100743.
204 Y. Zheng, L. Gao, S. He and H. Jin, *Front. Energy*, 2023, **17**, 390–399, DOI: 10.1007/s11708-023-0864-x.
205 Y. Zhu, C. Zhang, M. Yan, Z. Liu, W. Li, H. Li and Y. Wang, *Energy*, 2024, **304**, 132096, DOI: 10.1016/j.energy.2024.132096.
206 A. Shabruhi Mishamandani, A. Qatarani Nejad, N. Shabani and G. Ahmadi, *Renewable Energy Focus*, 2024, **50**, 100610, DOI: 10.1016/j.ref.2024.100610.
207 L. Yan, L. Wang, Z. Wang, Y. Cao and B. He, *J. Cleaner Prod.*, 2021, **285**, 125424, DOI: 10.1016/j.jclepro.2020.125424.
208 N. Pour, P. A. Webley and P. J. Cook, *Int. J. Greenh. Gas Control.*, 2018, **68**, 1–15, DOI: 10.1016/j.ijggc.2017.11.007.
209 J. Mohn, S. Szidat, J. Fellner, H. Rechberger, R. Quartier, B. Buchmann and L. Emmenegger, *Bioresour. Technol.*, 2008, **99**, 6471–6479, DOI: 10.1016/j.biortech.2007.11.042.

210 M. P. S. Santos and D. P. Hanak, *Int. J. Hydrogen Energy*, 2022, **47**, 6586–6604, DOI: **10.1016/j.ijhydene.2021.12.037**.
211 J. P. Mercado, A. T. Ubando, J. A. Gonzaga and S. R. Naqvi, *Environ. Res.*, 2023, **217**, 114876, DOI: **10.1016/j.envres.2022.114876**.
212 U. Mohamed, Y. Zhao, Y. Huang, Y. Cui, L. Shi, C. Li, M. Pourkashanian, G. Wei, Q. Yi and W. Nimmo, *Energy*, 2020, **205**, 117904, DOI: **10.1016/j.energy.2020.117904**.
213 Z. Xu, J. Huang, T. Muhammad, M. K. Agrawal, M. Ayadi, M. A. Ahmed, J. B. Ooi and F. Xiao, *Process Saf. Environ. Prot.*, 2024, **183**, 925–944, DOI: **10.1016/j.psep.2024.01.040**.
214 Y. P. Liu, Y. Wang and D. G. Huang, *Energy*, 2019, **189**, 115900, DOI: **10.1016/j.energy.2019.115900**.
215 J. Y. Cao, L. Zheng, Z. Y. Zheng, J. Q. Peng, M. K. Hu, Q. L. Wang and M. K. H. Leung, *Appl. Therm. Eng.*, 2023, **231**, 120903, DOI: **10.1016/j.applthermaleng.2023.120903**.
216 M. Chahartaghi, N. Dahmardeh, S. M. Hashemian and R. Malek, *Energy Sources, Part A*, 2021, 1–25, DOI: **10.1080/15567036.2021.1968074**.
217 Q. W. Pan, X. Y. Li, B. Wang, J. F. Li, S. H. Jin, J. Xu and T. S. Ge, *Appl. Therm. Eng.*, 2024, **251**, 123614, DOI: **10.1016/j.applthermaleng.2024.123614**.
218 Z. Zhong, M. Burhan, K. C. Ng, X. Cui and Q. Chen, *Desalination*, 2024, **576**, 117325, DOI: **10.1016/j.desal.2024.117325**.
219 J. Liu, H. Sun, H. Chen, W. Li, P. Pan, L. Wu, G. Xu and W. Liu, *Appl. Therm. Eng.*, 2023, **230**, 120825, DOI: **10.1016/j.applthermaleng.2023.120825**.
220 A. Lampropoulos, G. Varvoutis, E. Mandela, M. Konsolakis, G. E. Marnellos, D. Ipsakis and C. Athanasiou, *Int. J. Hydrogen Energy*, 2023, **48**, 39463–39483, DOI: **10.1016/j.ijhydene.2023.06.335**.
221 S. Li, H. Chen, X. Yuan, P. Pan, G. Xu, X. Wang and L. Wu, *Energy*, 2024, **295**, 130806, DOI: **10.1016/j.energy.2024.130806**.
222 G. Su, P. Jiang, H. C. Ong, J. Zhu, N. A. S. Amin, N. W. M. Zulkifli and S. Ibrahim, *J. Cleaner Prod.*, 2023, **423**, 138749, DOI: **10.1016/j.jclepro.2023.138749**.
223 A. Dufour, P. Girods, E. Masson, Y. Rogaume and A. Zoulalian, *Int. J. Hydrogen Energy*, 2009, **34**, 1726–1734, DOI: **10.1016/j.ijhydene.2008.11.075**.
224 D. Neves, H. Thunman, A. Matos, L. Tarelho and A. Gómez-Barea, *Prog. Energy Combust. Sci.*, 2011, **37**, 611–630, DOI: **10.1016/j.pecs.2011.01.001**.
225 M. Kong, X. Ye, D. Liu and C. Li, *Energy*, 2024, **296**, 131161, DOI: **10.1016/j.energy.2024.131161**.
226 Y. Wang, H. Xu, Y. Li, N. Lin and P. Xu, *Chemosphere*, 2023, **340**, 139818, DOI: **10.1016/j.chemosphere.2023.139818**.
227 A. Kumar Tripathi, I. Patra, N. Bharath Kumar, A. Majdi, I. Muda and A. Mahdavi, *Energy Sources, Part A*, 2022, **44**, 8490–8511, DOI: **10.1080/15567036.2022.2123070**.
228 N. D. Montiel-Bohórquez, A. F. Agudelo and J. F. Pérez, *Energy Convers. Manage.*, 2021, **238**, 114138, DOI: **10.1016/j.enconman.2021.114138**.
229 G. Biancini, L. Cioccolanti, R. Moradi and M. Moglie, *Appl. Therm. Eng.*, 2024, **241**, 122437, DOI: **10.1016/j.applthermaleng.2024.122437**.
230 V. Zare, *Energy Convers. Manage.*, 2020, **225**, 113479, DOI: **10.1016/j.enconman.2020.113479**.
231 C. Fu, J. Wang, Q. Shen, Z. Cui and S. Ding, *Energy Convers. Manage.*, 2024, **299**, 117802, DOI: **10.1016/j.enconman.2023.117802**.
232 S. Yang, A. Liang, S. Peng, Z. Liu, C. Deng and N. Xie, *Appl. Therm. Eng.*, 2024, **246**, 122924, DOI: **10.1016/j.applthermaleng.2024.122924**.
233 Z. Wu, P. Zhu, J. Yao, S. Zhang, J. Ren, F. Yang and Z. Zhang, *Appl. Energy*, 2020, **279**, 115794, DOI: **10.1016/j.apenergy.2020.115794**.
234 M. S. Khan, Q. Huan, J. G. Lin, R. D. Zheng, Z. L. Gao and M. Yan, *Energy Convers. Manage.*, 2022, **258**, 115506, DOI: **10.1016/j.enconman.2022.115506**.
235 Y. Cao, H. A. Dhahad, N. Farouk, W.-F. Xia, H. Nikafshan Rad, A. Ghasemi, S. Kamranfar, M. Mostafavi Sani and A. Akbar Shayesteh, *Appl. Therm. Eng.*, 2021, **196**, 117339, DOI: **10.1016/j.applthermaleng.2021.117339**.
236 W. Peng, H. Chen, J. Liu, X. Zhao and G. Xu, *Energy Convers. Manage.*, 2021, **245**, 114622, DOI: **10.1016/j.enconman.2021.114622**.
237 H. Zhao, R. Lu and T. Zhang, *Energy Convers. Manage.*, 2023, **280**, 116817, DOI: **10.1016/j.enconman.2023.116817**.
238 A. Kasaeian, H. Hadavi, Y. Amirhaeri and F. Pourfayaz, *Renewable Energy*, 2022, **195**, 1174–1193, DOI: **10.1016/j.renene.2022.06.101**.
239 P. Zhu, Z. Wu, L. Guo, J. Yao, M. Dai, J. Ren, S. Kurko, H. Yan, F. Yang and Z. Zhang, *Energy Convers. Manage.*, 2021, **240**, 114245, DOI: **10.1016/j.enconman.2021.114245**.
240 Z. Sun and M. Aziz, *Energy Convers. Manage.*, 2021, **244**, 114517, DOI: **10.1016/j.enconman.2021.114517**.
241 J. Zhang, H. Cheng, Z. Xu, Y. Zhou, K. Yin, X. Wang, Y. Gao, C. Sun, Y. Wang and P. Cui, *J. Cleaner Prod.*, 2023, **402**, 136844, DOI: **10.1016/j.jclepro.2023.136844**.
242 J. Liu, Y. Li, X. Meng and J. Wu, *Int. J. Green Energy*, 2023, **20**, 1524–1544, DOI: **10.1080/15435075.2022.2163589**.
243 X. Zhang, W. Liu, J. Pan, B. Zhao, Z. Yi, X. He, Y. Liu and H. Li, *Energy*, 2024, **295**, 131112, DOI: **10.1016/j.energy.2024.131112**.
244 C. Liu, C.-Y. Hsu, M. K. Agrawal, J. Zhang, S. F. Ahmad, A. H. Seikh, V. Mohanavel, S. Tahir Chauhdary and F. Chi, *J. Cleaner Prod.*, 2024, **443**, 141137, DOI: **10.1016/j.jclepro.2024.141137**.
245 L. Wang, G. Bo, R. Gao, M. Ayadi, W. Chammam, J. B. Ooi and M. Qin, *Process Saf. Environ. Prot.*, 2024, **184**, 151–169, DOI: **10.1016/j.psep.2024.01.073**.
246 T. U. K. Nutakki, M. K. Agrawal, S. Tahir Chauhdary, S. F. Ahmad, M. Ayadi, E. Hedi, T. Muhammad and F. Xiao, *Desalination*, 2024, **577**, 117404, DOI: **10.1016/j.desal.2024.117404**.

247 J. Zhang, P. Cui, S. Yang, Y. Zhou, W. Du, Y. Wang, C. Deng and S. Wang, *Appl. Energy*, 2023, **336**, 120822, DOI: 10.1016/j.apenergy.2023.120822.
248 H. Chen, J. R. Li, T. Y. Li, G. Xu, X. Jin, M. Wang and T. Liu, *Energy*, 2022, **245**, 123156, DOI: 10.1016/j.energy.2022.123156.
249 M. Singh, D. Zappa and E. Comini, *Int. J. Hydrogen Energy*, 2021, **46**, 27643–27674, DOI: 10.1016/j.ijhydene.2021.06.020.
250 J. Lv, Y. Wang, H. Chen, W. Li, P. Pan, L. Wu, G. Xu and R. Zhai, *Energy*, 2023, **282**, 128866, DOI: 10.1016/j.energy.2023.128866.
251 T. Hai, A. S. El-Shafay, A. H. Mohammed, K. Sharma and H. Rajab, *Int. J. Hydrogen Energy*, 2024, **49**, 252–265, DOI: 10.1016/j.ijhydene.2023.07.338.
252 T. Hai, M. A. Ali, A. Alizadeh, S. F. Almojil, A. I. Almohana, B. S. Chauhan, A. F. Alali and A. Raise, *Appl. Therm. Eng.*, 2023, **223**, 119884, DOI: 10.1016/j.applthermaleng.2022.119884.
253 H. Tian, R. H. Li and Y. P. Zhu, *Energy*, 2023, **285**, 129425, DOI: 10.1016/j.energy.2023.129425.
254 P. Jiang, A. Mahmud Parvez, Y. Meng, X. Dong, M. Xu, X. Luo, K. Shi and T. Wu, *Energy Convers. Manage.*, 2021, **236**, 114066, DOI: 10.1016/j.enconman.2021.114066.
255 W. G. Mei, R. R. Zhai and Z. H. Qian, *Appl. Therm. Eng.*, 2023, **223**, 119998, DOI: 10.1016/j.applthermaleng.2023.119998.
256 D. Lu, H. Chen, B. Li, J. An, P. Pan, G. Xu, Q. Zhao and T. Liu, *Energy Technol.*, 2023, **11**, 2300012, DOI: 10.1002/ente.202300012.
257 F. Ghorbannejad, M. H. Khoshgoftar Manesh, M. Nemati and A. Ghasemi, *Energy Rep.*, 2022, **8**, 9057–9080, DOI: 10.1016/j.egyr.2022.07.001.
258 K. Yang, Y. Y. He, N. Du, P. Yan, N. Zhu, Y. Z. Chen, J. Wang and P. D. Lund, *Energy*, 2024, **301**, 131605, DOI: 10.1016/j.energy.2024.131605.
259 J. Ren, Z. Q. Qian, C. G. Fei, D. Lu, Y. C. Zou, C. Xu and L. Liu, *Energy*, 2023, **269**, 126676, DOI: 10.1016/j.energy.2023.126676.
260 Y. Casas-Ledón, F. Spaudo and L. E. Arteaga-Pérez, *J. Cleaner Prod.*, 2017, **164**, 187–197, DOI: 10.1016/j.jclepro.2017.06.211.
261 Y. D. Fu, L. Cai, C. M. Liu, M. L. Wu and Y. W. Guan, *Renewable Energy*, 2024, **226**, 120290, DOI: 10.1016/j.renene.2024.120290.
262 N. Hashemian, A. Noorpoor and M. Amidpour, in *Synergy Development in Renewables Assisted Multi-carrier Systems*, ed. M. Amidpour, M. Ebadollahi, F. Jabari, M. R. Kolahi and H. Ghaebi, Springer, Cham, 2022, DOI: 10.1007/978-3-030-90720-4_5.
263 Y. Xiao, H. L. You, B. Hu, G. X. Li, J. T. Han, A. Lysyakov and D. F. Chen, *Int. J. Hydrogen Energy*, 2024, **63**, 82–102, DOI: 10.1016/j.ijhydene.2024.03.144.
264 Y. Ayub, J. Zhou, J. Ren and C. He, *Energy Convers. Manage.*, 2023, **292**, 117426, DOI: 10.1016/j.enconman.2023.117426.
265 L. Mu, P. Xie, T. Hu, Y. Shang, H. Pu, M. Dong and Z. Huo, *Biomass Convers. Biorefin.*, 2024, DOI: 10.1007/s13399-024-05684-1.
266 M. Parvez, O. Khan, S. Lal and M. Ahmad, Thermodynamic analysis of a solar-biomass cogeneration power and cooling by employing an ejector and single-effect absorption refrigeration system, *Biomass Bioenergy*, 2024, **184**, 107143, DOI: 10.1016/j.biombioe.2024.107143.
267 A. Behzadi, A. Arabkoohsar and V. S. Peric, *Appl. Therm. Eng.*, 2021, **190**, 116824, DOI: 10.1016/j.applthermaleng.2021.116824.
268 A. Biboum, A. Yilanci, S. M. O. Thierry, N. Yimen and R. Mouangue, *Energy Sources, Part A*, 2023, **45**, 9668–9683, DOI: 10.1080/15567036.2023.2239747.
269 X. Qi, C. Yang, M. Huang, Z. Ma, A. Hnydiuk-Stefan, K. Feng, P. Siarry, G. Królczyk and Z. Li, Conventional and advanced exergy-exergoeconomic-exergoenvironmental analyses of an organic Rankine cycle integrated with solar and biomass energy sources, *Energy*, 2024, **288**, 129657, DOI: 10.1016/j.energy.2023.129657.
270 A. R. Razmi, H. Heydari Afshar, A. Pourahmadiyan and M. Torabi, *Sustain. Energy Technol. Assess.*, 2021, **46**, 101253, DOI: 10.1016/j.seta.2021.101253.
271 T. Hai, M. A. Ali, A. Alizadeh, S. F. Almojil, A. I. Almohana, B. S. Chauhan, A. F. Alali and A. Raise, Optimization next to environmental analysis of harvesting waste heat from a biomass-driven externally-fired gas turbine cycle for sub-zero cooling and production of hydrogen, freshwater, and hot water, *Appl. Therm. Eng.*, 2023, **223**, 119884, DOI: 10.1016/j.applthermaleng.2022.119884.
272 X. J. Xue, J. Y. Lv, H. Chen, G. Xu and Q. B. Li, *Energy*, 2022, **261**, 125367, DOI: 10.1016/j.energy.2022.125367.
273 T. Uchino, T. Yasui and C. Fushimi, *Energy Convers. Manage.*, 2021, **243**, 114366, DOI: 10.1016/j.enconman.2021.114366.
274 T. Uchino, T. Yasui and C. Fushimi, *J. Energy Storage*, 2023, **61**, 106720, DOI: 10.1016/j.est.2023.106720.
275 S. Yi, H. Lin, A. M. Abed, A. Shawabkeh, M. Marefati and A. Deifalla, *Sustain. Cities Soc.*, 2023, **91**, 104412, DOI: 10.1016/j.scs.2023.104412.
276 H. Ishaq, S. Islam, I. Dincer and B. S. Yilbas, *J. Cleaner Prod.*, 2020, **256**, 120625, DOI: 10.1016/j.jclepro.2020.120625.
277 S. Zhang, W. Jian, J. Zhou, J. Li and G. Yan, *Fuel*, 2023, **334**, 126825, DOI: 10.1016/j.fuel.2022.126825.
278 N. Ding, W. Wu, L. Wang and H. Yin, *Int. J. Hydrogen Energy*, 2024, **52**, 485–504, DOI: 10.1016/j.ijhydene.2023.03.364.
279 M. Ishaq and I. Dincer, *Sustain. Cities Soc.*, 2024, **104**, 105291, DOI: 10.1016/j.scs.2024.105291.
280 B. Hosseingholilou, N. Tavakoli and M. Saidi, *Process Saf. Environ. Prot.*, 2024, **187**, 533–548, DOI: 10.1016/j.psep.2024.04.086.
281 K. Ma, T. Shi, Y. Hu, S. Yang, W. Shen, C. He, Y. Liu, Z. Liu and J. Ren, *Energy Convers. Manage.*, 2022, **269**, 116135, DOI: 10.1016/j.enconman.2022.116135.
282 N. Lümmen and E. V. Røstbø, *Energy*, 2020, **211**, 118996, DOI: 10.1016/j.energy.2020.118996.
283 Z. Xu, Y. Zhou, K. Yin, J. Zhang, Z. Zhu, Y. Wang and P. Cui, *J. Cleaner Prod.*, 2023, **386**, 135835, DOI: 10.1016/j.jclepro.2022.135835.

284 K. Yin, Y. Wang, Q. Wu, J. Zhang, Y. Zhou, Z. Xu, Z. Zhu, J. Qi, Y. Wang and P. Cui, *Renewable Energy*, 2024, **222**, 119893, DOI: 10.1016/j.renene.2023.119893.
285 K. Yin, R. Zhang, M. Yan, L. Sun, Y. Ma, P. Cui, Z. Zhu and Y. Wang, *Process Saf. Environ. Prot.*, 2023, **178**, 8–17, DOI: 10.1016/j.psep.2023.08.007.
286 Z. F. Xu, H. Q. Qi, D. Yao, J. F. Zhang, Z. Y. Zhu, Y. L. Wang and P. Z. Cui, *Energy Convers. Manage.*, 2022, **258**, 115509, DOI: 10.1016/j.enconman.2022.115509.
287 R. Ren, H. Wang, X. Feng and C. You, *Energy Convers. Manage.*, 2023, **292**, 117401, DOI: 10.1016/j.enconman.2023.117401.
288 J. Zhou, C. Liu, J. Ren and C. He, *Energy*, 2024, **310**, 133272, DOI: 10.1016/j.energy.2024.133272.
289 Z. Ma, X. Liu, G. Li, X. Qiu, D. Yao, Z. Zhu, Y. Wang, J. Gao and P. Cui, *J. Environ. Chem. Eng.*, 2021, **9**, 106752, DOI: 10.1016/j.jece.2021.106752.
290 K. Lan and Y. Yao, *Commun. Earth Environ.*, 2022, **3**, 300, DOI: 10.1038/s43247-022-00632-1.
291 N. Wu, K. Lan and Y. Yao, *Resour. Conserv. Recycl.*, 2023, **188**, 106693, DOI: 10.1016/j.resconrec.2022.106693.
292 T. Shi, J. Zhou, J. Ren, Y. Ayub, H. Yu, W. Shen, Q. Li and A. Yang, *Energy*, 2023, **272**, 127131, DOI: 10.1016/j.energy.2023.127131.
293 C. Zhao, J. Huang, D. Xie, Y. Qiao and M. Xu, *Energy Convers. Manage.*, 2024, **299**, 117826, DOI: 10.1016/j.enconman.2023.117826.
294 G. Li, S. Wang, J. Zhao, H. Qi, Z. Ma, P. Cui, Z. Zhu, J. Gao and Y. Wang, *Energy*, 2020, **199**, 117488, DOI: 10.1016/j.energy.2020.117488.
295 M. Shamsi, A. A. Obaid, S. Farokhi and A. Bayat, *Int. J. Hydrogen Energy*, 2022, **47**, 772–781, DOI: 10.1016/j.ijhydene.2021.10.055.
296 A. Poluzzi, G. Guandalini and M. C. Romano, *Sustainable Energy Fuels*, 2022, **6**, 3830–3851, DOI: 10.1039/d2se00661h.
297 R. Demol, A. Dufour, Y. Rogaume and G. Mauviel, *Energy Fuels*, 2021, **36**, 488–501, DOI: 10.1021/acs.energyfuels.1c03528.
298 D. J. Nouwe Edou and J. A. Onwudili, *Renewable Energy*, 2022, **189**, 704–716, DOI: 10.1016/j.renene.2022.02.074.
299 Y. A. Situmorang, Z. Zhao, P. An, T. Yu, J. Rizkiana, A. Abudula and G. Guan, *Appl. Energy*, 2020, **268**, 115122, DOI: 10.1016/j.apenergy.2020.115122.
300 T. Li, J. Wang, H. Chen, W. Li, P. Pan, L. Wu, G. Xu and H. Chen, *Energy Convers. Manage.*, 2023, **287**, 117085, DOI: 10.1016/j.enconman.2023.117085.
301 A. Perejón, L. M. Romeo, Y. Lara, P. Lisbona, A. Martínez and J. M. Valverde, *Appl. Energy*, 2016, **162**, 787–807, DOI: 10.1016/j.apenergy.2015.10.121.
302 Z. Chu, Y. Li, C. Zhang and Y. Fang, *Fuel*, 2023, **342**, 127916, DOI: 10.1016/j.fuel.2023.127916.
303 C. Zhang, Y. Li, Z. Chu and Y. Fang, *Energy Convers. Manage.*, 2023, **278**, 116710, DOI: 10.1016/j.enconman.2023.116710.
304 S. Khosravi, E. Neshat and R. K. Saray, *Renewable Energy*, 2023, **214**, 140–153, DOI: 10.1016/j.renene.2023.06.003.
305 C. Zhang, Y. Li, L. Yang, X. Fan and L. Chu, *Energy Convers. Manage.*, 2022, **253**, 115169, DOI: 10.1016/j.enconman.2021.115169.
306 G. Dziva, Z. Jia, Y. Xue and L. Zeng, *Fuel*, 2023, **352**, 129024, DOI: 10.1016/j.fuel.2023.129024.
307 G. Dziva, Q. Cheng, K. Liu and L. Zeng, *Int. J. Hydrogen Energy*, 2023, **48**, 38602–38616, DOI: 10.1016/j.ijhydene.2023.06.216.
308 J. H. Tang, Y. T. Tang, Y. C. Liu, Z. W. Sun, J. M. Deng, W. L. Chen, Z. Qin and X. Q. Ma, *Energy Convers. Manage.*, 2023, **292**, 117375, DOI: 10.1016/j.enconman.2023.117375.
309 X. Chen, Z. Sun, P.-C. Kuo and M. Aziz, *Chem. Eng. J.*, 2024, **485**, 149734, DOI: 10.1016/j.cej.2024.149734.
310 J. Qi, J. Liu, G. Chen, J. Yao, B. Yan, W. Yi, H. Zao and S. Xu, *Energy Convers. Manage.*, 2023, **294**, 117562, DOI: 10.1016/j.enconman.2023.117562.
311 G. C. Liu, Y. Zhao, S. Heberlein, A. Veksha, A. Giannis, W. P. Chan, T. T. Lim and G. Lisak, *Energy Convers. Manage.*, 2022, **269**, 116087, DOI: 10.1016/j.enconman.2022.116087.
312 C. Rai, B. Bhui and P. V, *Int. J. Hydrogen Energy*, 2022, **47**, 11177–11189, DOI: 10.1016/j.ijhydene.2022.01.159.
313 R. Mallick and P. Prabu, *Energy Convers. Manage.*, 2022, **271**, 116320, DOI: 10.1016/j.enconman.2022.116320.
314 D. Wu, Z. Gao, S. Wu and R. Xiao, *Energy Fuels*, 2023, **37**, 14033–14045, DOI: 10.1021/acs.energyfuels.3c02405.
315 D. Wu, Z. Gao, S. Wu and R. Xiao, *Int. J. Hydrogen Energy*, 2024, **66**, 24–32, DOI: 10.1016/j.ijhydene.2024.04.078.
316 C. Xu, Y. Liu, Q. Zhang, T. Xin, R. Zhao, M. Wang, W. Saw and S. Lu, *Energy Convers. Manage.*, 2021, **247**, 114746, DOI: 10.1016/j.enconman.2021.114746.
317 G. Acikalin and I. Dincer, *Process Saf. Environ. Prot.*, 2023, **178**, 776–785, DOI: 10.1016/j.psep.2023.08.043.
318 G. Dziva, C. Luan, G. Ding, A. Boré, K. Jean Ives Kouakou, T. Tembo, A. Ullah, M. Zaman, S. Li and L. Zeng, *Chem. Eng. J.*, 2024, **490**, 151666, DOI: 10.1016/j.cej.2024.151666.
319 Z. Sun, S. Wang and M. Aziz, *Energy Convers. Manage.*, 2022, **251**, 115013, DOI: 10.1016/j.enconman.2021.115013.
320 K. Miyahira and M. Aziz, *J. Cleaner Prod.*, 2022, **372**, 133827, DOI: 10.1016/j.jclepro.2022.133827.
321 J. Tang, L. Kang and Y. Liu, *Ind. Eng. Chem. Res.*, 2022, **61**, 8128–8140, DOI: 10.1021/acs.iecr.2c00616.
322 D. Wen and M. Aziz, *Appl. Energy*, 2022, **319**, 119272, DOI: 10.1016/j.apenergy.2022.119272.
323 R. Yan, M. Wu, J. Fan, C. Sun, J. Wang, Y. He, H. Liu, P. Li and J. Zhang, *Energy Convers. Manage.*, 2024, **306**, 118263, DOI: 10.1016/j.enconman.2024.118263.
324 Q. Weng, S. Toan, R. Ai, Z. Sun and Z. Sun, *J. Cleaner Prod.*, 2021, **289**, 125749, DOI: 10.1016/j.jclepro.2020.125749.
325 M. Akbari and A. Kumar, *Fuel*, 2024, **358**, 130107, DOI: 10.1016/j.fuel.2023.130107.

326 X. Cui, G. Song, A. Yao, H. Wang, L. Wang and J. Xiao, *Process Saf. Environ. Prot.*, 2021, **156**, 417–428, DOI: 10.1016/j.psep.2021.10.025.
327 A. S. R. Subramanian, T. Gundersen and T. A. Adams, *Energy*, 2020, **205**, 117830, DOI: 10.1016/j.energy.2020.117830.
328 M. Schmid, C. Schmidberger, S. Hafner and G. Scheffknecht, *Fuel*, 2024, **360**, 130491, DOI: 10.1016/j.fuel.2023.130491.
329 A. L. Rispoli, N. Verdone and G. Vilardi, *Fuel Process. Technol.*, 2021, **221**, 106922, DOI: 10.1016/j.fuproc.2021.106922.
330 H. Zhang, L. Wang, J. Van herle, F. Maréchal and U. Desideri, *Appl. Energy*, 2020, **270**, 115113, DOI: 10.1016/j.apenergy.2020.115113.
331 J. Wang, K. A. Al-attab and T. Y. Heng, *J. Cleaner Prod.*, 2024, **449**, 141712, DOI: 10.1016/j.jclepro.2024.141712.
332 J. Wang, K. A. Al-attab and T. Y. Heng, *Energy Convers. Manage.*, 2023, **280**, 116762, DOI: 10.1016/j.enconman.2023.116762.
333 A. AlNouss, G. McKay and T. Al-Ansari, *Energy Convers. Manage.*, 2020, **208**, 112612, DOI: 10.1016/j.enconman.2020.112612.
334 S. Wang, C. Li, Y.-j. Hu, H. Wang, G. Xu, G. Zhao and S. Wang, *Fuel*, 2024, **358**, 130255, DOI: 10.1016/j.fuel.2023.130255.
335 T. Shi, Y. Liu, A. Yang, S. Sun, W. Shen and J. Ren, *Energy Convers. Manage.*, 2022, **260**, 115600, DOI: 10.1016/j.enconman.2022.115600.
336 C. Y. A. Nwai and B. Patel, *Waste Biomass Valorization*, 2023, **14**, 4155–4171, DOI: 10.1007/s12649-023-02115-6.
337 Z. Sun and M. Aziz, *Appl. Energy*, 2022, **323**, 119635, DOI: 10.1016/j.apenergy.2022.119635.
338 M. Del Grosso, B. Sridharan, C. Tsekos, S. Klein and W. de Jong, *Biomass Bioenergy*, 2020, **136**, 105529, DOI: 10.1016/j.biombioe.2020.105529.
339 A. AlNouss, M. Shahbaz, G. McKay and T. Al-Ansari, *J. Cleaner Prod.*, 2022, **341**, 130849, DOI: 10.1016/j.jclepro.2022.130849.
340 H. Y. Liu, Y. T. Tang, X. Q. Ma, J. H. Tang and W. C. Yue, *Energy Convers. Manage.*, 2024, **309**, 118428, DOI: 10.1016/j.enconman.2024.118428.
341 K. Im-orb, A. N. Phan and A. Arpornwichanop, *Energy Convers. Manage.*, 2020, **226**, 113493, DOI: 10.1016/j.enconman.2020.113493.
342 U. Safder, J. Loy-Benitez and C. Yoo, *Energy*, 2024, **290**, 130104, DOI: 10.1016/j.energy.2023.130104.
343 Q. J. Zhang, H. Chen, B. Li, P. Y. Pan, G. Xu, Q. X. Zhao and X. Jiang, *Appl. Therm. Eng.*, 2023, **225**, 120234, DOI: 10.1016/j.applthermaleng.2023.120234.
344 Y. T. Wang, H. Chen, S. C. Qiao, P. Y. Pan, G. Xu, Y. H. Dong and X. Jiang, *Energy*, 2023, **267**, 126490, DOI: 10.1016/j.energy.2022.126490.
345 E. Anetjärvi, E. Vakkilainen and K. Melin, *Energy*, 2023, **276**, 127202, DOI: 10.1016/j.energy.2023.127202.
346 Y. Sun, *Process Saf. Environ. Prot.*, 2024, **185**, 225–238, DOI: 10.1016/j.psep.2024.02.086.
347 S. Pratschner, F. Radosits, A. Ajanovic and F. Winter, *J. CO_2 Util.*, 2023, **75**, 102563, DOI: 10.1016/j.jcou.2023.102563.
348 F. Rajaee, G. Guandalini, M. C. Romano and J. Ritvanen, *Energy Convers. Manage.*, 2024, **301**, 118009, DOI: 10.1016/j.enconman.2023.118009.
349 M. Ostadi, G. Y. Zang, L. Bromberg, D. R. Cohn and E. Gençer, *Energy Convers. Manage.*, 2024, **302**, 118142, DOI: 10.1016/j.enconman.2024.118142.
350 M. Ostadi, L. Bromberg, D. R. Cohn and E. Gençer, *Fuel*, 2023, **334**, 126697, DOI: 10.1016/j.fuel.2022.126697.
351 J. H. Tang, Y. T. Tang, H. Y. Liu, S. B. Peng, Z. W. Sun, Y. C. Liu, J. M. Deng, W. L. Chen and X. Q. Ma, *Energy Convers. Manage.*, 2024, **314**, 118727, DOI: 10.1016/j.enconman.2024.118727.
352 G. Butera, R. O. Gadsboll, G. Ravenni, J. Ahrenfeldt, U. B. Henriksen and L. R. Clausen, *Energy*, 2020, **199**, 117405, DOI: 10.1016/j.energy.2020.117405.
353 Y. Sun, Z. Qin, Y. T. Tang, C. F. Liao, Y. C. Liu and X. Q. Ma, *Process Saf. Environ. Prot.*, 2022, **161**, 611–627, DOI: 10.1016/j.psep.2022.03.060.
354 A. Poluzzi, G. Guandalini, S. Guffanti, C. Elsido, S. Moioli, P. Huttenhuis, G. Rexwinkel, E. Martelli, G. Groppi and M. C. Romano, *Fuel*, 2022, **310**, 122113, DOI: 10.1016/j.fuel.2021.122113.
355 D. Klüh, E. Anetjärvi, K. Melin and E. Vakkilainen, *Energy Convers. Manage.*, 2024, **314**, 118649, DOI: 10.1016/j.enconman.2024.118649.
356 L. Y. Zhang, R. X. Gao, Z. Y. Tang, C. D. Zhang, K. W. Jun, S. K. Kim, T. S. Zhao, H. Wan and G. F. Guan, *Energy Convers. Manage.*, 2024, **311**, 118504, DOI: 10.1016/j.enconman.2024.118504.
357 W. W. Xu, J. F. Zhang, Q. M. Wu, Y. Y. Wang, W. X. Zhao, Z. Y. Zhu, Y. L. Wang and P. Z. Cui, *Appl. Energy*, 2024, **374**, 124031, DOI: 10.1016/j.apenergy.2024.124031.
358 J. Zhang, Y. Wang, Y. Zhang, Q. Wu, L. Xin, Y. Zhou, K. Yin, Y. Wang, X. Li and P. Cui, *Energy Convers. Manage.*, 2024, **299**, 117808, DOI: 10.1016/j.enconman.2023.117808.
359 K. Im-orb and P. Piroonlerkgul, *Renewable Energy*, 2023, **208**, 324–330, DOI: 10.1016/j.renene.2023.03.092.
360 K. Im-orb and A. Arpornwichanop, *Energy Convers. Manage.*, 2022, **258**, 115511, DOI: 10.1016/j.enconman.2022.115511.
361 R. Kofler, N. Campion, M. Hillestad, W. Meesenburg and L. R. Clausen, *Energy Fuels*, 2024, **38**, 8777–8803, DOI: 10.1021/acs.energyfuels.4c00311.
362 R. Kofler and L. R. Clausen, *Energy Convers. Manage.*, 2023, **281**, 116815, DOI: 10.1016/j.enconman.2023.116815.
363 J. Byun, O. Kwon, J. Kim and J. Han, *ACS Sustainable Chem. Eng.*, 2022, **10**, 4512–4521, DOI: 10.1021/acssuschemeng.1c08300.
364 H. Zhou, A. Meng, Y. Long, Q. Li and Y. Zhang, *Renewable Sustainable Energy Rev.*, 2014, **36**, 107–122, DOI: 10.1016/j.rser.2014.04.024.
365 M. Rybaczewska-Błażejowska and D. Jezierski, *Int. J. Life Cycle Assess.*, 2024, **29**, 1799–1817, DOI: 10.1007/s11367-024-02326-6.
366 Y. Zhao, J. Yao, G. Chen, J. Liu, Z. Cheng, L. Wang, W. Yi and S. Xu, *Energy Convers. Manage.*, 2023, **295**, 117623, DOI: 10.1016/j.enconman.2023.117623.

367 H. Lee, J. Im, H. Cho, S. Jung, H. Choi, D. Choi, J. Kim, J. Lee and E. E. Kwon, *Chem. Eng. J.*, 2024, **481**, 148741, DOI: 10.1016/j.cej.2024.148741.
368 I. R. E. Agency, *Innovation Outlook: Renewable Methanol*, Abu Dhabi, 2021.
369 B. Eisavi, F. Ranjbar, H. Nami and A. Chitsaz, *Energy Convers. Manage.*, 2022, **253**, 115163, DOI: 10.1016/j.enconman.2021.115163.
370 B. Eisavi, H. Nami, F. Ranjbar and A. Sharifi, *Int. J. Hydrogen Energy*, 2024, **52**, 869–888, DOI: 10.1016/j.ijhydene.2023.11.025.
371 M. Cortazar, L. Santamaria, G. Lopez, J. Alvarez, L. Zhang, R. Wang, X. Bi and M. Olazar, *Energy Convers. Manage.*, 2023, **276**, 116496, DOI: 10.1016/j.enconman.2022.116496.
372 J. Ren and Y.-L. Liu, *J. Hazard. Mater. Lett.*, 2020, **1**, 100008, DOI: 10.1016/j.hazl.2020.100008.
373 X. S. Zhang, J. W. Pan, L. Wang, T. L. Qian, Y. Z. Zhu, H. Q. Sun, J. Gao, H. J. Chen, Y. Gao and C. Liu, *Appl. Energy*, 2019, **251**, 113314, DOI: 10.1016/j.apenergy.2019.113314.
374 M. L. V. Rios, A. M. González, E. E. S. Lora and O. A. A. del Olmo, *Biomass Bioenergy*, 2018, **108**, 345–370, DOI: 10.1016/j.biombioe.2017.12.002.
375 F. Zhou, L. Zhu, L. Yang, Y. Hong and J. Xu, *Appl. Therm. Eng.*, 2023, **233**, 121148, DOI: 10.1016/j.applthermaleng.2023.121148.
376 X. H. Wang, Y. F. Zhang and K. N. Ma, *Sustain. Cities Soc.*, 2024, **111**, 105555, DOI: 10.1016/j.scs.2024.105555.
377 A. De Meyer, S. Verdonck, I. Storms, J. López, M. Tschulkow, T. Compernolle, S. Van Passel, J. Van Orshoven, B. Verbist, R. Guisson, W. Arts, S. Van den Bosch, J. Van Aelst, B. Sels and B. Muys, *J. Cleaner Prod.*, 2024, **440**, 140873, DOI: 10.1016/j.jclepro.2024.140873.
378 T. N. O. Mensah, A. S. Oyewo, D. Bogdanov, A. Aghahosseini and C. Breyer, *Renewable Energy*, 2024, **234**, 121198, DOI: 10.1016/j.renene.2024.121198.
379 L. Izquierdo-Horna, R. Kahhat and I. Vázquez-Rowe, *Sustain. Prod. Consum.*, 2022, **33**, 809–819, DOI: 10.1016/j.spc.2022.08.008.
380 D. Bisen, A. P. S. Chouhan, M. Pant and S. Chakma, *Renewable Sustainable Energy Rev.*, 2025, **208**, 115016, DOI: 10.1016/j.rser.2024.115016.
381 Z. Ghaemi and A. D. Smith, *Sustain. Energy Technol. Assess.*, 2022, **51**, 101986, DOI: 10.1016/j.seta.2022.101986.
382 P. M. De Oliveira-De Jesus, *Renewable Sustainable Energy Rev.*, 2019, **101**, 516–526, DOI: 10.1016/j.rser.2018.11.030.
383 M. Jia, Z. Zhang, L. Zhang, L. Zhao, X. B. Lu, L. Y. Li, J. H. Ruan, Y. L. Wu, Z. M. He, M. Liu, L. L. Jiang, Y. J. Gao, P. C. Wu, S. Y. Zhu, M. C. Niu, H. T. Zheng, B. F. Cai, L. Tang, Y. B. Shu and J. N. Wang, *Appl. Energy*, 2024, **373**, 123838, DOI: 10.1016/j.apenergy.2024.123838.
384 P. Glavic, Z. N. Pintaric, H. Levicnik, V. Dragojlovic and M. Bogataj, *Processes*, 2023, **11**, 2647, DOI: 10.3390/pr11092647.
385 Y. Teng, C. Z. Li, G. Q. P. Shen, Q. W. Yang and Z. Peng, *Build. Environ.*, 2023, **243**, 110648, DOI: 10.1016/j.buildenv.2023.110648.
386 M. Kalverkamp, E. Helmers and A. Pehlken, *J. Cleaner Prod.*, 2020, **269**, 121329, DOI: 10.1016/j.jclepro.2020.121329.
387 C. Ding, *Environ. Sanit. Eng.*, 2024, **32**, 36–40, DOI: 10.19841/j.cnki.hjwsgc.2024.05.006.
388 J. P. Xu, Y. D. Huang, Y. Shi and R. L. Li, *Socio-Econ. Plan. Sci.*, 2022, **81**, 101180, DOI: 10.1016/j.seps.2021.101180.
389 Y. Xin, X. Xing, X. Li and H. Hong, *Appl. Energy*, 2024, **356**, 122419, DOI: 10.1016/j.apenergy.2023.122419.
390 S. J. Ma, C. B. Zhou, C. Chi, Y. J. Liu and G. Yang, *Environ. Sci. Technol.*, 2020, **54**, 9609–9617, DOI: 10.1021/acs.est.0c01802.
391 M. M. Billal, R. M. Sebastian and A. Kumar, *J. Cleaner Prod.*, 2024, **434**, 139865, DOI: 10.1016/j.jclepro.2023.139865.
392 A. Shah Irshad, M. Naseer Zakir, S. Shah Rashad, M. Elsayed Lotfy, A. Mikhaylov, M. H. Elkholy, G. Pinter and T. Senjyu, *Energy Convers. Manag.: X*, 2024, **23**, 100640, DOI: 10.1016/j.ecmx.2024.100640.
393 K. Kocsis, J. Kövendi and B. Bokor, *Sustain. Cities Soc.*, 2024, **117**, 105953, DOI: 10.1016/j.scs.2024.105953.
394 X. Cheng, J. Yang, Z. Han, G. Shi, D. Pan, L. Meng, Z. Zeng and Z. Shen, *Int. J. Appl. Earth Obs. Geoinf.*, 2024, **135**, 104219, DOI: 10.1016/j.jag.2024.104219.
395 A. L. Croella and L. Fraccascia, *Comput. Ind. Eng.*, 2024, **198**, 110714, DOI: 10.1016/j.cie.2024.110714.
396 T. Morató, M. Vaezi and A. Kumar, *Renewable Sustainable Energy Rev.*, 2020, **134**, 110154, DOI: 10.1016/j.rser.2020.110154.
397 Y. Tang, Y. Li and T. T. Cockerill, *Biomass Bioenergy*, 2024, **184**, 107187, DOI: 10.1016/j.biombioe.2024.107187.
398 J. J. Wu, J. Zhang, W. M. Yi, H. Z. Cai, Y. Li and Z. P. Su, *Energy*, 2022, **239**, 122374, DOI: 10.1016/j.energy.2021.122374.
399 K. Altayib and I. Dincer, *Energy Convers. Manage.*, 2023, **298**, 117793, DOI: 10.1016/j.enconman.2023.117793.
400 S. Li, T. Laukkanen, D. Jiang, V. Vuorinen and M. Järvinen, *Energy Convers. Manage.*, 2024, **306**, 118318, DOI: 10.1016/j.enconman.2024.118318.
401 S. Maimaiti, Y. Gu, Q. Chen and Z. Tang, *J. Cleaner Prod.*, 2023, **425**, 139002, DOI: 10.1016/j.jclepro.2023.139002.
402 W. Wu, M. I. Taipabu, W.-C. Chang, K. Viswanathan, Y.-L. Xie and P.-C. Kuo, *Renewable Energy*, 2022, **196**, 707–719, DOI: 10.1016/j.renene.2022.07.007.
403 L. Muriuki, D. Wafula Wekesa and F. Njoka, *Energy Convers. Manage.*, 2024, **299**, 117813, DOI: 10.1016/j.enconman.2023.117813.
404 L. Wang, Y. Zhang, C. Li, M. Pérez-Fortes, T.-E. Lin, F. Maréchal, J. Van herle and Y. Yang, *Appl. Energy*, 2020, **280**, 115987, DOI: 10.1016/j.apenergy.2020.115987.
405 T. Otgonbayar and M. Mazzotti, *Energy*, 2024, **290**, 130087, DOI: 10.1016/j.energy.2023.130087.